



Abblaihed, Khaled Abdulmohsen H. (2025) *Antenna design and characterization for future wireless communication enabled V2X applications*. PhD thesis.

<https://theses.gla.ac.uk/85295/>

Copyright and moral rights for this work are retained by the author

A copy can be downloaded for personal non-commercial research or study, without prior permission or charge

This work cannot be reproduced or quoted extensively from without first obtaining permission from the author

The content must not be changed in any way or sold commercially in any format or medium without the formal permission of the author

When referring to this work, full bibliographic details including the author, title, awarding institution and date of the thesis must be given

Enlighten: Theses

<https://theses.gla.ac.uk/>  
[research-enlighten@glasgow.ac.uk](mailto:research-enlighten@glasgow.ac.uk)

# Antenna Design and Characterization for Future Wireless Communication enabled V2X Applications

Khaled Abdulmohsen H Alblaihed

Submitted in fulfilment of the requirements for the  
Degree of Doctor of Philosophy

James Watt School of Engineering  
College of Science and Engineering  
University of Glasgow



University  
of Glasgow

January 2025

# Abstract

The evolution of 5G technology has significantly impacted the advancement of Vehicle-to-Everything (V2X) communications, enabling high-speed, low-latency interactions critical for autonomous driving, road safety, and infotainment systems. Operating in the millimeter-wave (mmWave) band, particularly in dynamic vehicular environments, presents challenges such as signal propagation loss, atmospheric attenuation, and polarization mismatches. Addressing these challenges is essential to meet the stringent requirements of 5G V2X applications, which demand wide impedance bandwidth, high gain, efficient beamsteering, and robust polarization control. Achieving these objectives necessitates innovative, cost-effective antenna designs that ensure reliable communication while supporting high data rates and scalability for next-generation networks.

This thesis presents antenna solutions to overcome these challenges, focusing on linearly polarized (LP) and circularly polarized (CP) designs. The LP antenna designs include an annular ring patch antenna offering a wide impedance bandwidth of 35.17% and a 9-element series-fed array achieving a high realized gain of 16.6 dBi with low sidelobe levels (SLLs). Building on this, 2x9 and 4x9 series-fed arrays enhance the realized gain to 17.9 dBi and 21.1 dBi, respectively, while maintaining wide bandwidths. Additionally, a four-port phased array enables dynamic beamsteering, achieving beam control across multiple angles with configurable realized gain up to 21.5 dBi. To address polarization mismatches and multipath interference, CP antenna designs are developed, including a single-element CP patch with wide axial ratio (AR) and impedance bandwidths. The single-element design extends to a 9-element series-fed CP array achieving a realized gain of 15.2 dBi and low SLLs. These solutions emphasize structural simplicity, reducing fabrication costs and enhancing scalability for large-scale deployment.

The proposed designs are validated through simulation, fabrication, and experimental measurements, demonstrating close agreement between simulation and measurement results. Compared to the state-of-the-art, these designs offer advancements in bandwidth, gain, polarization control, and beamsteering while maintaining cost-effectiveness and scalability. The outcomes of this research contribute to the development of high-performance antennas that address the critical demands of 5G V2X systems, enabling reliable, efficient, and robust communication in next-generation vehicular applications.

# Acknowledgements

I want to begin by extending my profound gratitude to the Almighty God for preserving my health and guiding me through the challenges of my PhD journey. I am forever thankful for the inspiration, knowledge, strength, and His grace that allowed me to attain this scholarship.

I want to express my heartfelt gratitude to my primary supervisor, Dr. Lina Mohjazi, who accepted me as her PhD student and provided invaluable mentorship, encouragement, and support throughout my doctoral journey. Her unwavering passion for academic research excellence has profoundly influenced both my academic development and personal growth. Additionally, I extend my immense appreciation to my co-supervisor, Prof. Qammer Abbasi, who has consistently offered strong support for my research endeavor. I am deeply thankful for his enthusiasm, patience, and the valuable insights that have sparked numerous intriguing research ideas and broadened my scholarly horizons.

I would also like to thank Prof. Muhammad Ali Imran for his unwavering support, which has been essential in helping me complete my PhD.

I would like to express my sincere gratitude to Jouf University for awarding me the scholarship that enabled me to undertake this PhD research. Their support has provided me with the resources and opportunity to fully focus on my academic and research goals, for which I am truly thankful.

I would like to extend my deepest gratitude to my dear parents. Their unwavering love and sacrifices have empowered me to pursue my dream. Their constant support and encouragement have been a continual source of inspiration and motivation, without which I would not have reached this significant milestone in my life.

My deepest appreciation goes to my wife, *Shatha*, and my children, *Khuzama* and *Abdalmohsen*, for their patience, understanding, and support throughout this journey. Their love has been my anchor, providing comfort and motivation in the face of challenges.

I also want to thank my friends and colleagues who provided intellectual stimulation and emotional support during this challenging process.

Thank you to everyone who contributed, no matter how small, to the completion of this research during my PhD journey.

**University of Glasgow**  
College of Science & Engineering  
**Statement of Originality**

**Name:** Khaled Abdulmohsen H Alblaihed

**Registration Number:** xxxxxxxx

I certify that the thesis presented here for examination for a PhD degree of the University of Glasgow is solely my own work other than where I have clearly indicated that it is the work of others (in which case the extent of any work carried out jointly by me and any other person is clearly identified in it) and that the thesis has not been edited by a third party beyond what is permitted by the University's PGR Code of Practice.

The copyright of this thesis rests with the author. No quotation from it is permitted without full acknowledgement.

I declare that the thesis does not include work forming part of a thesis presented successfully for another degree.

I declare that this thesis has been produced in accordance with the University of Glasgow's Code of Good Practice in Research.

I acknowledge that if any issues are raised regarding good research practice based on review of the thesis, the examination may be postponed pending the outcome of any investigation of the issues.

**Signature:** Khaled

**Date:** 30/01/2025

# Contents

|  |             |
|--|-------------|
| <b>Abstract</b>  | <b>i</b>    |
| <b>Acknowledgements</b>  | <b>ii</b>   |
| <b>Declaration</b>   | <b>iii</b>  |
| <b>List of Tables</b>  | <b>vii</b>  |
| <b>List of Figures</b>   | <b>viii</b> |
| <b>List of Abbreviations</b>   | <b>xi</b>   |
| <b>List of Symbols</b>   | <b>xii</b>  |
| <b>1 Introduction</b>  | <b>1</b>    |
| 1.1 Scope and Motivation . . . . .   | 1           |
| 1.1.1 Bandwidth, Polarization, and Gain Challenges in Antenna Design . . . . . | 2           |
| 1.1.2 Beamsteering for 5G V2X Communications . . . . .                         | 3           |
| 1.2 Problem Statement and Objectives . . . . .                                 | 4           |
| 1.2.1 Problem Statement . . . . .  | 5           |
| 1.2.2 Objectives . . . . .   | 6           |
| 1.3 Contributions and Research Outcome . . . . .                               | 8           |
| 1.3.1 Contributions . . . . .  | 8           |
| 1.3.2 Research Outcome . . . . .   | 9           |
| 1.4 Thesis Outline . . . . .   | 10          |
| <b>2 Literature Review</b>   | <b>12</b>   |
| 2.1 Overview of Antenna Design . . . . .                                       | 12          |
| 2.1.1 Low-Frequency Antenna Characteristics . . . . .                          | 13          |
| 2.1.2 mmWave Antenna Characteristics . . . . .                                 | 15          |
| 2.1.3 Antenna Design for 5G V2X Communication Systems . . . . .                | 16          |
| 2.2 Antenna Polarization Characteristics . . . . .                             | 21          |

|          |   |           |
|----------|---|-----------|
| 2.2.1    | Linearly Polarized . . . . .                                      | 22        |
| 2.2.2    | Circularly Polarized . . . . .                                    | 23        |
| 2.3      | Antenna Array . . . . .   | 25        |
| 2.3.1    | Feeding Techniques for Antenna Arrays . . . . .                   | 27        |
| 2.4      | Phased Array Beamsteering . . . . .                               | 28        |
| 2.4.1    | Fundamentals of Phased Array Beamsteering . . . . .               | 29        |
| 2.4.2    | Beamsteering Angle Calculation for 4-Port Phased Arrays . . . . . | 30        |
| 2.5      | Summary . . . . .   | 31        |
| <b>3</b> | <b>Linearly Polarized Antennas Design</b>                         | <b>33</b> |
| 3.1      | Introduction . . . . .  | 33        |
| 3.2      | Contributions . . . . .   | 34        |
| 3.3      | Rectangular Patch Antenna . . . . .                               | 35        |
| 3.3.1    | Antenna Configuration . . . . .                                   | 35        |
| 3.3.2    | Simulated Optimization of the Antenna Design . . . . .            | 37        |
| 3.4      | Annular Ring Patch Antenna . . . . .                              | 39        |
| 3.4.1    | Antenna Configuration and Analysis . . . . .                      | 39        |
| 3.4.2    | Evolution of the Antenna Design . . . . .                         | 40        |
| 3.4.3    | Experimental Validation and Discussion . . . . .                  | 41        |
| 3.5      | Annular Ring Patch Antenna Array . . . . .                        | 46        |
| 3.5.1    | Design and Analysis of the Antenna Array . . . . .                | 46        |
| 3.5.2    | Simulation Analysis . . . . .                                     | 47        |
| 3.5.3    | Measurement Results and Discussion . . . . .                      | 48        |
| 3.6      | Summary . . . . .   | 51        |
| <b>4</b> | <b>Beamsteering Antenna</b>                                       | <b>55</b> |
| 4.1      | Introduction . . . . .  | 55        |
| 4.2      | Contributions . . . . .   | 56        |
| 4.3      | 2x9 series-fed LP patch antenna array . . . . .                   | 57        |
| 4.3.1    | Design and Analysis of 2x9 Antenna Array . . . . .                | 57        |
| 4.3.2    | Simulation Results . . . . .                                      | 58        |
| 4.3.3    | Experimental Discussion . . . . .                                 | 58        |
| 4.4      | 4x9 series-fed LP patch antenna array . . . . .                   | 63        |
| 4.4.1    | 4x9 Antenna Array Configuration . . . . .                         | 63        |
| 4.4.2    | Simulation Analysis of 4x9 Antenna Array . . . . .                | 63        |
| 4.4.3    | Experimental Validation . . . . .                                 | 64        |
| 4.5      | Phased Array with Beamsteering Capabilities . . . . .             | 69        |
| 4.5.1    | An Overview . . . . .   | 69        |
| 4.5.2    | Simulation Results of the Proposed Phased Antenna Array . . . . . | 70        |

|          |  |           |
|----------|--|-----------|
| 4.5.3    | Experimental Validation and Discussion . . . . .                   | 71        |
| 4.6      | Summary . . . . .  | 75        |
| <b>5</b> | <b>Circularly Polarized Antenna Design</b>                         | <b>76</b> |
| 5.1      | Introduction . . . . .   | 76        |
| 5.2      | Contributions . . . . .  | 77        |
| 5.3      | Circularly Polarized Patch Antenna . . . . .                       | 78        |
| 5.3.1    | Antenna Configuration and Analysis . . . . .                       | 78        |
| 5.3.2    | Simulation Analysis of CP Antennas . . . . .                       | 80        |
| 5.3.3    | Experimental Validation and Discussion . . . . .                   | 82        |
| 5.4      | Circularly Polarized Patch Antenna Array . . . . .                 | 86        |
| 5.4.1    | Antenna Configuration and Analysis . . . . .                       | 86        |
| 5.4.2    | Simulation Analysis of Series-Fed CP Antenna Array . . . . .       | 87        |
| 5.4.3    | Experimental Validation and Discussion . . . . .                   | 90        |
| 5.5      | Summary . . . . .  | 94        |
| <b>6</b> | <b>Conclusions and Future Works</b>                                | <b>95</b> |
| 6.1      | Concluding Remarks . . . . .                                       | 95        |
| 6.2      | Future Work . . . . .  | 97        |
| 6.2.1    | Advanced Antenna Materials and Fabrication Techniques . . . . .    | 97        |
| 6.2.2    | Optimizing Phased Array Design for Enhanced Beamsteering . . . . . | 98        |
| 6.2.3    | Further Enhancement of CP Antenna Arrays . . . . .                 | 98        |

# List of Tables

|     |  |    |
|-----|--|----|
| 3.1 | Rectangular Patch Antenna Design Parameters . . . . .                      | 36 |
| 3.2 | Annular Ring Patch Antenna Design Parameters . . . . .                     | 41 |
| 3.3 | Comparison of the proposed LP design with other similar works. . . . .     | 46 |
| 3.4 | The Dolph-Chebyshev approach for 9-element array weights. . . . .          | 48 |
| 3.5 | Optimized feedline widths between adjacent elements. . . . .               | 48 |
| 4.1 | Comparison of the proposed work with other similar works. . . . .          | 75 |
| 5.1 | Comparison of the proposed CP design with other closely related works. . . | 86 |
| 5.2 | Comparison of the proposed CP array design with other similar works. . .   | 94 |

# List of Figures

|      |  |    |
|------|--|----|
| 1.1  | Coverage zones for various vehicular application scenarios in dynamic environments. . . . .  | 3  |
| 2.1  | V2X communications. . . . .  | 17 |
| 2.2  | Different Antenna Shapes. . . . .  | 19 |
| 2.3  | Polarization types. . . . .  | 21 |
| 2.4  | Array feeding structures (a) parallel structure (b) series-fed structure. . . .  | 28 |
| 3.1  | Geometry of the proposed rectangular patch antenna. . . . .  | 36 |
| 3.2  | Evolution of the proposed rectangular patch antenna. . . . .   | 37 |
| 3.3  | Evolution of simulated reflection coefficients during the design process. . . .  | 38 |
| 3.4  | Simulated realized gain of the proposed rectangular patch antenna. . . . .   | 38 |
| 3.5  | Simulated radiation pattern of the proposed rectangular patch antenna in the E-plane ( $\phi = 0^\circ$ ) and H-plane ( $\phi = 90^\circ$ ). . . . . | 39 |
| 3.6  | Structure of the annular ring patch antenna (a) top view (b) side view. . . .  | 40 |
| 3.7  | Evolution of the proposed annular ring patch antenna. . . . .  | 41 |
| 3.8  | Simulated reflection coefficients in the process of evolution. . . . .   | 42 |
| 3.9  | Measurement system and the LP annular ring antenna prototype. . . . .  | 44 |
| 3.10 | Reflection coefficient of the simulated and measured proposed LP annular ring antenna. . . . .   | 45 |
| 3.11 | Simulated and measured gain and efficiency for the proposed LP antenna. . .  | 45 |
| 3.12 | Simulated and measured radiation pattern of the proposed LP annular ring antenna (a) $\phi = 0^\circ$ and (b) $\phi = 90^\circ$ . . . . .            | 46 |
| 3.13 | Structure of the proposed antenna array (a) single-element top view (b) array top view (c) side view. . . . .  | 47 |
| 3.14 | Reflection coefficient of the simulated proposed LP antenna array. . . . .   | 49 |
| 3.15 | Evolution of the proposed LP antenna array (a) 7-element (b) 9-element. . .  | 49 |
| 3.16 | Evolution of the gain for the proposed LP antenna array. . . . .   | 50 |
| 3.17 | Current distribution of the proposed LP antenna array. . . . .   | 50 |
| 3.18 | Reflection coefficient of the simulated and measured proposed LP antenna array. . . . .  | 51 |

|      |   |    |
|------|---|----|
| 3.19 | Measurement system and the LP antenna array prototype. . . . .  | 52 |
| 3.20 | Simulated and measured realized gain and SLLs results as a function of the frequency. . . . .   | 53 |
| 3.21 | Simulated and measured radiation pattern of the proposed LP antenna array (a) $\phi = 0^\circ$ and (b) $\phi = 90^\circ$ . . . . .  | 53 |
| 4.1  | Structure of the proposed 2x9 series-fed antenna array. . . . .   | 58 |
| 4.2  | Reflection coefficient of the simulated proposed 2x9 LP antenna array. . . . .  | 59 |
| 4.3  | Realized gain of the simulated proposed 2x9 LP antenna array. . . . .   | 59 |
| 4.4  | Reflection coefficient of the simulated and measured proposed 2x9 LP antenna array. . . . .   | 60 |
| 4.5  | Measurement system and the 2x9 LP antenna array prototype. . . . .  | 61 |
| 4.6  | Simulated and measured realized gain results of the proposed 2x9 LP antenna array. . . . .  | 62 |
| 4.7  | Simulated and measured radiation pattern of the proposed 2x9 LP antenna array (a) $\phi = 0^\circ$ and (b) $\phi = 90^\circ$ . . . . .  | 62 |
| 4.8  | Structure of the proposed 4x9 series-fed antenna array. . . . .   | 64 |
| 4.9  | Reflection coefficient of the simulated proposed 4x9 LP antenna array. . . . .  | 65 |
| 4.10 | Realized gain of the simulated proposed 4x9 LP antenna array. . . . .   | 65 |
| 4.11 | Reflection coefficient of the simulated and measured proposed 4x9 LP antenna array. . . . .   | 66 |
| 4.12 | Measurement system and the 4x9 LP antenna array prototype. . . . .  | 67 |
| 4.13 | Simulated and measured realized gain of the proposed 4x9 LP antenna array. . . . .  | 68 |
| 4.14 | Simulated and measured radiation pattern of the proposed 4x9 LP antenna array (a) $\phi = 0^\circ$ and (b) $\phi = 90^\circ$ . . . . .  | 68 |
| 4.15 | Structure of the proposed series-fed phased antenna array. . . . .  | 70 |
| 4.16 | Reflection coefficient of the simulated proposed phased antenna array. . . . .  | 71 |
| 4.17 | The proposed series-fed phased antenna array and its corresponding simulated radiation pattern results. . . . .   | 72 |
| 4.18 | Reflection coefficient of the simulated and measured proposed phased array. . . . .   | 73 |
| 4.19 | Experimental validation of the proposed phased antenna array. (a) Measurement system and the prototype. (b) Simulated and measured radiation pattern. (c) Simulated and measured realized gain. . . . . | 74 |
| 5.1  | Structure of the circularly polarized antenna (a) air-gaps (b) cross-stubs (c) side view. . . . .   | 79 |
| 5.2  | Simulated reflection coefficient of the proposed CP antennas. . . . .   | 81 |
| 5.3  | Axial ratio in the process of the CP antennas evolution. . . . .  | 81 |
| 5.4  | Measurement system and the CP antennas prototype. . . . .   | 83 |

|      |   |    |
|------|---|----|
| 5.5  | Reflection coefficient of the simulated and measured CP antennas. . . . .   | 84 |
| 5.6  | Simulated and measured AR of the proposed CP antennas. . . . .  | 84 |
| 5.7  | Simulated and measured gain and efficiency for the proposed CP antennas.  | 85 |
| 5.8  | Simulated and measured radiation pattern of CP antennas (a) air-gaps and<br>(b) cross-stubs. . . . .                                  | 85 |
| 5.9  | Structure of the proposed series-fed CP patch antenna array. . . . .  | 87 |
| 5.10 | Evolution of the proposed CP antenna array (a) 7-element (b) 9-element. .   | 88 |
| 5.11 | Evolution of the simulated gain for the proposed antenna array. . . . .   | 88 |
| 5.12 | Current distribution of the proposed CP antenna array. . . . .  | 89 |
| 5.13 | Sidelobe levels of the proposed CP antenna array. . . . .   | 89 |
| 5.14 | Measurement system and the CP antenna array prototype. . . . .  | 91 |
| 5.15 | Simulated and measured $S_{11}$ of the proposed CP antenna array. . . . .   | 92 |
| 5.16 | Simulated and measured AR of the proposed CP antenna array. . . . .   | 92 |
| 5.17 | Simulated and measured realized gain and SLLs of the proposed CP antenna<br>array. . . . .  | 93 |
| 5.18 | Simulated and measured radiation pattern of the proposed CP antenna<br>array (a) $\phi = 0^\circ$ and (b) $\phi = 90^\circ$ . . . . . | 93 |

# List of Abbreviations

|        |                                  |
|--------|----------------------------------|
| 5G     | Fifth Generation                 |
| mmWave | Millimetre Wave                  |
| V2X    | Vehicle-to-Everything            |
| V2V    | Vehicle-to-Vehicle               |
| V2I    | Vehicle-to-Infrastructure        |
| V2N    | Vehicle-to-Network               |
| V2P    | Vehicle-to-Pedestrian            |
| FR1    | Frequency Range 1                |
| FR2    | Frequency Range 2                |
| MPAs   | Microstrip patch antennas        |
| LP     | Linearly Polarized               |
| CP     | Circularly Polarized             |
| RHCP   | Right-Hand Circular Polarization |
| LHCP   | Left-Hand Circular Polarization  |
| AR     | Axial Ratio                      |
| SLLs   | Sidelobe levels                  |
| NLoS   | Non Line of Sight                |
| LoS    | Line of Sight                    |
| CWP    | Coplanar Waveguide Port          |
| CATR   | Compact Antenna Test Range       |
| OTA    | Over-The-Air                     |
| AUT    | Antenna Under Test               |
| VNA    | Vector Network Analyzer          |

# List of Symbols

|               |  |
|---------------|--|
| $\Delta\phi$  | Phase shift                                      |
| $\lambda$     | Wavelength                                       |
| $\log(\cdot)$ | Base-10 logarithm of ( $\cdot$ )                 |
| $\phi_1$      | Outer radius air-gap angle                       |
| $\phi_2$      | Inner radius air-gap angle                       |
| $\phi_n$      | Phase of the antenna array elements              |
| $\theta_s$    | Steering angle                                   |
| $AR_{dB}$     | Axial Ratio                                      |
| $C$           | Speed of light                                   |
| $d$           | Distance between adjacent antenna array elements |
| $D_n$         | Dolph-Chebyshev element weight                   |
| $E_{max}$     | Maximum electric field intensity                 |
| $E_{min}$     | Minimum electric field intensity                 |
| $f_{rmm}$     | Resonant frequency                               |
| $G_{AUT}$     | Antenna under test gain                          |
| $G_{ref}$     | Reference antenna gain                           |
| $h$           | Substrate thickness                              |
| $L$           | Antenna substrate length                         |
| $L_f$         | Antenna array feed length                        |
| $L_n$         | Antenna slot length                              |
| $L_{RA}$      | Rectangular antenna length                       |
| $n$           | Antenna array elements                           |
| $P_{AUT}$     | Antenna under test power                         |
| $P_{ref}$     | Reference antenna power                          |
| $R_1$         | Annular ring antenna outer radius                |
| $R_2$         | Annular ring antenna inner radius                |
| $R_x$         | Receiver   |
| $S_{11}$      | Antenna reflection coefficients                  |

|          |                              |
|----------|------------------------------|
| $T_x$    | Transmitter                  |
| $W$      | Antenna substrate width      |
| $W_f$    | Antenna array feed width     |
| $W_n$    | Antenna array elements width |
| $W_{RA}$ | Rectangular antenna width    |
| $W_s$    | Antenna slot width           |
| $X_{nm}$ | First-order Bessel function  |

# Chapter 1

## Introduction

### 1.1 Scope and Motivation

The rapid evolution of wireless communication technologies, particularly with the introduction of 5G networks, has opened up vast opportunities for numerous applications in diverse sectors such as transportation, healthcare, and smart cities. One of the most promising and transformative fields is Vehicle-to-Everything (V2X) communications, which is critical for enhancing future transportation systems by enabling applications ranging from road safety to autonomous driving, vehicle diagnostics, and passenger infotainment [1]. V2X communications facilitate multiple interaction types, including Vehicle-to-Vehicle (V2V), Vehicle-to-Infrastructure (V2I), Vehicle-to-Network (V2N), and Vehicle-to-Pedestrian (V2P), all of which require reliable, low-latency, and high-throughput communication links [2].

V2X communications operate across two primary frequency bands: Frequency Range 1 (FR1), covering from 410 MHz to 7.125 GHz, and Frequency Range 2 (FR2), spanning 24.25 GHz to 52.6 GHz [3]. While FR1 is commonly used for long-range communications with moderate data rates, FR2, especially the millimeter-wave (mmWave) band, offers the potential to deliver much higher data rates with shorter range. Among the mmWave frequencies, the 28 GHz band has garnered particular attention due to its ability to offer high data rates, enhanced reliability, low latency, and reduced power consumption, which are essential for critical safety applications in dynamic vehicular environments [4]. However, mmWave communication faces significant challenges, including atmospheric attenuation, signal propagation loss, and limited coverage, all of which can compromise the reliability of communication links, particularly in highly dynamic environments like vehicular networks [5]. Furthermore, the imperative for V2X communications to accommodate an extensive array of sensors necessitates an antenna design characterized by a wide impedance bandwidth, adding complexity to the design requirements.

To overcome these challenges, antenna designs must offer not only high gain to

counteract signal attenuation but also wide impedance bandwidth to ensure consistent performance across the mmWave frequency range. Additionally, practical considerations such as cost, simplicity, and compactness are crucial, especially since modern vehicles may require multiple antennas integrated into limited spaces. Microstrip patch antennas (MPAs) are highly promising for V2X communication systems, particularly in the mmWave band, due to their compact size, low cost, and ease of fabrication [6].

In the context of this thesis, these challenges will be addressed through the design and development of innovative antenna solutions that focus on enhancing gain, expanding impedance bandwidth, and integrating beamsteering techniques to ensure reliable communication in 5G V2X environments.

### 1.1.1 Bandwidth, Polarization, and Gain Challenges in Antenna Design

Antenna design for V2X communication systems must address the need for both wide impedance bandwidth and high gain to ensure reliable communication, particularly in the mmWave band, where signal attenuation is more pronounced. Linearly Polarized (LP) antennas have been widely employed in various V2X applications due to their ability to provide wide impedance bandwidth and high gain. However, LP antennas can experience limitations in environments where multipath interference and polarization mismatches occur [7]. In such cases, Circularly Polarized (CP) antennas offer an advantage, as they provide greater resilience to polarization mismatches and enhance signal stability in dynamic environments like those encountered in V2X communications. Both LP and CP antennas are therefore essential, depending on the specific environmental and operational requirements of V2X systems.

Various techniques have been introduced to enhance the impedance bandwidth and axial ratio (AR) bandwidth in both LP and CP antenna designs. For LP antennas, solutions such as aperture-coupled patches, stacked patches, and metamaterial-based low-profile antennas have been explored [8], [9], [10], though many of these designs come with higher complexity and fabrication costs. CP antennas, which are better suited to mitigate multipath interference, must also provide wide AR bandwidth and high gain to be effective in dynamic vehicular environments. Achieving these requirements often involves innovative design techniques that enable wide impedance and AR bandwidth while maintaining simple antenna structures for ease of fabrication and integration into vehicular communication systems.

Increasing the gain of antennas can be effectively achieved by developing antenna arrays, where multiple elements are combined to enhance the overall performance. Arrays not only improve the gain but also maintain compactness and simplicity in design. The choice of feeding techniques is crucial in array designs, as they directly impact the

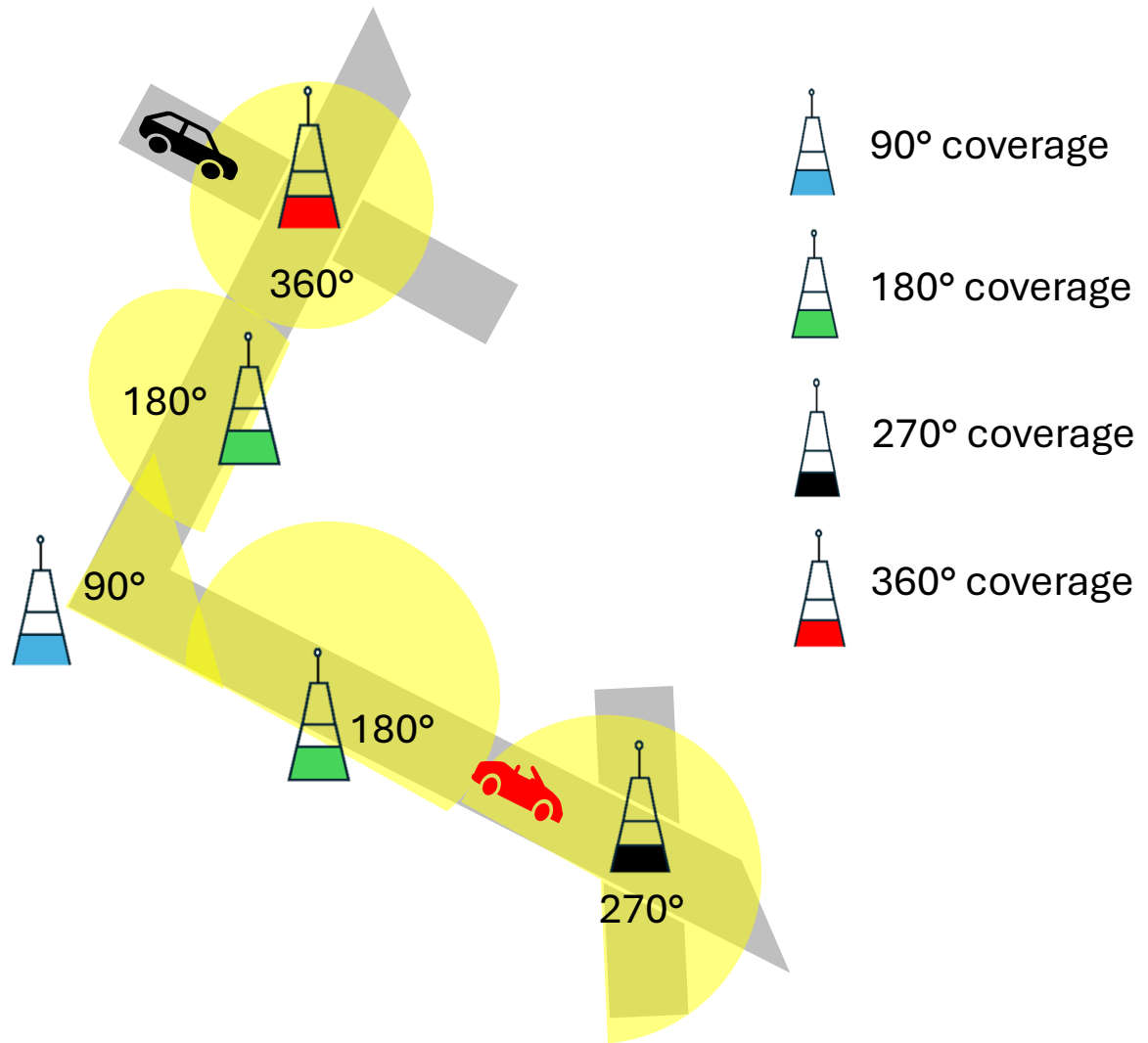


Figure 1.1: Coverage zones for various vehicular application scenarios in dynamic environments.

efficiency, size, and performance of the antenna. While parallel-fed arrays are commonly used, they tend to create bulkier designs with higher losses. On the other hand, series-fed arrays offer a more compact structure with simpler feed networks, which is particularly beneficial for 5G V2X applications. By applying the Dolph-Chebyshev weighting method, series-fed arrays can balance beamwidth and sidelobe levels (SLLs), ensuring high gain and low interference, which are critical for reliable 5G V2X communications [11], [12].

### 1.1.2 Beamsteering for 5G V2X Communications

Beyond the challenges of gain and bandwidth, beamsteering techniques are critical for V2X communication systems, particularly in environments where dynamic coverage is required. In real-world scenarios, an antenna system might need to offer 360° coverage for highway

applications or  $90^\circ$  or  $180^\circ$  coverage in confined environments like urban intersections or trackside locations, as illustrated in Fig. 1.1. Beamsteering allows the antenna to adjust its radiation pattern dynamically, ensuring that coverage adapts to the vehicle's location and movement patterns [13], [14].

Phased array designs have emerged as an effective solution for enabling dynamic beam control, allowing the coverage configuration to be adjusted based on application requirements. Such arrays can provide  $90^\circ$ ,  $180^\circ$ ,  $270^\circ$ , or  $360^\circ$  beam coverage, making them ideal for the varied needs of 5G V2X communication systems. For instance, phased arrays allow beamsteering to dynamically adjust the radiation pattern and maintain reliable links as vehicles move through different environments, such as highways, urban areas, or intersections [15].

The development of phased arrays with beamsteering capabilities marks a significant advancement in antenna technology for 5G V2X applications. These phased arrays can achieve dynamic beam control to meet the evolving communication needs of vehicular systems, with multi-unit configurations providing full  $360^\circ$  coverage when required. This adaptability ensures that the system can maintain reliable communication links across a variety of environments, making it an ideal solution for next-generation vehicular networks, where dynamic coverage is essential.

## 1.2 Problem Statement and Objectives

As the demand for advanced communication systems continues to rise with the evolution of 5G networks, V2X communications emerge as a cornerstone technology for future transportation systems. V2X applications, which include V2V, V2I, V2P, and V2N communications, require reliable, low-latency, and high-throughput communication links to support a wide range of critical services, such as road safety, autonomous driving, and passenger infotainment. These communication systems operate across both FR1 and FR2, where the mmWave band offers considerable benefits in terms of high data rates and low latency, but it also introduces significant challenges, including atmospheric attenuation, signal propagation loss, and limited coverage.

One of the primary challenges facing 5G V2X communication systems is the design and development of antennas that can overcome these obstacles while maintaining wide impedance bandwidth, high gain, and stable communication links in dynamic vehicular environments. MPAs offer a promising solution due to their compact size, ease of fabrication, and low cost. However, achieving the wide impedance bandwidth, high gain, and polarization flexibility needed to ensure reliable communication remains a challenge, particularly in environments with multipath interference and polarization mismatches. Additionally, modern vehicles often require multiple antennas within limited spaces,

further complicating the design process.

This thesis addresses these challenges by focusing on the design and development of innovative antenna solutions that enhance gain, expand impedance bandwidth, and incorporate beamsteering capabilities. By employing advanced design techniques, such as series-fed arrays, multi-element configurations, and phased arrays with dynamic beamsteering, the research aims to improve antenna performance for 5G V2X applications. The objective is to provide high-performance antenna designs that support wide coverage, minimize interference, and adapt to various dynamic environments, ensuring robust and reliable communication in next-generation vehicular networks.

## 1.2.1 Problem Statement

### Challenges in Antenna Design for 5G V2X Communications

The design of antennas for 5G V2X communication systems faces several challenges that arise from the unique demands of these dynamic vehicular environments.

*Challenge 1) Achieving wide impedance bandwidth in designing 5G V2X antennas.* V2X communication systems operating in the mmWave band require antennas with wide impedance bandwidth to ensure stable and reliable links, especially in high-data-rate scenarios like real-time traffic updates and autonomous driving. The shorter wavelengths in the mmWave range lead to increased atmospheric attenuation and propagation losses, which are further intensified in non-line-of-sight (NLoS) conditions, such as urban intersections or tunnels [5]. Additionally, the high mobility of vehicles exacerbates communication disruptions, necessitating antenna designs that balance wide impedance bandwidth with robust performance under dynamic conditions. Addressing these challenges is essential to support the stringent requirements of 5G V2X applications, including low latency and high reliability.

*Challenge 2) Mitigating polarization mismatches and multipath interference.* In highly dynamic vehicular environments, polarization mismatches and multipath interference present additional challenges that can degrade signal quality and reliability. While LP antennas can be effective in certain environments, they may struggle in scenarios with significant multipath interference, such as urban areas with dense building structures or highway overpasses where signals reflect off surrounding surfaces. In such conditions, CP antennas offer better resilience by mitigating polarization mismatches [7]. However, achieving both wide AR bandwidth and wide impedance bandwidth in CP antennas, while maintaining a compact and efficient design, remains a key challenge for 5G V2X antenna designs.

*Challenge 3) Optimizing antenna arrays for gain and SLLs control.* To overcome the limitations of single-element antennas in achieving the necessary gain for long-range communication, antenna arrays are often employed. Increasing the number of elements in an array can significantly enhance the gain, but this introduces additional complexity in terms of feeding structures and array configurations. Series-fed arrays, which offer a compact and simple feeding structure, must be optimized to balance gain, beamwidth, and SLLs. Achieving high gain and low SLLs in mmWave arrays while maintaining a compact design is critical for reliable 5G V2X communications.

*Challenge 4) Integrating beamsteering in phased arrays.* In V2X communication systems, dynamic coverage requirements demand the use of beamsteering techniques to ensure reliable links across varying environments. However, achieving efficient beamsteering in phased arrays introduces its own set of challenges. While multi-port phased arrays can provide beamsteering capabilities, the ability to cover wide angles (such as  $\pm 45^\circ$ ) with minimal loss in gain and without introducing excessive complexity in the design is a major hurdle. Additionally, phased arrays must be designed to maintain low SLLs, which is critical for minimizing interference in dense urban environments. Optimizing these arrays for 5G V2X applications requires addressing the trade-offs between beamwidth, gain, and SLLs, while ensuring that the antennas remain practical for integration into vehicles.

## 1.2.2 Objectives

In light of the previously mentioned technical challenges, the objectives of this thesis are outlined as follows:

*O1 :* Conduct an in-depth exploration of antenna design principles for 5G V2X communication systems, focusing on LP antennas, CP antennas, array configurations, and phased array techniques. This review analyzes state-of-the-art techniques for achieving wide impedance bandwidth, high gain, and efficient beamsteering, while addressing challenges related to polarization, multipath interference. The exploration covers various approaches, including single-element designs and array-based solutions, examining their suitability for 5G V2X applications based on their performance outcomes. This objective sets the foundation for the subsequent design and development work in this thesis, providing a comprehensive understanding of the existing literature and identifying key areas where further innovation is needed.

- O2* : Investigate and design high-performance antennas capable of achieving wide impedance bandwidth and high gain to ensure reliable communication across the mmWave frequency range for future V2X applications. These designs focus on overcoming the inherent challenges of atmospheric attenuation and signal propagation loss, prevalent in the mmWave band. The work begins with the development of a single-element antenna offering wide bandwidth, essential for supporting the high data rates required in 5G V2X communications. This single element is then extended into a 9-element series-fed array to enhance gain, providing a practical solution to improve signal strength and communication reliability over longer distances. By optimizing both bandwidth and gain, this objective ensures that the antenna designs support stable, consistent communication in dynamic vehicular environments.
- O3* : Develop and optimize phased array antennas with beamsteering capabilities to address the dynamic coverage requirements of 5G V2X applications. This objective involves designing multi-element arrays, such as 2x9 and 4x9 series-fed arrays, that offer high realized gain while maintaining compactness and simplicity. The phased arrays are designed to achieve dynamic beamsteering, allowing for flexible coverage across various vehicular environments, such as intersections, highways, and urban areas. The research focuses on achieving wide-angle beamsteering (up to  $\pm 45^\circ$ ) while minimizing losses in gain and maintaining low SLLs, which are crucial for reducing interference in dense environments. This objective provides adaptable phased array solutions that ensure reliable communication links regardless of the vehicle's position or movement, supporting a range of 5G V2X scenarios.
- O4* : Design CP antennas that provide wide AR bandwidth and wide impedance bandwidth to mitigate polarization mismatches and enhance signal stability in dynamic vehicular environments. The research focuses on both single-element CP antennas and their extension into series-fed arrays, providing solutions that operate effectively in environments with significant multipath interference. The CP antenna designs are optimized to achieve high gain, ensuring robust communication links in scenarios where polarization mismatches could otherwise degrade signal quality. Additionally, this objective explores innovative techniques to enhance AR bandwidth while maintaining a compact, low-profile design, making these antennas suitable for integration into modern vehicles equipped with multiple communication systems.

## 1.3 Contributions and Research Outcome

Based on the objectives outlined earlier, this thesis contributes to advancing antenna design for 5G V2X communications by addressing critical challenges and trade-offs related to impedance bandwidth, gain, beamsteering, and polarization. This section highlights the primary contributions and research outcomes of this work.

### 1.3.1 Contributions

The major contributions of this thesis are summarized as follows:

- Design and development of a novel LP annular ring patch antenna and series-fed array: This research introduces a novel LP annular ring patch antenna operating at 28 GHz, designed to provide a wide impedance bandwidth of 35.71% and a radiation efficiency exceeding 90%. This single-element antenna is optimized for 5G V2X applications, where wide bandwidth and high radiation efficiency are crucial to ensuring reliable communication links in dynamic vehicular environments. To enhance gain, the design is extended into a 9-element series-fed antenna array, which achieves a realized gain of 16.6 dBi and low SLLs exceeding -17 dB. The series-fed configuration offers a compact and simple feed network, demonstrating that high gain can be achieved without adding excessive complexity. Both the single-element and the array provide practical solutions for overcoming atmospheric attenuation and propagation loss, making them suitable for integration into modern vehicles with limited space for antenna installations.
- Development and optimization of phased array antennas for beamsteering: One of the key contributions of this thesis is the design of phased array antennas capable of dynamic beamsteering to meet the diverse coverage needs of 5G V2X applications. The thesis presents the development of 2x9 and 4x9 series-fed arrays, optimized for high realized gain and low SLLs, while maintaining compactness and simplicity. These arrays are integrated into a phased array design with four ports, enabling dynamic beamsteering across angles of 90°, 180°, 270°, and 360°, depending on the specific vehicular communication scenario. The research demonstrates that wide-angle beamsteering, up to  $\pm 45^\circ$ , can be achieved while minimizing loss in gain, ensuring reliable communication links even in highly dynamic environments such as intersections and urban areas. This contribution addresses the challenges of maintaining consistent communication coverage as vehicles move through varied and complex environments, providing flexible phased array solutions for next-generation vehicular networks.

- Design and extension of CP antennas for wide impedance and AR bandwidths: A significant contribution of this thesis is the design of novel CP antenna, which is optimized for 5G V2X applications where polarization mismatches and multipath interference are common challenges. The single-element CP antenna achieves an AR bandwidth of 20.35% and an impedance bandwidth of 35.71%, using innovative design techniques such as cross-stubs. This design ensures stable communication links in dynamic vehicular environments, where maintaining polarization stability is crucial. The CP antenna design is then extended into a 9-element series-fed array, achieving a realized gain of 15.2 dBi and low SLLs exceeding -17 dB. The series-fed array configuration enhances gain and beam stability while preserving the benefits of circular polarization, making it ideal for long-range, high-performance vehicular communication. This contribution demonstrates that CP antennas can be both cost-effective and high-performing, addressing the complexity and implementation challenges typically associated with mmWave antennas for 5G V2X applications.

### 1.3.2 Research Outcome

The outcomes of this thesis, derived from focused research in 5G V2X antenna design, have resulted in the following publications:

#### Journals

- [J1] **K. A. Alblaihed**, K. Jalil ur Rehman, Q. H. Abbasi, M. A. Imran, and L. Mohjazi, ‘Bandwidth Enhancement of Microstrip Patch Antenna Using Air Holes for WLAN Applications’, *International Journal of Simulation: Systems, Science & Technology*, vol. 23, no. 2, pp1-3, Apr. 2022.
- [J2] **K. A. Alblaihed**, A. Abohmra, M. U. Rehman, Q. H. Abbasi, M. A. Imran, and L. Mohjazi, ‘Wideband Series-Fed Patch Antenna Array With High Gain and Low Sidelobe: Linearly and Circularly Polarized for 5G V2X Applications’, *IEEE Open Journal of Antenna and Propagation*, vol. 5, no. 6, pp. 1580-1591, Dec. 2024. DOI: 10.1109/OJAP.2024.3424330.
- [J3] **K. A. Alblaihed**, A. Abohmra, Q. H. Abbasi, M. A. Imran, and L. Mohjazi, ‘High-Gain Series-Fed Phased Antenna Array Beamsteering for 5G V2X Communication’, submitted to *IEEE Open Journal of Antenna and Propagation*. (**Under review**).
- [J4] **K. A. Alblaihed**, Q. H. Abbasi, M. A. Imran, and L. Mohjazi, ‘Advancements in Antenna Design for 5G V2X Communication Systems: Addressing Challenges in

Polarization, Beamsteering, and Bandwidth’, submitted to IEEE Access. (**Under review**).

## Conference Proceedings

- [C1] **K. A. Alblaihed**, Q. H. Abbasi, M. A. Imran, and L. Mohjazi, ‘Gain Enhancement of Microstrip Patch Antenna for 28 GHz 5G Applications’, In 2022 IEEE International Symposium on Antennas and Propagation and USNC-URSI Radio Science Meeting (AP-S/URSI), Denver, CO, USA, Jul. 2022. DOI: 10.1109/AP-S/USNC-URSI47032.2022.9886673.
- [C2] **K. A. Alblaihed**, Q. H. Abbasi, M. A. Imran, and L. Mohjazi, ‘Wideband of Microstrip Patch Antenna for 28 GHz 5G Applications’, In 2023 IEEE International Symposium on Antennas and Propagation and USNC-URSI Radio Science Meeting (USNC-URSI), Portland, OR, USA, Jul. 2023. DOI: 10.1109/USNC-URSI52151.2023.10237641.
- [C3] **K. A. Alblaihed**, Q. H. Abbasi, M. A. Imran, and L. Mohjazi, ‘Gain Enhancement Using Superstrate of Microstrip Patch Antenna Array for 5G Applications’, In 2024 IEEE International Symposium on Antennas and Propagation and INC/USNC-URSI Radio Science Meeting (AP-S/INC-USNC-URSI), Firenze, Italy, Jul. 2024. DOI: 10.1109/AP-S/INC-USNC-URSI52054.2024.10686327.

## 1.4 Thesis Outline

The rest of this thesis is structured as follows. Chapter 2 provides a comprehensive review of the literature related to antenna design for 5G V2X communication systems, covering LP antennas, CP antennas, antenna arrays, and phased array techniques. The chapter focuses on state-of-the-art methods for achieving wide impedance bandwidth, high gain, and efficient beamsteering, while addressing the challenges of polarization mismatches and multipath interference in vehicular environments. Chapter 3 introduces the design and development of a novel single-element LP antenna, optimized for wide bandwidth and high radiation efficiency, and extends this work by developing a 9-element series-fed array to enhance gain and reduce SLLs, providing practical solutions to mitigate signal attenuation and propagation loss. In Chapter 4, the focus shifts to the design and optimization of phased array antennas capable of dynamic beamsteering, with the development of 2x9 and 4x9 series-fed arrays leading to a phased array design that supports flexible coverage angles, ranging from 90° to 360°, depending on the specific vehicular communication requirements. Chapter 5 presents the design of CP antennas to address polarization mismatches and

improve signal stability, beginning with the development of a novel single-element CP antenna that achieves wide AR and impedance bandwidths, followed by the extension of this design into a 9-element series-fed CP array to further enhance gain and beam stability. Finally, Chapter 6 concludes the thesis by summarizing the key research findings and discussing potential future work, including further optimization of antenna designs for next-generation vehicular communication systems.

# Chapter 2

## Literature Review

In this chapter, the fundamental advantages of mmWave technology are examined to highlight its transformative potential for high-speed, low-latency communications. The discussion then narrows to its applications within 5G V2X communication systems, where mmWave frequencies enable high data rates and robust connectivity for advanced vehicular applications. A detailed overview of the essential requirements for designing effective antennas for 5G V2X communication systems is presented, with particular attention to achieving wide impedance bandwidth, high gain, and optimal polarization. This chapter also provides a comprehensive review of linearly and circularly polarized antennas, focusing on their roles and performance characteristics in dynamic vehicular environments. The benefits of gain enhancement through array configurations, particularly within the mmWave spectrum, are explored, followed by an analysis of feeding structures that compares series and parallel configurations in terms of simplicity and performance. Finally, phased array techniques and beamsteering capabilities are discussed as essential components for achieving dynamic coverage in 5G V2X communication systems, establishing a foundation for the phased array designs covered in later chapters. This comprehensive review aligns with the objectives outlined in *O1*, providing a foundational understanding of the design principles and techniques that support the antenna innovations presented in this thesis.

### 2.1 Overview of Antenna Design

Antenna design is a fundamental aspect of wireless communication, central to converting electrical signals into electromagnetic waves that transmit and receive data across diverse environments [16]. The design of antennas varies significantly based on specific requirements like bandwidth, gain, polarization, and operating frequency, each of which affects the antenna's form, functionality, and size. Generally, the size of an antenna is inversely related to its frequency of operation: higher frequencies, such as those within

the mmWave range, enable more compact antenna designs, while lower frequencies require larger structures to achieve efficiency. This scalability allows antennas to be tailored for a broad array of applications, from compact mobile devices to large-scale broadcast systems.

Several types of antennas are commonly used, each serving specific purposes and offering unique benefits. Microstrip patch antennas, for example, are lightweight, compact, and relatively easy to fabricate, making them suitable for high-frequency applications where space and efficiency are critical [17]. Yagi-Uda antennas, with their high gain and directivity, are often used in fixed, directional applications [18], while dipole antennas offer simple omnidirectional coverage that is ideal for low-cost communication systems [19]. Horn antennas, known for their broad bandwidth and high gain, are commonly employed in high-power applications, especially at microwave and mmWave frequencies [20]. Each antenna type brings distinct advantages in terms of gain, bandwidth, and coverage pattern, allowing designers to select configurations best suited for specific operational requirements.

The frequency of operation also influences the achievable data rate. Higher frequencies offer expanded bandwidth, allowing for greater data rates essential in applications that demand rapid data transmission [21]. However, at these elevated frequencies, particularly in the mmWave spectrum, communication links face unique challenges due to atmospheric attenuation, reduced range, and greater susceptibility to signal degradation from obstacles, making antenna design more challenging. Thus, antenna design at higher frequencies requires a careful balance of size, efficiency, and environmental resilience. This section provides an overview of antenna design principles, exploring how size, frequency, and performance are interlinked and setting the stage for understanding the technical intricacies in advanced antenna applications.

### 2.1.1 Low-Frequency Antenna Characteristics

Low-frequency antennas, typically operating in the sub-6 GHz range, are foundational to many communication systems due to their robust propagation characteristics, reliable signal strength, and ability to maintain effective coverage over longer distances. This frequency range is often preferred in applications such as cellular networks, Wi-Fi, and satellite communications, where signal integrity and penetration capabilities are critical for maintaining quality connections across various environments [22]. Due to the inverse relationship between an antenna's size and its operating frequency, low-frequency antennas are generally larger, requiring more space for optimal resonance and efficiency. These antennas are known for their resilience in overcoming physical obstructions, such as buildings and natural terrain, making them especially advantageous in both urban and rural settings. For example, an antenna designed to operate at 3.5 GHz may require dimensions of 21.7 mm by 10.2 mm in width and length to achieve the necessary performance characteristics [23]. As frequencies increase within this lower frequency

spectrum, such as around 5.5 GHz, dimensions vary depending on bandwidth needs. Designs can range from 21.7 mm x 27 mm for antennas with a bandwidth of 0.7 GHz [24] to significantly larger sizes, such as 50 mm x 40 mm for narrower bandwidths of 0.05 GHz [25]. These variations highlight the intricate relationship between frequency, bandwidth, and size in low-frequency antenna design, where careful balancing is essential to meet specific performance requirements effectively.

The structural requirements of low-frequency antennas often lead to larger designs, especially in applications where reliability and signal quality are paramount [26]. Antennas operating around 4.5 GHz with broader bandwidths, such as 2 GHz, maintain relatively compact dimensions of length and width at 35 mm x 27.5 mm [27]. In contrast, antennas with narrower bandwidths at similar frequencies can demand substantially larger structures, reaching sizes of approximately 75 mm x 68 mm [28]. These design choices illustrate the trade-offs between bandwidth, efficiency, and compactness. In many cases, low-frequency antennas are configured for stable, long-distance communication, providing consistent connections well-suited to applications that prioritize coverage over device integration. Despite their advantages in stability and reliability, the larger physical size of low-frequency antennas presents challenges for integration into compact devices or space-constrained environments, making them less practical for modern applications that require smaller, embedded components.

Another critical aspect of low-frequency antennas is their data rate capabilities, which are influenced by the bandwidth available within these lower frequency bands. Limited bandwidth at low frequencies constrains data rates, making these antennas less ideal for applications demanding high-speed data transfer or substantial throughput [29]. For instance, while a 5.5 GHz antenna offering a 1 GHz bandwidth with dimensions of 25 mm x 22 mm [30] can achieve moderate data rates, these capabilities remain insufficient for the high data demands of emerging applications. The limitations in data rate potential within the low-frequency spectrum thus create a performance gap for applications that require rapid and continuous data transmission. As the need for faster and more reliable data transfer grows in fields like streaming, autonomous systems, and high-frequency trading, low-frequency antennas become increasingly limited in meeting these demands, highlighting the need to explore higher frequency solutions.

Transitioning to higher frequencies, particularly within the mmWave spectrum, offers considerable benefits in addressing the data rate limitations inherent in low-frequency antennas. Operating at higher frequencies allows for greater bandwidth, which directly supports higher data rates and more efficient data handling. The shorter wavelengths at mmWave frequencies also enable smaller, more compact antenna designs, which are easier to integrate into diverse devices without sacrificing performance. This shift in frequency, however, introduces unique challenges such as increased atmospheric attenuation and

reduced range, factors that must be carefully managed in antenna design. While low-frequency antennas remain essential for applications that require extensive coverage and robust signal penetration, the advantages of mmWave technology provide a compelling alternative for meeting the demands of high-speed, high-capacity communication [31]. The following sub-section will discuss mmWave antenna design, examining both the opportunities and challenges that arise when adapting these high-frequency antennas for advanced wireless applications.

### 2.1.2 mmWave Antenna Characteristics

Antenna designs operating in the mmWave frequency range, typically between 24 GHz and 100 GHz, are indispensable for modern communication systems due to their ability to support high data rates and extensive bandwidth [32]. This frequency range enables the development of smaller, more compact antennas, which can be seamlessly integrated into devices with limited space, such as mobile devices, vehicular systems, and wearables. Unlike low-frequency antennas, which require larger dimensions to maintain efficiency, mmWave antennas leverage shorter wavelengths to achieve compactness without compromising performance. This compact design is particularly advantageous for applications requiring rapid data transmission, precise directional control, and high-density deployments, such as smart cities and advanced transportation systems. Furthermore, mmWave antennas are well-suited for multi-antenna configurations, making them a cornerstone for advanced wireless systems that demand enhanced spectral efficiency and low-latency connectivity.

The significant size reduction achieved at mmWave frequencies provides a critical advantage for compact and high-performance systems. For instance, antennas operating at 28 GHz with a 3 GHz bandwidth can achieve dimensions as small as  $10 \text{ mm} \times 10 \text{ mm}$  [33], while designs at 32 GHz and 38 GHz typically measure approximately  $13 \text{ mm} \times 13 \text{ mm}$  and  $14.7 \text{ mm} \times 11.4 \text{ mm}$ , respectively [34, 35]. In comparison, low-frequency antennas generally require larger dimensions due to their longer wavelengths, which can make integration into space-constrained environments more challenging. This size reduction not only simplifies integration into space-constrained environments but also facilitates the deployment of phased arrays and other complex configurations. Such systems enable precise beamforming, making efficient use of available bandwidth and ensuring optimal performance in compact devices and advanced applications like autonomous vehicles and urban infrastructure.

Despite their benefits, mmWave antennas face challenges stemming from the unique propagation characteristics of higher frequencies. Shorter wavelengths, while advantageous for compact design, are more susceptible to attenuation caused by environmental factors such as buildings, trees, and atmospheric particles. This attenuation significantly impacts

the effective range and reliability of mmWave signals, especially in non-line-of-sight (NLoS) conditions and dynamic environments. To overcome these limitations, antenna designers employ innovative solutions such as adaptive beamforming, materials with low dielectric losses, and phased array configurations that dynamically steer beams toward intended targets [36]. These techniques not only mitigate signal degradation but also optimize connectivity in challenging urban scenarios, where maintaining robust links is critical.

The high data rate capabilities of mmWave antennas further underscore their importance in modern communication systems. By leveraging the wider bandwidths available at mmWave frequencies, these antennas enable applications requiring instantaneous data exchange, such as real-time industrial automation, immersive augmented reality, and intelligent transportation systems [37]. Unlike low-frequency antennas, which excel in long-range communication but are constrained by narrow bandwidths, mmWave antennas are optimized for short-range, high-capacity environments. For instance, in urban centers, mmWave antennas facilitate seamless communication between smart devices and IoT networks, enabling data-intensive tasks such as smart traffic management and real-time monitoring. Additionally, these antennas support advanced technologies like carrier aggregation, which enhances network efficiency by combining multiple frequency bands to deliver higher data throughput.

The compact design and exceptional performance of mmWave antennas have also contributed to their widespread adoption across diverse applications. In medical imaging, for instance, their high resolution and compact size enable accurate diagnostics using portable devices. In remote sensing, mmWave antennas provide precise data collection for environmental monitoring and disaster management. Moreover, in wearable technology, their small size and efficiency support continuous connectivity for health monitoring and augmented reality applications. These use cases highlight the adaptability of mmWave technology. Similarly, in 5G V2X applications, mmWave antennas enable high-speed, low-latency communication critical for autonomous driving, collision avoidance, and real-time traffic management, further underlining their indispensability in environments demanding reliable, high-performance communication systems.

### 2.1.3 Antenna Design for 5G V2X Communication Systems

As mentioned in 2.1.2, mmWave technology is a critical enabler for the high-speed, low-latency communication demands of 5G V2X communication systems. Operating primarily at 28 GHz, mmWave antennas offer a balance between bandwidth capacity and manageable propagation characteristics, making them an ideal choice for vehicular applications [38]. V2X communication encompasses interactions such as V2V, V2I, V2P, and V2N, as illustrated in Fig. 2.1. These interactions are the foundation of intelligent transportation systems, supporting real-time safety alerts, traffic optimization, and autonomous driving

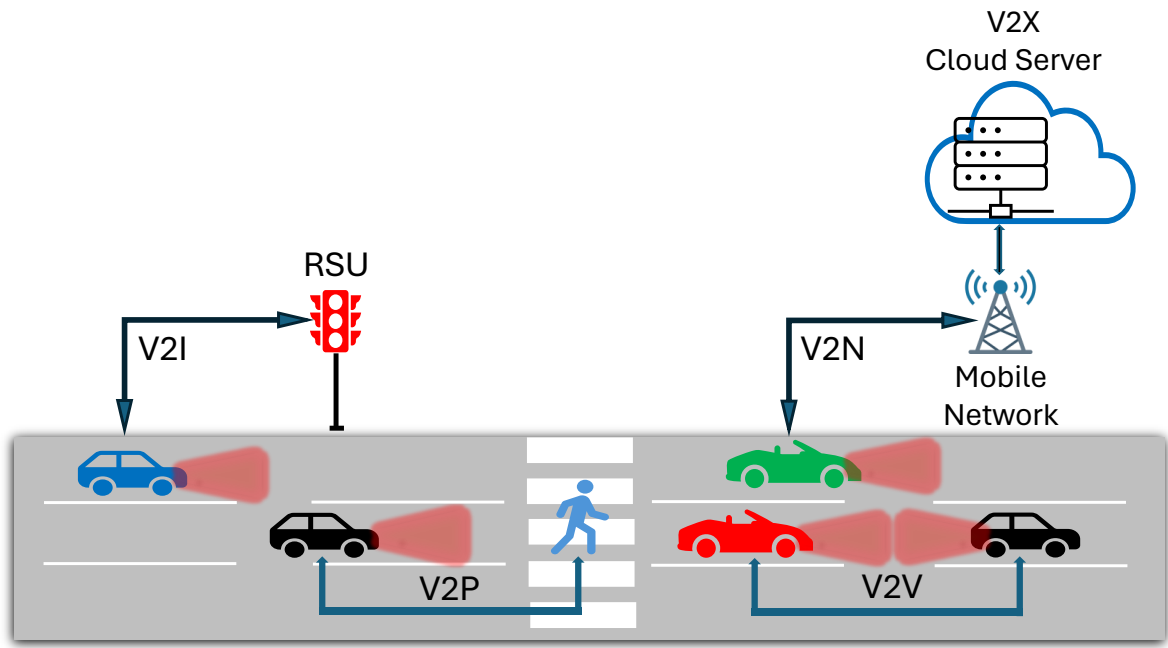


Figure 2.1: V2X communications.

technologies. However, the dynamic nature of vehicular environments presents unique challenges, including severe multipath effects caused by urban infrastructure, interference in congested areas, and the requirement for full azimuthal coverage to maintain seamless connectivity [39].

The compact size and low weight of mmWave antennas enable their integration into various vehicle components, such as side mirrors, bumpers, or rooftops, without compromising vehicle aerodynamics or aesthetics. Microstrip patch antennas (MPAs) are particularly well-suited for V2X systems due to their low cost, ease of fabrication, and compatibility with phased array configurations [40]. These designs deliver highly directional beams capable of mitigating interference and maintaining reliable communication in dynamic vehicular environments. For instance, in dense urban areas, phased arrays allow vehicles to maintain stable connections with roadside units (RSUs) and other vehicles, ensuring uninterrupted data exchange even in challenging conditions.

Wideband performance is a critical requirement for V2X antennas, as it directly impacts the ability to handle real-time, high-data-rate applications such as collision avoidance, vehicle platooning, and advanced infotainment systems [41]. In smart intersections, for example, mmWave antennas enable vehicles to exchange critical information such as traffic updates and pedestrian alerts within milliseconds, significantly enhancing road safety. The 28 GHz frequency band is particularly suited for these applications, offering the bandwidth required for seamless communication while maintaining spectral efficiency [42]. Additionally, phased array designs enhance coverage

by dynamically adapting to changing network topologies, ensuring stable performance across diverse vehicular scenarios. Moreover, cost-effective designs are essential for large-scale deployment, especially in applications requiring multiple antennas per vehicle [43]. By prioritizing compact, scalable designs that deliver high performance, mmWave antennas align with the cost and integration requirements of next-generation V2X communication systems, enabling widespread adoption of advanced communication technologies in the automotive sector.

### **Influence of Antenna Shape on Wideband Performance**

Bandwidth is a critical parameter in antenna design for V2X communication systems, as it directly determines the ability to handle high data rates and support applications like real-time collision avoidance, vehicle platooning, and advanced infotainment systems. A wider bandwidth ensures seamless data transmission, accommodating the diverse and data-intensive demands of V2X networks. However, this advantage comes with the challenge of potential interference, as wideband signals overlap with other signals in the frequency spectrum, especially in congested environments [44]. Effective management of interference is crucial to maintain robust communication links while maximizing the benefits of wideband operation. For V2X systems, achieving a balance between bandwidth and interference mitigation is essential to meet the stringent performance requirements of next-generation vehicular communication.

MPAs are widely used in V2X communication systems due to their compact size, low weight, and ease of fabrication. These antennas are inherently well-suited for automotive applications, offering low-profile designs that integrate seamlessly into limited spaces such as vehicle roofs, bumpers, or mirrors. Among MPAs, the shape of the radiating element plays a significant role in determining the achievable bandwidth. Rectangular patch antennas, for instance, are among the most common and simplest designs. However, they typically offer narrow bandwidths due to their limited ability to support multiple resonant modes [45]. This constraint arises from the confined surface currents within the rectangular geometry, which restricts the range of frequencies at which the antenna can effectively operate. On the other hand, circular patch antennas provide broader bandwidths, as their symmetrical shape supports multiple modes of resonance, allowing for more efficient current distribution. The annular ring patch antenna, with its unique geometry that distributes currents across both the inner and outer edges, achieves the widest bandwidth among these designs [46]. This capability to support multiple resonances makes the annular ring shape particularly advantageous for applications requiring seamless, high-speed communication. The distinct characteristics of these shapes are illustrated in Fig. 2.2, which compares rectangular, circular, and annular ring patch antennas.

The practical impact of these shapes on bandwidth performance can be seen through

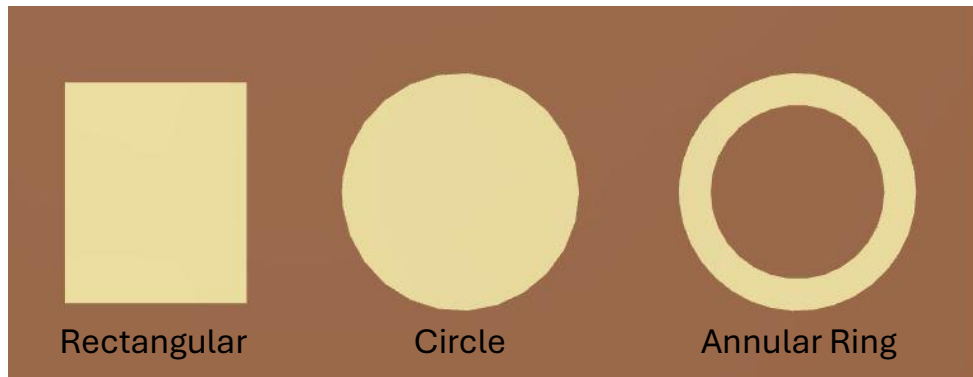


Figure 2.2: Different Antenna Shapes.

specific examples of antennas designed for 28 GHz. A rectangular patch antenna achieves a bandwidth of 0.5 GHz, reflecting its limited wideband capability [47]. A circular patch antenna demonstrates a significant improvement with a bandwidth of 2 GHz, benefiting from its symmetrical structure [48]. The annular ring patch antenna provides an impressive bandwidth of 10 GHz, showcasing its superior performance for wideband applications [49]. These designs, despite their varying bandwidths, share the advantage of simplicity, as they rely on single-layer structures. This simplicity is particularly valuable for V2X systems, where cost-effectiveness and ease of production are key considerations for large-scale deployment.

While the antenna shape is a key determinant of bandwidth, other design parameters also play a significant role in achieving optimal performance. Factors such as substrate material, dielectric constant, and feeding techniques can significantly influence the achievable bandwidth and overall efficiency of the antenna. These additional considerations highlight the intricate balance required between design simplicity and technical complexity. For 5G-enabled V2X communication systems, innovative strategies that optimize both shape and other design parameters are essential to achieving the desired wideband performance without compromising scalability or cost-effectiveness. This interplay between simplicity and complexity sets the stage for the next discussion on addressing design complexity in antenna development.

### **Influence of Design Complexity on Wideband Performance**

As mentioned in 2.1.3, achieving wideband performance can be significantly influenced by the shape of the antenna. However, antenna shape is not the sole determinant of bandwidth. Various design techniques can be employed to enhance bandwidth, often involving increased structural complexity. While these approaches are effective in achieving wideband performance, they frequently come with trade-offs such as higher fabrication costs, more intricate fabrication processes, and increased design challenges. Understanding these trade-offs is essential for determining when complex designs may be justified for

specific applications and when simpler, cost-effective solutions, such as those required in V2X communication systems, should be prioritized.

Antenna stacking is one of the widely used techniques to enhance bandwidth. For instance, a rectangular patch antenna resonating at 28 GHz typically offers a bandwidth of around 0.5 GHz in its simplest form. By introducing a stacked patch configuration, the bandwidth can be significantly improved to approximately 3 GHz, as demonstrated in [50]. This enhancement is achieved by adding multiple layers to the antenna structure, which enables additional resonance modes, thereby broadening the bandwidth. However, the resulting design involves up to five stacked layers, significantly increasing the complexity of fabrication and the associated costs. This makes the technique less favorable for cost-sensitive applications such as V2X, where scalability and affordability are critical considerations.

Another technique involves cavity-backed antenna designs, which leverage enclosed metallic cavities to enhance bandwidth. A conventional rectangular patch antenna offering a 0.7 GHz bandwidth can be redesigned with a cavity-backed structure to achieve up to 4 GHz, as reported in [51]. The cavity creates an additional path for resonance, improving the antenna's overall performance. However, this design requires multiple layers and intricate vias, which further complicate the fabrication process and increase material costs. While the enhanced bandwidth is advantageous for applications requiring robust performance, the added complexity may limit its practical deployment in scenarios like vehicular communication systems, where simplicity and cost-effectiveness are paramount.

Slot-loading techniques also demonstrate the potential to achieve wideband performance by modifying the surface current distribution. For example, a circular patch antenna with a simple design typically achieves a bandwidth of around 1 GHz. By incorporating five carefully designed slots into the patch, the bandwidth can be expanded to 4 GHz, as illustrated in [52]. The slots introduce multiple resonance paths, thereby broadening the frequency range. However, the increased use of metallic materials and the precise fabrication requirements make this approach more expensive and technically demanding, potentially reducing its scalability for mass production in V2X systems.

While these advanced techniques illustrate how structural complexity can achieve wideband performance, they also highlight the trade-offs involved. Techniques such as stacking, cavity-backed structures, and slot-loading often lead to increased design intricacies and higher fabrication costs. These challenges must be carefully considered, especially in applications like V2X, where affordability, scalability, and ease of integration are as important as achieving high performance. Importantly, V2X communication systems demand antennas with simple structures that provide wideband performance to balance the need for high efficiency with cost-effective scalability. This balance is critical to ensuring that the antennas meet the stringent requirements of next-generation vehicular

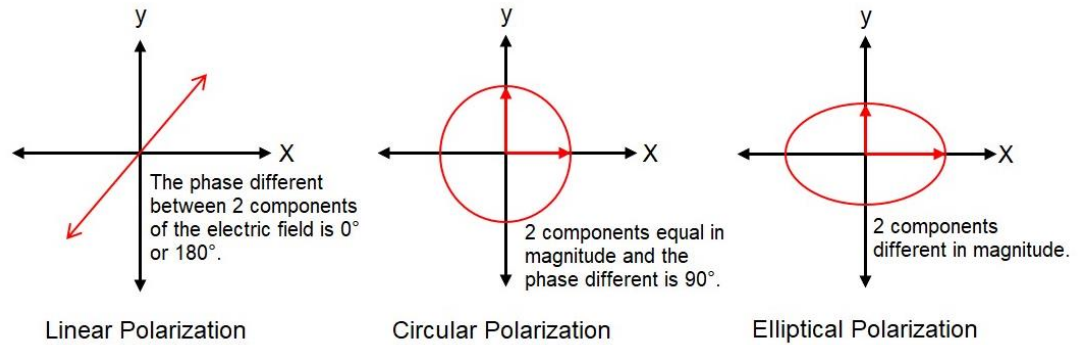


Figure 2.3: Polarization types.

networks while remaining practical for widespread adoption.

## 2.2 Antenna Polarization Characteristics

Polarization is a key characteristic of electromagnetic waves that significantly influences antenna performance, especially in high-frequency and dynamic environments. It defines the orientation of the electric field vector as the wave propagates, and proper polarization alignment between transmitting and receiving antennas is essential for minimizing power loss and maximizing signal integrity [53]. In advanced wireless systems such as 5G, where high data rates and robust connectivity are expected under varying conditions, polarization plays a crucial role in link reliability and interference mitigation. The importance of polarization characteristics has been emphasized in standardization efforts for 5G mmWave systems, such as those outlined by 3GPP, due to their impact on system interoperability and performance consistency across diverse vehicular scenarios [54].

There are three main types of polarization in antennas: linear, circular, and elliptical [55]. Linearly polarized antennas radiate electromagnetic waves with a constant electric field orientation, while circularly polarized antennas generate a rotating electric field that traces a circular path. These two are most commonly used in practical applications, whereas elliptical polarization, although theoretically useful, is rarely adopted due to its design complexity and narrow applicability. Figure 2.3 illustrates the fundamental polarization types, serving as a visual reference for their geometric characteristics.

In the context of V2X communication systems, polarization directly affects link robustness, especially in the presence of mobility, reflections, and multipath propagation. LP and CP antennas are the most relevant for V2X applications due to their respective advantages [56]. LP antennas are generally more efficient in line-of-sight (LoS) conditions, such as highway scenarios, due to their simplicity and low loss under stable alignment. In contrast, CP antennas offer improved resilience in non-line-of-sight (NLoS) and urban environments by mitigating polarization mismatch and reflection-induced degradation.

Selecting the appropriate polarization type based on the operating environment is therefore critical to achieving reliable and efficient V2X communication.

### 2.2.1 Linearly Polarized

LP antennas remain a dominant choice in high-frequency antenna systems due to their straightforward design, ease of integration, and reliable performance under proper alignment. These characteristics are particularly valuable in vehicular environments, where compact and low-cost solutions are essential for deployment on car rooftops, mirrors, or infrastructure nodes. The structural simplicity of LP antennas also supports scalable fabrication and integration into phased arrays, making them a practical choice for 5G V2X systems operating in the mmWave band.

In V2X communication scenarios where line-of-sight (LoS) conditions are generally maintained, such as highway-based V2V, V2I, and V2P communication, LP antennas are especially advantageous. These applications benefit from predictable antenna alignment and minimal multipath, enabling LP antennas to deliver high signal integrity with minimal polarization mismatch. However, as V2X systems operate at 28 GHz and beyond, one of the most pressing physical-layer requirements is wide impedance bandwidth, which ensures robust high-data-rate communication across dynamic channels [57].

Several LP antenna designs in the literature have been proposed at or near the 28 GHz band, offering a spectrum of performance trade-offs. For instance, the design in [58] achieves a broad impedance bandwidth from 25.2 to 32.8 GHz, fulfilling the bandwidth demand for mmWave V2X communication. However, this wideband response comes at the cost of a complex structure that includes multiple slots, metal enhancements, and vias, increasing fabrication difficulty and potential signal losses. In contrast, the design presented in [59] offers a simpler, more compact structure using a Rogers RT 5880 substrate, a material well-suited for mmWave applications [60], but achieves a narrower bandwidth from 27.1 to 29.2 GHz. While its structural simplicity is beneficial, the limited bandwidth may constrain performance in future 5G-V2X systems, particularly if channel shifting is required. Similarly, the antenna proposed in [61] covers the 25.5 to 29.5 GHz band with moderate complexity, incorporating slots and vias to enhance performance. Despite its wideband claim, the upper frequency edge lies just above 28 GHz, which may restrict flexibility in real-world deployments where frequency shifts for channel isolation or coexistence are necessary.

However, LP antennas face challenges in dynamic environments where severe multipath effects and polarization mismatches caused by signal reflections are prevalent. For instance, in dense urban areas, signals reflected from buildings and other structures can degrade the performance of LP antennas. These limitations necessitate the use of alternative polarization strategies, such as circular polarization, to complement LP antennas in more

complex V2X scenarios [62]. Nonetheless, the simplicity, low cost, and efficiency of LP antennas ensure their continued relevance in addressing the evolving demands of vehicular communication systems.

### 2.2.2 Circularly Polarized

CP antennas radiate electromagnetic waves whose electric field vector rotates in a helical manner as the wave propagates. This rotation can be either right-hand circular polarization (RHCP) or left-hand circular polarization (LHCP), depending on the direction of rotation relative to wave propagation. Ensuring proper polarization matching between transmitter and receiver, i.e., RHCP to RHCP or LHCP to LHCP, is essential in maintaining link quality, as mismatched polarization states naturally reject each other and can reduce co-channel interference [63]. In the context of vehicular communication systems, CP antennas are particularly valuable for addressing dynamic and multipath-prone environments. Their ability to mitigate polarization mismatch, maintain signal consistency under varying orientations, and reduce the effects of reflections makes them well-suited for V2X applications [64], especially in dense urban settings and high-mobility conditions [65].

To achieve circular polarization, various antenna design techniques have been established in the literature. One common approach is to introduce small perturbations to the radiating structure, such as notches or slots, to excite two orthogonal modes with a  $90^\circ$  phase difference [66]. Another technique involves introducing angular air gaps within loop-like structures to support traveling-wave behavior and induce phase progression [67]. Stub loading is also widely used, where carefully placed linear stubs generate desired current distributions that support circular polarization [68]. Other methods include truncating patch corners [69] or leveraging structural asymmetry [70] to control the phase and amplitude of orthogonal modes. While these techniques are effective, each comes with trade-offs in terms of structural complexity, design sensitivity, and integration feasibility in compact vehicular systems.

Recent works have explored these CP techniques in the mmWave band near 28 GHz, aiming to balance axial ratio bandwidth, impedance bandwidth, and physical complexity. For instance, the CP antenna in [71] offers a compact structure resonating at 28 GHz, achieving an impedance bandwidth from 27.5 to 28.5 GHz and an axial ratio bandwidth from 27.8 to 28.2 GHz. While the design benefits from low complexity, its narrow bandwidth limits adaptability in V2X systems, where frequency agility and channel isolation are critical. In contrast, the design presented in [72] achieves a significantly broader bandwidth, covering from 26 to 33 GHz for both impedance and AR bandwidth. However, this performance comes at the cost of a highly complex multilayered structure with intricate slot arrangements, which may increase fabrication difficulty, cost, and

integration constraints for vehicular deployment. These contrasting examples reflect a broader design challenge, CP antennas must provide robust polarization purity and wide bandwidth while remaining mechanically simple and suitable for high-mobility platforms such as vehicles.

A critical parameter in evaluating CP antennas is the AR, which quantifies polarization purity [73]. The AR measures the ratio of the major to the minor axis of the polarization ellipse, with a value of 3 dB or less indicating effective CP. Achieving a low AR ensures robust communication, while a wide AR bandwidth allows consistent CP performance across a broad frequency range. This capability is especially important in V2X systems, where maintaining reliable polarization performance under varying conditions is crucial for applications like real-time traffic management, cooperative driving, and long-range communication links. The significance of AR in defining CP performance will be explored further in the following sub-subsection.

### Axial Ratio

The AR is a fundamental parameter that defines the quality of CP in antennas. It represents the ratio of the magnitudes of the electric field components along the major and minor axes of the polarization ellipse and is commonly expressed in decibels (dB). The AR provides a quantitative measure of how closely the polarization of an antenna approximates ideal CP, where the magnitudes of the electric field components are equal, and their phases differ by exactly 90°. Circular polarization with a low AR ensures that the antenna radiates or receives energy with minimal polarization distortion, making it highly desirable in scenarios with varying signal orientations. In practical terms, the AR can be calculated using the equation [74]

$$AR_{\text{dB}} = 20 \log_{10} \left( \frac{E_{\text{max}}}{E_{\text{min}}} \right), \quad (2.1)$$

where  $E_{\text{max}}$  is the maximum electric field intensity in the major axis direction of the antenna's radiation pattern. It corresponds to the direction of the maximum radiation.  $E_{\text{min}}$  is the minimum electric field intensity in the minor axis direction of the radiation pattern. This equation quantifies the evaluation of antenna polarization by analyzing the AR to determine how effectively the antenna maintains the polarization of transmitted or received signals [75]. An AR value of 1 (or 0 dB) indicates perfect circular polarization, while an AR below 3 dB signifies effective CP operation. Conversely, when the AR exceeds 3 dB, the polarization shifts to elliptical or linear. By ensuring an AR below 3 dB, the antenna achieves robust CP, minimizing polarization mismatches and enhancing communication reliability.

Circular polarization in patch antennas at mmWave frequencies is often achieved

through innovative design techniques. These include integrating multiple radiating elements with precise phase and amplitude control or implementing dual-polarized patch arrays with feeding networks that introduce a  $90^\circ$  phase difference between orthogonal elements. Such configurations ensure that the antenna generates CP radiation with high quality, as characterized by a low AR. These approaches enable antennas to maintain consistent polarization across various operational conditions, which is essential for dynamic communication environments.

The AR bandwidth, defined as the frequency range over which the AR remains below 3 dB, is a critical factor in evaluating CP antenna performance. A wide AR bandwidth allows the antenna to sustain circular polarization across a broader frequency range, accommodating variations in operational conditions and supporting seamless communication. This feature is particularly crucial in V2X communication systems, where maintaining consistent polarization performance over a wide frequency range enhances resilience to multipath effects caused by signal reflections from buildings, vehicles, and other structures.

In the context of V2X applications, achieving a low AR across a wide frequency range directly impacts the reliability of key functionalities such as collision avoidance, cooperative driving, and vehicle-to-infrastructure communication. By maintaining consistent circular polarization, CP antennas reduce signal degradation and polarization mismatches, ensuring efficient energy transfer between transmitting and receiving antennas. This capability is particularly valuable in dynamic vehicular scenarios, where maintaining stable communication links under varying orientations and environmental conditions is crucial. The concept and significance of AR, along with its role in defining circular polarization, make it a cornerstone for advancing CP antenna design in next-generation V2X networks.

## 2.3 Antenna Array

In the mmWave frequency range, enhancing antenna gain is essential for overcoming the inherent challenges associated with high-frequency signal propagation, such as increased atmospheric attenuation and limited range [76]. A higher antenna gain enables more focused energy transmission and reception, improving signal strength and reducing susceptibility to interference [77]. Various techniques can be employed to increase antenna gain, including the use of reflectors, lenses, and metamaterial designs. However, the most widely adopted and effective method is the creation of antenna arrays, where multiple radiating elements are combined to achieve higher overall gain [78]. This approach offers a balance between design complexity and performance improvement, making it particularly suited to advanced communication systems operating in the mmWave band.

The concept of an antenna array involves combining multiple radiating elements, which work together to achieve a collective gain much higher than that of a single element. Each additional element contributes to the overall directivity and gain of the array, although the extent of improvement depends on factors such as the array configuration, spacing between elements, and operating frequency [79]. For instance, a single-element antenna with a gain of approximately 6.7 dBi can achieve a gain of 12 dBi when arranged in a 2 x 2 array, as demonstrated in [80]. Similarly, a single element with a gain of 4.5 dBi in [81] achieves 11.5 dBi with a four-element array, illustrating a significant improvement. In [82], a single antenna element offering 7 dBi gain was transformed into an array with four elements, achieving a gain of 13.8 dBi. This study also explored a 16 x 16 array configuration, which reached a remarkable 28 dBi gain, demonstrating how large-scale arrays can produce high directivity. The relationship between the number of elements and the resulting gain follows a logarithmic trend, where each additional element contributes less incrementally to the overall gain as the array size increases. For small arrays, such as 2 x 2 configurations, the gain improvement per element can be substantial, often exceeding 1 dBi per element, as seen in the examples provided. However, in larger arrays like the 16 x 16 configuration, the per-element contribution to gain diminishes due to factors such as mutual coupling, impedance mismatches, and array efficiency losses [83]. Additionally, the spacing between elements plays a critical role in determining the overall gain, with optimal spacing minimizing destructive interference and enhancing constructive wave addition [84]. These insights highlight that while increasing the number of elements remains a fundamental approach to achieving higher gain, the efficiency of this approach depends on careful array design and optimization.

For 5G V2X communication systems, the increased gain offered by antenna arrays provides critical advantages in addressing the unique challenges of vehicular communication. High-gain arrays enable focused radiating, which enhances signal strength and extends coverage, ensuring reliable connectivity even in dynamic environments with dense obstacles [85]. The ability to achieve high directivity mitigates signal attenuation caused by atmospheric absorption and minimizes interference from neighboring signals, both of which are prevalent in the mmWave band. Additionally, enhanced gain improves the system's energy efficiency, reducing the power required for transmission and allowing for longer operational lifespans in battery-powered devices or vehicles [86]. These benefits are particularly valuable for key 5G V2X applications, such as collision avoidance, cooperative driving, and vehicle-to-infrastructure communication, where reliable, high-speed data exchange is paramount. By leveraging antenna arrays, 5G V2X systems can achieve the high-performance metrics necessary for next-generation intelligent transportation networks, ensuring robust and efficient communication in even the most challenging vehicular environments.

### 2.3.1 Feeding Techniques for Antenna Arrays

Antenna arrays are essential for enhancing gain, improving directional control, and enabling advanced beamforming, particularly in high-performance systems such as mmWave communication and 5G V2X applications. A critical component of array design is the feeding structure, which distributes power to the individual elements while ensuring proper impedance matching, typically  $50 \Omega$  per element. Among the most widely used feeding techniques are parallel and series-fed structures, each offering unique advantages and challenges in terms of design complexity, physical size, and performance [87]. The choice of feeding structure directly influences the array's overall efficiency, scalability, and ease of fabrication, making it a key consideration in the design process.

Parallel feeding structures deliver equal power to each antenna element through individual transmission lines, enabling precise control over power distribution and phase alignment across the array [88]. This approach ensures consistent excitation, making it ideal for applications requiring high precision. However, parallel-fed structures are inherently complex due to their multiple feedlines and intricate network designs. This complexity often translates to larger physical dimensions and increased fabrication challenges, especially in high-frequency mmWave systems where precision is critical. In contrast, series-fed structures simplify the feeding network by connecting elements sequentially along a single feedline. This design reduces the number of feedlines, significantly minimizing the physical footprint and simplifying the fabrication process. These structural differences highlight the trade-offs between the two techniques, particularly in balancing performance, size, and complexity. The practical implications of these feeding techniques are evident in comparative designs. A parallel-fed array resonating at 28 GHz demonstrates a gain of 11.4 dBi with a feeding network that spans a bulky 44.1 x 42.6 mm, emphasizing its larger size and complexity [89]. On the other hand, a series-fed array operating at the same frequency achieves the same gain but features a more compact size of 41.2 x 17.2 mm, with a streamlined feeding network [90]. Fig. 2.4 illustrates examples of parallel and series-fed configurations, highlighting the fundamental differences in structure and simplicity. The series-fed structure's simplicity and reduced dimensions make it an attractive choice for applications with stringent space and integration constraints, particularly in mmWave systems where compact designs are essential for efficient operation.

The compact and streamlined design of series-fed arrays makes them particularly advantageous for V2X communication systems, which require antennas that combine high performance with simplicity and cost-effectiveness [91]. These designs are well-suited for vehicular applications, where space constraints and integration challenges demand compact solutions. Furthermore, series-fed arrays can employ advanced tapering techniques, such as Dolph-Chebyshev weighting, to achieve low sidelobe levels [92]. For

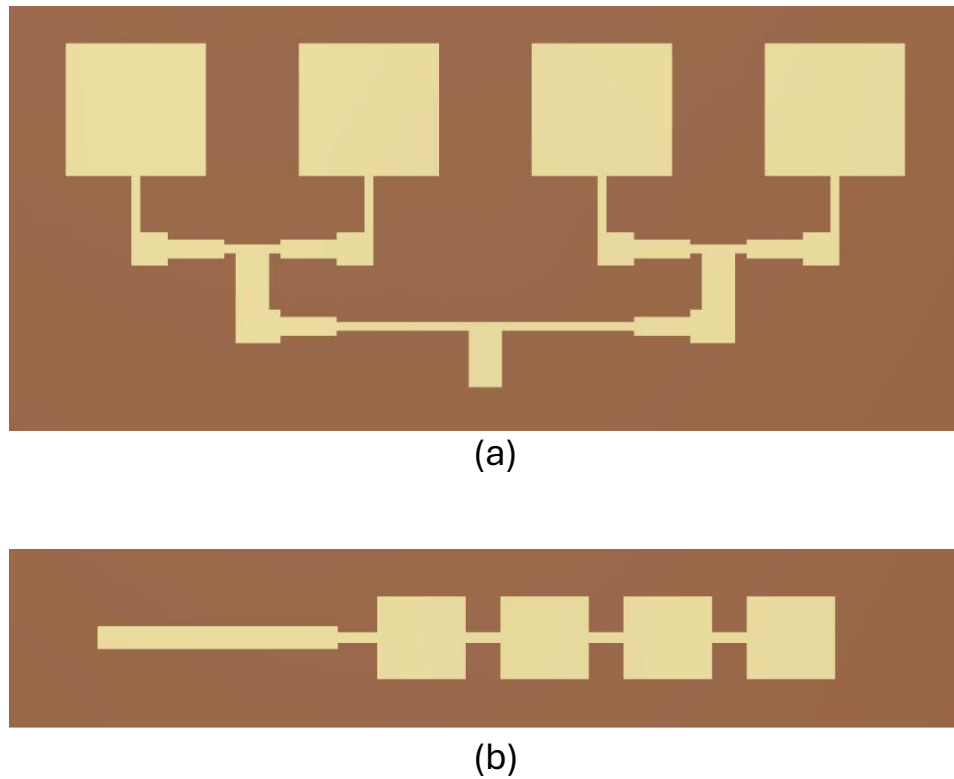


Figure 2.4: Array feeding structures (a) parallel structure (b) series-fed structure.

example, a 9-element series-fed array with symmetrical dimensions can reduce sidelobes while maintaining high gain, minimizing interference and enhancing signal clarity. This ability to balance performance with simplicity makes series-fed arrays an ideal choice for 5G V2X systems, supporting reliable and efficient communication in high-density and dynamic environments.

## 2.4 Phased Array Beamsteering

Phased array antennas play a critical role in modern communication systems by enabling precise control over beam direction without relying on mechanical movement. This electronically steerable capability is particularly valuable in dynamic environments such as V2X, where vehicles operate under fast-changing conditions and maintaining reliable, directional connectivity is essential [93]. Beamsteering supports more efficient spectrum utilization, stronger signal focus, and reduced interference, factors that are key to robust and responsive V2X links.

Traditional phased array designs generally fall into two categories: fully digital and hybrid configurations. Fully digital arrays offer high precision by assigning independent phase and amplitude control to each element, but this results in substantial hardware complexity, cost, and power consumption [94]. Hybrid arrays, which combine analog and

digital techniques, offer a compromise in terms of flexibility and efficiency, yet still demand intricate feeding networks and sophisticated signal processing [95]. These architectures, while powerful, are often impractical for vehicular applications due to their integration and cost challenges.

A more practical alternative for 5G V2X systems is the use of simplified phased array configurations based on series-fed structures. These designs reduce fabrication complexity and minimize the number of required components by grouping elements into sub-arrays, each driven by a single port. Beamsteering is achieved by introducing predefined phase shifts at each port, enabling fixed-angle directional coverage with low overhead. This approach offers an efficient balance between performance, simplicity, and scalability, attributes that align well with the constraints of vehicular platforms and the demands of real-time communication in high-mobility environments.

### 2.4.1 Fundamentals of Phased Array Beamsteering

Phased array beamsteering is a technique used to electronically direct the main lobe of an antenna array's radiation pattern by applying phase shifts to the excitation signals of individual elements. This capability is especially critical in mmWave and V2X communication systems, where narrow beams are needed to overcome high atmospheric losses and maintain reliable links between fast-moving or dynamically positioned nodes [96], [97].

A variety of techniques have been explored in the literature to implement beamsteering in phased arrays. One common approach involves applying a uniform phase progression across the array to steer the beam toward a desired direction, as demonstrated in [98], where varactor-loaded elements were used to dynamically tune phase shifts. The linear arrays offer simple, narrow-beam control in one dimension, while 2D planar arrays enable more flexible beam steering in both azimuth and elevation, as shown in a metamaterial-based design in [99]. Feeding techniques also significantly impact complexity and performance. In [100], a series-fed phased array was employed to simplify the network and achieve beamsteering with reduced loss and footprint. Conversely, the design in [101] used a parallel-fed structure with independent control for each element, providing fine steering resolution but requiring a complex and bulky feeding system.

Designing phased arrays for V2X environments introduces specific constraints that influence trade-offs between complexity, beam performance, and integration. High gain and narrow beamwidth are required to overcome mmWave propagation loss, but achieving these with fully adaptive systems is often cost-prohibitive and unsuitable for vehicular platforms. Additionally, V2X systems require fast response to environmental changes, making simpler beamsteering architectures more attractive for real-time operation [102]. Mutual coupling, grating lobes, and limited physical space on vehicles further constrain

element spacing and array scalability. Therefore, beamsteering solutions targeting V2X must strike a balance between directional control, physical compactness, and ease of fabrication.

To address these challenges, simplified phased array designs with low complexity and fixed-angle beamsteering offer a practical solution. Configurations based on a small number of ports and predefined phase shifts, such as the 4-port series-fed array, reduce hardware demands while enabling directional coverage suitable for V2X scenarios. These approaches align well with vehicular requirements for integration, scalability, and cost-efficiency, making them a compelling choice for next-generation 5G V2X systems. The methodology for calculating steering angles in such configurations is further detailed in the following subsection.

### 2.4.2 Beamsteering Angle Calculation for 4-Port Phased Arrays

Phased arrays enable beamsteering by applying progressive phase shifts to antenna elements, allowing the main radiation beam to be steered electronically without any mechanical movement. In V2X communication systems, where vehicles operate in unpredictable, multipath-rich environments, this directional control becomes essential for maintaining robust links and minimizing interference [103]. The 4-port phased array architecture offers a practical beamsteering solution that simplifies hardware complexity by dividing the antenna into four independently driven subarrays, each typically constructed using a series-fed design [104]. This configuration enables compact and low-cost implementation while retaining effective angular coverage, traits well-aligned with the demands of 5G-enabled vehicular platforms.

Beamsteering in a phased array relies on the principle of electronically controlling the phase of signals fed to each antenna element. Constructive interference of radiated signals determines the direction of the main beam, while destructive interference suppresses unwanted radiation in other directions [105]. The steering angle  $\theta_s$  is influenced by the relative phase shifts  $\Delta\phi$  introduced between adjacent elements. For a phased array operating at a wavelength  $\lambda$  and with element spacing  $d$ , the required phase shift is calculated as [106]

$$\Delta\phi = \frac{2\pi d}{\lambda} \sin(\theta_s), \quad (2.2)$$

where  $d$  is the distance between adjacent elements, typically set at half the wavelength ( $d=\lambda/2$ ) to avoid grating lobes,  $\lambda$  is the wavelength corresponding to the operating frequency, and  $\theta_s$  is the desired steering angle. Within each subarray of the 4-port phased array, the phase for the  $n$ -th element is determined by [107]

$$\phi_n = (n - 1)\Delta\phi, \quad (2.3)$$

where  $n$  is the index of the element (e.g.,  $n = 1, 2, 3, \dots$ ). This equation ensures that each element contributes the appropriate phase shift to steer the beam collectively toward the desired angle. By controlling the phase shifts applied at each port, the overall radiation pattern of the array can be dynamically steered, providing flexibility to adapt to changing communication requirements.

While the mathematical foundation is well-established, translating it into practical mmWave designs presents a balance between performance and fabrication. The literature demonstrates a clear trade-off between steering range and design complexity. For instance, the phased array in [108] achieves  $\pm 35^\circ$  beamsteering at 28 GHz but employs a five-layer structure with embedded vias, making it bulky and costly for vehicular integration. In contrast, the two-layer design in [109] achieves a simpler and more compact structure with beamsteering limited to  $\pm 23^\circ$ . This contrast reflects a common theme in mmWave phased arrays, wide steering angles often require architectural complexity, while simplicity tends to limit directional flexibility.

Addressing this trade-off remains a central challenge for V2X antenna design. Arrays must deliver sufficient angular coverage to handle dynamic link scenarios, such as overtaking, intersection crossing, and variable traffic patterns, without introducing excess hardware overhead. Simplified multi-port configurations, like the 4-port phased array, represent a promising solution by offering fixed-angle beamsteering through controlled excitation at the subarray level. These designs eliminate the need for high-resolution phase shifters and complex feeding networks, helping strike a meaningful balance between performance, cost, and integration feasibility. As research advances, identifying architectures that maintain this balance while adapting to vehicular mobility will continue to be a priority in the development of practical phased array solutions for 5G V2X systems.

## 2.5 Summary

This chapter presented a literature-driven review of antenna design approaches relevant to 5G V2X communication systems, focusing on the key requirements of wide impedance bandwidth, polarization stability, gain enhancement, and compact structure. It began by comparing various antenna shapes and structures reported in the literature in terms of bandwidth and implementation complexity. The polarization characteristics of linearly and circularly polarized antennas were examined, highlighting their operational suitability across different V2X scenarios and reviewing published techniques for generating circular polarization. The axial ratio was also discussed as a key metric for evaluating CP performance. The chapter then evaluated antenna array configurations, with a

comparative analysis of parallel and series-fed techniques, emphasizing their trade-offs in size and complexity. Finally, the state of the art in phased array beamsteering was reviewed, and recent works were critically analysed to illustrate the design trade-offs between angular coverage and fabrication complexity. These insights establish a strong foundation for the technical contributions presented in the upcoming chapters.

# Chapter 3

## Linearly Polarized Antennas Design

In this chapter, the focus is placed on the design and development of a single-element LP patch antenna, optimized to achieve a wide impedance bandwidth and low profile, which are critical requirements for 5G V2X applications. Additionally, this chapter presents the design of a series-fed 9-element antenna array, which enhances the gain and performance of the single element. The primary objective, aligned with *O2*, is to achieve a wide impedance bandwidth to support reliable and efficient communication in 5G networks. Through careful design considerations, this work ensures that both the single element and the series-fed array meet the demanding specifications of 5G V2X technology, providing a robust platform for uninterrupted vehicular communications. The chapter further elaborates on the design methodology, simulation results, and the steps taken to achieve the desired impedance bandwidth and high gain, positioning these antennas as key elements in advancing future V2X systems.

### 3.1 Introduction

Vehicle-to-everything communications represent a promising technology for future transportation systems, enabling advanced applications in areas such as road safety, passenger infotainment, automaker services, and vehicle optimization [110]. V2X facilitates various forms of communication, including V2V, V2I, V2P, and V2N, integrating these interactions seamlessly within the transportation network. V2X operates within two frequency ranges: the FR1 spans 410 MHz to 7.125 GHz, while the FR2 covers 24.25 GHz to 52.6 GHz [111]. The 28 GHz mmWave band, in particular, has garnered significant attention due to its ability to support high data rates, enhanced reliability, and reduced power consumption [112]. These capabilities are vital for high-level safety applications in V2X, such as minimizing road accidents, where ultra-reliable communication and ultra-low latency are essential.

Furthermore, the broad use of sensors in V2X communications necessitates antenna

designs with wide impedance bandwidth [113]. Achieving this requires antennas that are cost-effective, simple in structure, and miniaturized, meeting the stringent demands of V2X communications [114], [115]. MPAs emerge as excellent candidates due to their compact size, lightweight construction, low cost, and ease of fabrication [116].

However, the mmWave band suffers from significant propagation loss, which affects the reliability of communication links [117]. This challenge underscores the need for antennas with wide impedance bandwidth and high gain. Numerous approaches have been proposed in the literature to enhance the bandwidth of LP single-element patch antennas operating in the mmWave band, such as aperture-coupled patches [118], [119], stacked patches [120], [121], strip-coupled dual patches [122], folded slotted patches [123], and metamaterial-based low-profile antennas [124], [125]. However, these solutions often come with high fabrication costs and complex designs.

MPAs are particularly suited to improve gain and counteract atmospheric attenuation in the mmWave band. While waveguide designs offer higher efficiency, microstrip arrays can suffer from dielectric and conductor losses, which are influenced by the substrate material and design dimensions, including the antenna's overall size [12]. To mitigate some of these challenges and optimize performance, the choice of feeding technique plays a critical role. Feeding techniques, such as series and parallel feeds, directly influence the array's compactness, simplicity, and SLLs. Parallel feeding, though widely used in array designs, tends to result in bulky structures with higher losses. Series-fed arrays, on the other hand, are favored for their compact design, simpler feed networks, and lower SLLs, which are crucial for minimizing interference and enhancing signal quality in wireless communication and sensor applications [126], [127].

## 3.2 Contributions

This chapter makes several key contributions to the field of 5G V2X communications, addressing critical challenges related to bandwidth and gain, which directly help to mitigate the effects of atmospheric attenuation. The focus is on the design and development of novel and efficient antenna solutions that are both technically advanced and practical for real-world vehicular communication systems. By introducing innovative yet simplified structures, these contributions not only address the high costs and complexity associated with current antenna designs but also demonstrate how the proposed solutions meet the rigorous demands of next-generation vehicular communication networks. Through a combination of design, optimization, and validation, the proposed antennas achieve significant improvements over existing solutions. The key contributions of this chapter are:

- Design of a novel LP annular ring patch antenna operating at 28 GHz with a wide

impedance bandwidth of 35.71% and a radiation efficiency exceeding 90%, ensuring reliable, high-performance communication in future V2X applications.

- Development of a 9-element series-fed antenna array with a low SLLs exceeding -17 dB and a realized gain of 16.6 dBi, demonstrating that high realized gain can be achieved with a compact design.
- Demonstration of significant performance improvements in bandwidth, gain, and SLLs, validated through fabrication and measurement, providing a consistent and practical solution to mitigate atmospheric attenuation and other challenges specific to future V2X communications.

The organization of this chapter is as follows: Several case studies are conducted to develop a simple antenna structure characterized by wide impedance bandwidth, as required for 5G V2X applications. First, a rectangular patch antenna operating at 28 GHz is designed. Next, the antenna's shape is modified to an annular ring patch, which offers an improved impedance bandwidth. Finally, to mitigate atmospheric attenuation, the annular ring patch antenna is developed into a 9-element series-fed patch antenna array.

### 3.3 Rectangular Patch Antenna

This section provides a detailed description of the design process for a rectangular patch antenna, along with the evolution of its simulation, gain, and radiation pattern results.

#### 3.3.1 Antenna Configuration

The rectangular patch antenna is designed and simulated using CST Studio 2019. The design consists of a patch antenna operating at 28 GHz, connected via a transmission line. The patch serves as the radiator, with three slots placed adjacent to the radiator to control the resonant frequency at the desired 28 GHz. These slots increase the effective current path length, allowing the antenna to resonate at a lower frequency, which enables fine-tuning to the target 28 GHz band. Additionally, two small square elements are positioned at the bottom of the patch to enhance antenna radiation. The patch antenna is placed on a Rogers TC600 substrate, which has a dielectric constant of 6.15 and a thickness of 0.16 mm. The substrate is located above the ground plane. The dimensions of the radiator patch are optimized, with a length ( $L_{RA}$ ) of 3.99 mm and a width ( $W_{RA}$ ) of 2 mm. The slots are further optimized, with lengths of 0.15 mm and widths of 2 mm. Fig. 3.1 illustrates the proposed antenna layout in CST, and the key design parameters are summarized in Table 3.1.

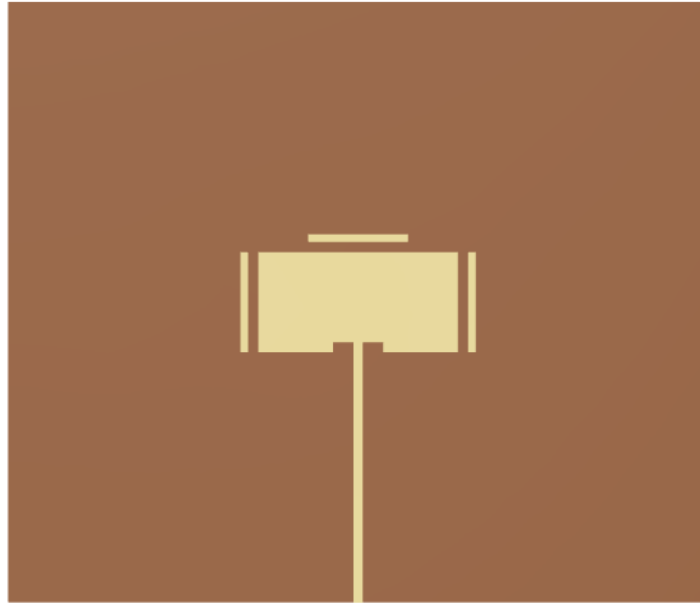


Figure 3.1: Geometry of the proposed rectangular patch antenna.

Table 3.1: Rectangular Patch Antenna Design Parameters

| Parameter                                | Value (mm) |
|--|------------|
| Length of the ground plane and substrate | 14         |
| Width of the ground plane and substrate  | 12         |
| Length of the patch                      | 3.99       |
| Width of the patch                       | 2          |
| Length of the slot                       | 0.15       |
| Width of the slot                        | 2          |
| Thickness of substrate                   | 0.16       |
| Width of the feed                        | 0.18       |

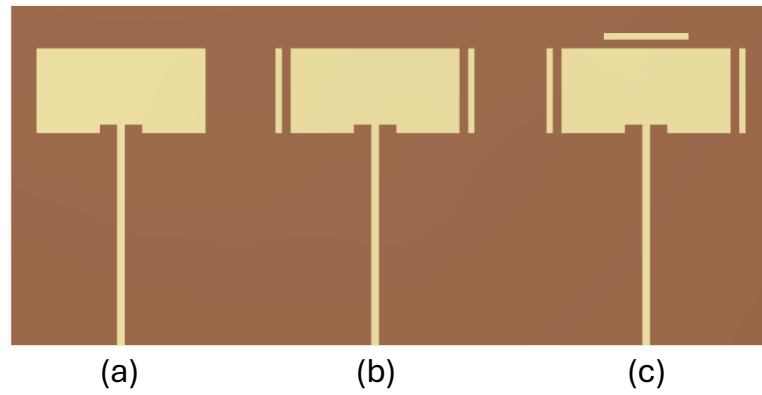


Figure 3.2: Evolution of the proposed rectangular patch antenna.

### 3.3.2 Simulated Optimization of the Antenna Design

The proposed rectangular patch antenna is designed to resonate at 28 GHz and undergoes development through three stages, as depicted in Fig. 3.2. The corresponding reflection coefficients ( $S_{11}$ ) are presented in Fig. 3.3. The initial objective is to achieve resonance at 28 GHz while also aiming for a wide impedance bandwidth. The first iteration begins with a rectangular patch antenna featuring two small squares at the bottom, as shown in Fig. 3.2 (a). This design resonates at 28.2 GHz and offers a bandwidth of approximately 0.4 GHz. In the second iteration, two slots are introduced on the left and right of the radiator to fine-tune the resonance to 28 GHz and potentially expand the bandwidth, as shown in Fig. 3.2 (b). This adjustment shifts the resonance to 27.9 GHz, though the bandwidth remains unchanged at 0.4 GHz. Finally, in the third iteration, depicted in Fig. 3.2 (c), an additional slot is added at the top of the radiator. This modification successfully tunes the resonance to 28 GHz and expands the bandwidth to 0.5 GHz.

The realized gain of the proposed antenna, as shown in Fig. 3.4, is 6.04 dBi, which compares favorably with single-element antennas in the open literature. The simulated radiation efficiency is 91%, indicating minimal losses within the structure. Furthermore, Fig. 3.5 presents the radiation pattern in both the E and H planes for the proposed antenna.

While the proposed rectangular patch antenna design demonstrates a simple structure, it offers a relatively narrow impedance bandwidth, which limits its suitability for the targeted future V2X applications. This limitation highlights the need for further design modifications, leading to the development of a more advanced antenna structure, which will be discussed in the following section.

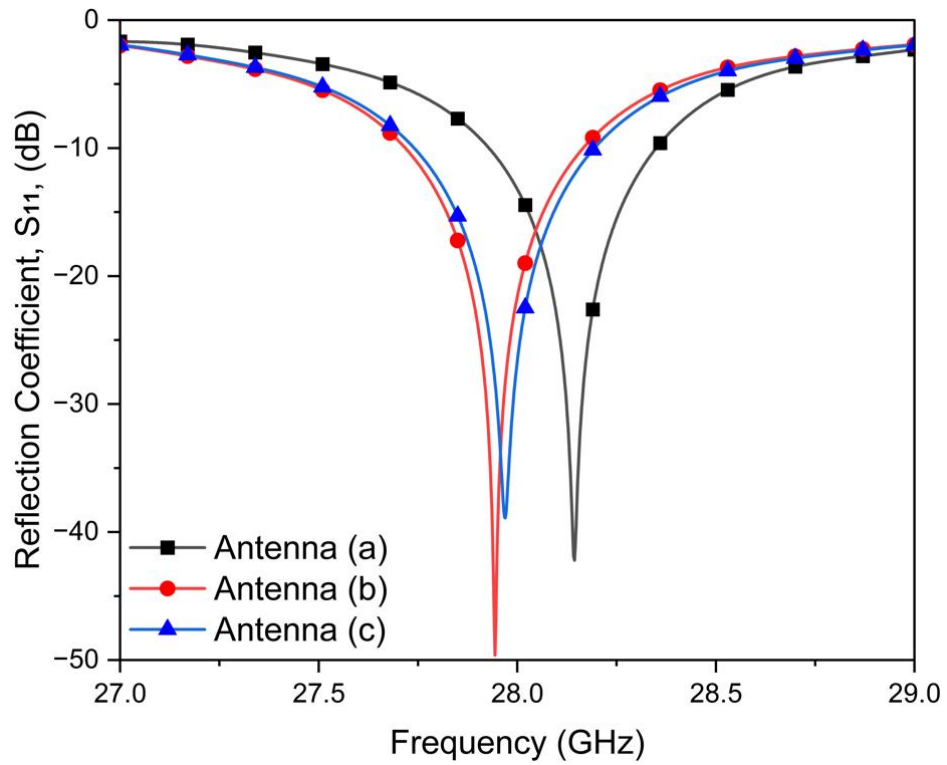


Figure 3.3: Evolution of simulated reflection coefficients during the design process.

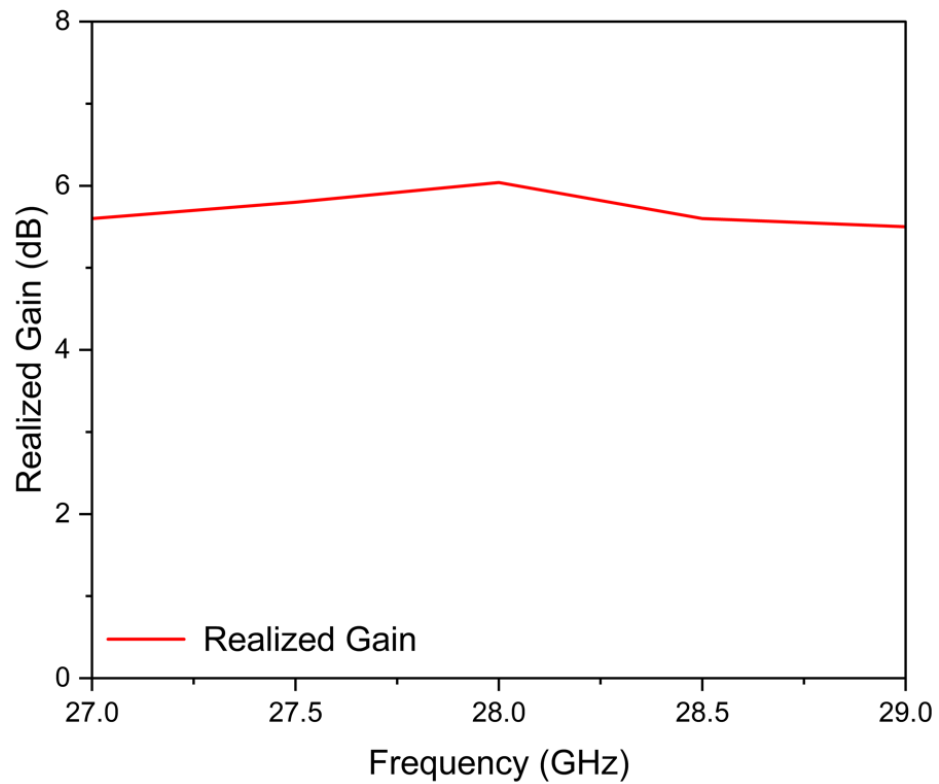


Figure 3.4: Simulated realized gain of the proposed rectangular patch antenna.

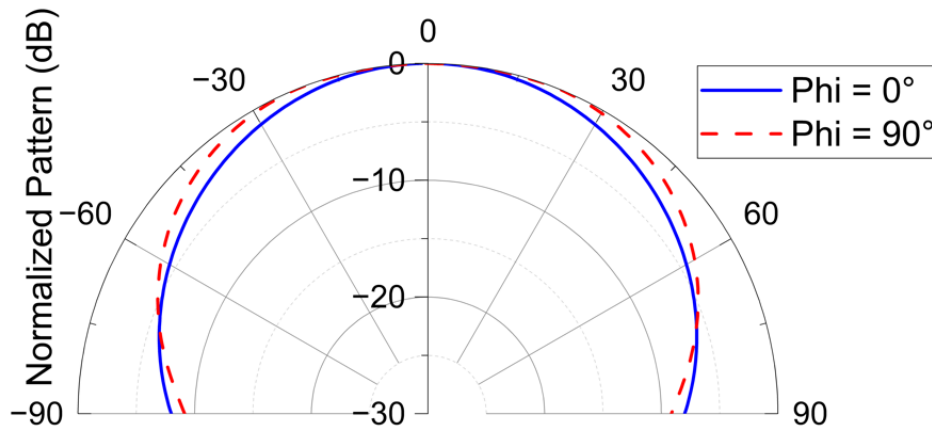


Figure 3.5: Simulated radiation pattern of the proposed rectangular patch antenna in the E-plane ( $\phi = 0^\circ$ ) and H-plane ( $\phi = 90^\circ$ ).

### 3.4 Annular Ring Patch Antenna

Given the bandwidth limitations of the rectangular patch antenna, a design modification is necessary to meet the wide impedance bandwidth requirements of future V2X applications. To overcome the mentioned limitation, the shape of the antenna is changed to an annular ring patch. The annular ring patch antenna is known for its ability to offer a wider impedance bandwidth due to the presence of multiple resonant modes, resulting from its circular geometry [128]. The increased flexibility in controlling resonant frequencies allows the annular ring patch to achieve enhanced bandwidth performance, making it a suitable candidate for high-frequency applications like 5G V2X. The design procedures for the linearly polarized annular ring patch antenna are presented and analyzed in this section.

#### 3.4.1 Antenna Configuration and Analysis

The design and simulation of the antenna are conducted using CST studio 2023, focusing on an annular ring patch antenna that resonates at 28 GHz, with the radius referred to as  $R_1$  in Fig. 3.6. This antenna is fabricated on a Rogers RT-duroid 5880 substrate, notable for its dielectric constant of 2.2 and a thickness of 0.787 mm. The substrate's dimensions, marked as  $L$  and  $W$ , are precisely set at 20 mm and 14.5 mm, respectively. A coplanar waveguide port (CWP) is employed to feed the antenna, which is excited by a single coaxial feed. To match a  $50 \Omega$  reference impedance, the optimal widths of the feed and its separation from the grounded pads are determined to be 0.23 mm and 0.18 mm, respectively. Furthermore, an inner annular ring, its radius identified as  $R_2$  in Fig. 3.6, is strategically added without direct electrical connection, enhancing the bandwidth without significantly increasing the antenna's size or complexity [129]. The radiator is fabricated onto the substrate, which is positioned above the ground plane, having a thickness of

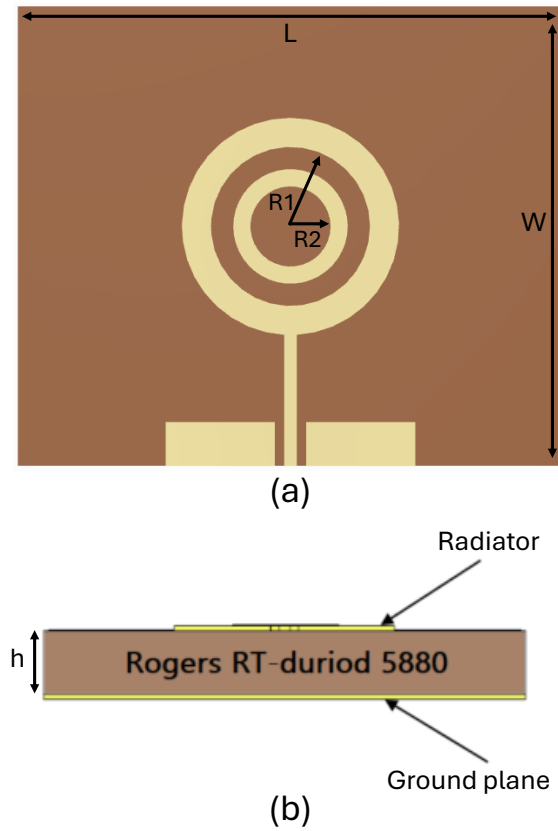


Figure 3.6: Structure of the annular ring patch antenna (a) top view (b) side view.

0.035 mm. The parameters defining the annular ring patch antenna are determined as follows [130]

$$f_{r_{\text{mm}}} = \frac{\chi_{\text{nm}} c}{2\pi a \sqrt{\epsilon_r}} \quad (3.1)$$

and

$$\frac{b - a}{b + a} < 0.35, \quad (3.2)$$

where  $f_{r_{\text{mm}}}$  is the resonant frequency,  $\chi_{\text{nm}}$  is the first-order Bessel function [131],  $c$  is the speed of light, and  $a$  and  $b$  represent the annular ring's outer and inner radii, respectively. Details of the design parameters are listed in Table 3.2.

### 3.4.2 Evolution of the Antenna Design

The development of the proposed antenna is structured into three stages, each designed to progressively enhance performance, as depicted in Fig. 3.7. The corresponding reflection coefficients are presented in Fig. 3.8. Initially, the objective is to achieve a wide impedance bandwidth starting from the lower limit of the FR2 band at 24 GHz. The first iteration began with a simple circular patch antenna, shown in Fig. 3.7 (a), which achieved a limited bandwidth ranging from 25.2 to 28.7 GHz. To expand this bandwidth, the second

Table 3.2: Annular Ring Patch Antenna Design Parameters

| Parameter  | Value (mm) |
|--|------------|
| Length of the substrate and ground plane (L)           | 20         |
| Width of the substrate and ground plane (W)            | 14.5       |
| Outer loop radius ( $R_1$ )                            | 1.74       |
| Inner loop radius ( $R_2$ )                            | 1.2        |
| Transmission line width                                | 0.23       |
| Pads length  | 1.64       |
| Pads width   | 0.84       |
| The distance between the pad and the transmission line | 0.18       |
| Thickness of substrate (h)                             | 0.787      |

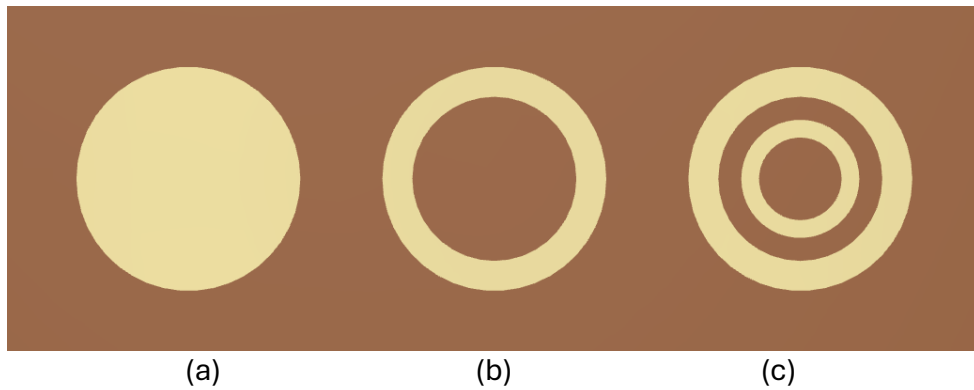


Figure 3.7: Evolution of the proposed annular ring patch antenna.

iteration introduced an annular ring configuration, illustrated in Fig. 3.7 (b), extending the impedance bandwidth from 27.2 to 30.7 GHz. In the third iteration, an inner annular ring was added, as depicted in Fig. 3.7 (c). This ring was designed without direct electrical connections to the main patch, maintaining simplicity in the antenna structure. This strategic modification significantly broadened the impedance bandwidth to cover 35.71% (24 to 34 GHz), achieving an  $S_{11}$  below -30 dB. These enhancements demonstrate the potential of our antenna design to support a wide range of mmWave applications, particularly for V2X communications, by effectively optimizing the antenna's bandwidth.

### 3.4.3 Experimental Validation and Discussion

The proposed LP patch antenna is fabricated utilizing PCB (printed circuit board) technology and is subsequently measured to confirm the accuracy of simulation results. The annular ring antenna design is optimized using the CST software and fabricated on a Rogers RT-duroid 5880 substrate with overall dimensions of 20 mm x 14.5 mm x 0.787 mm. Measurements are performed using a mmWave vector network analyzer and a 50  $\Omega$  coaxial cable to measure the reflection coefficient. For connection to the CPW feeding structure, a 2.4 mm SMA connector is utilized. In Fig. 3.9, the measurement chamber and

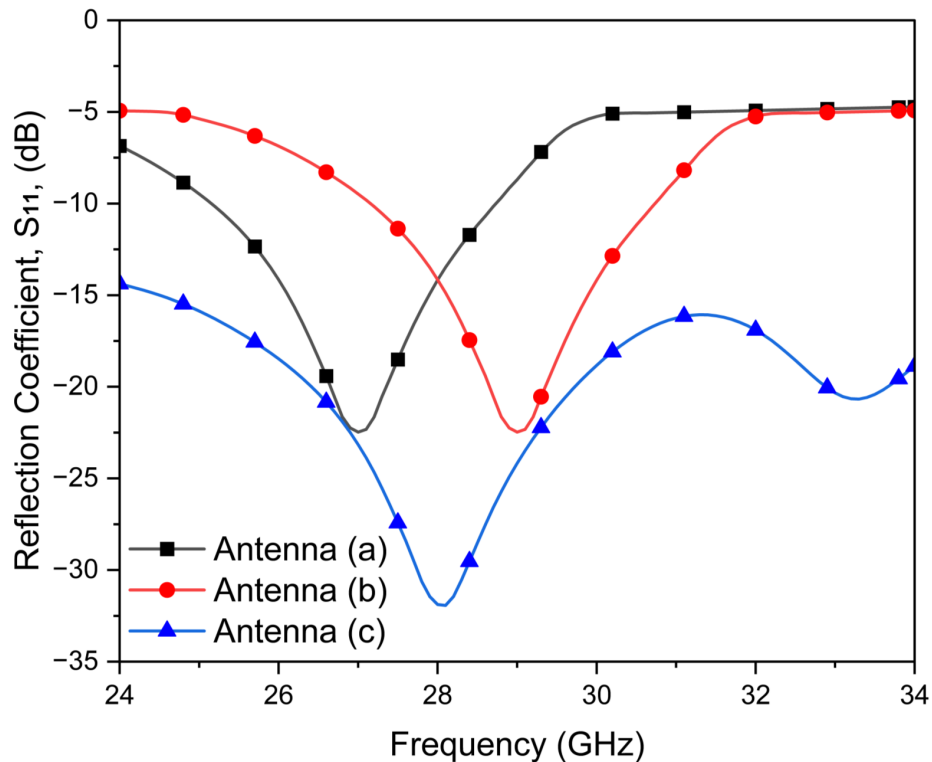


Figure 3.8: Simulated reflection coefficients in the process of evolution.

a prototype of the proposed antenna are presented. The gain and radiation pattern are measured using the far-field mmWave measurement system (R & S AT800B, Compact Antenna Test Range (CATR) benchtop Over-The-Air (OTA) system). An OTA antenna measurement setup is arranged in an open area within an indoor lab to measure the far-field radiation pattern and gain, as illustrated in Fig. 3.9. A standard gain antenna serves as the transmitter (Tx), while the proposed antenna, under test (AUT/Rx antenna), is positioned on a 360° rotator/turntable. This turntable, connected to a PI motor controller, enables automated rotation controlled by LabVIEW software, achieving a precise angular resolution of 1° per step. In the measurement system setup, a reflector is placed between the transmitter (Tx) and the receiver (Rx), as illustrated in Fig. 3.9, with the distances from the Tx to the reflector and from the reflector to the Rx being 75 cm and 120 cm, respectively. Expanding this gap maintains the similarity in the normalized radiation patterns, although the received power or the transmission coefficient ( $S_{21}$ ) level decreases following the Friis transmission equation due to path loss, which increases as the square of the distance between the Tx and Rx antennas, formulated as [132]

$$\text{Path loss} = 20 \times \log(4\pi d/\lambda). \quad (3.3)$$

The gain of the proposed antenna is evaluated through a relative gain comparison method, where measurements are conducted towards the direction of maximum power,

and  $S_{21}$  is recorded on a Vector Network Analyzer (VNA). For these evaluations,  $S_{21}$  is initially measured using two identical antennas; subsequently, one is substituted with the proposed antenna. The gain of the proposed antenna, expressed in dB, is determined using the equation [133]

$$G_{\text{AUT}(dB)} = G_{\text{ref}(dB)} + S_{21\text{AUT}(dB)} - S_{21\text{ref}(dB)}, \quad (3.4)$$

where  $G_{\text{AUT}}$  represents the proposed antenna's gain and  $G_{\text{ref}}$  denotes the gain of a standard antenna at a particular frequency.

The simulated and measured  $S_{11}$  for the proposed antenna, as illustrated in Fig. 3.10, confirm its excellent performance across a wide impedance bandwidth from 24 to 34 GHz, equivalent to 35.71% of the frequency spectrum. The close correlation between the measured and simulated  $S_{11}$  validates the precision of the antenna design and simulation approach. Furthermore, the measured peak value of  $S_{11}$  of approximately -30 dB highlights the antenna's high efficiency in radiating and receiving electromagnetic signals within the frequency range. Such robust performance underscores the antenna's potential for applications demanding high-frequency operation and extensive bandwidth, notably in 5G V2X communications, where reliable and efficient signal transmission is paramount.

Fig. 3.11 illustrates the radiation efficiency alongside the realized gain, both simulated and measured. The antenna achieves a peak realized gain of 5.5 dBi at 28 GHz, with a demonstrated efficiency of 94%.

The radiation pattern of the proposed LP annular ring patch antenna at 28 GHz is depicted in Fig. 3.12, utilizing a far-field mmWave measurement system to characterize the antenna's performance in both the E-plane and H-plane at angles  $0^\circ$  and  $90^\circ$ , respectively. The broadside radiation patterns, both simulated and measured, of the antenna are illustrated in the figure. The antenna demonstrates an exceptionally narrow beamwidth, suitable for future V2X applications. The consistency observed between the simulated and measured results affirms the antenna's operational effectiveness.

Table 3.3 provides a comparison of the proposed design against other related works in the state of the art, with a specific focus on implementation complexity and cost. It is worth to highlight that, although the literature on mmWave band antennas is extensive, with many designs aiming for wide impedance bandwidth, they often resort to complex structures to achieve this goal. In contrast, the proposed design not only attains a wide impedance bandwidth but does so with a notably simpler structure. This distinction underscores the innovative aspect of the design, potentially contributing to reduced production costs and ease of fabrication without compromising performance.

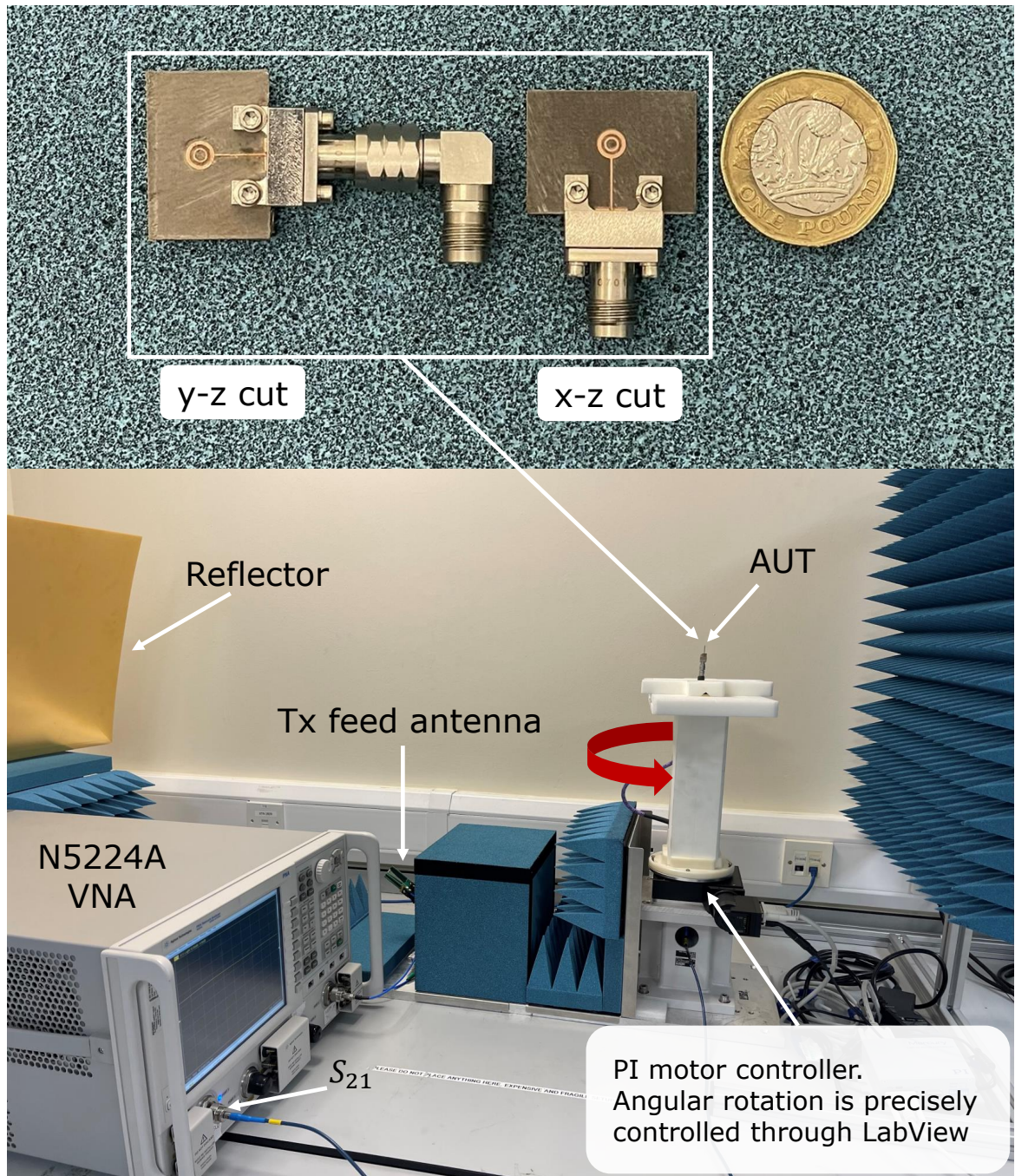


Figure 3.9: Measurement system and the LP annular ring antenna prototype.

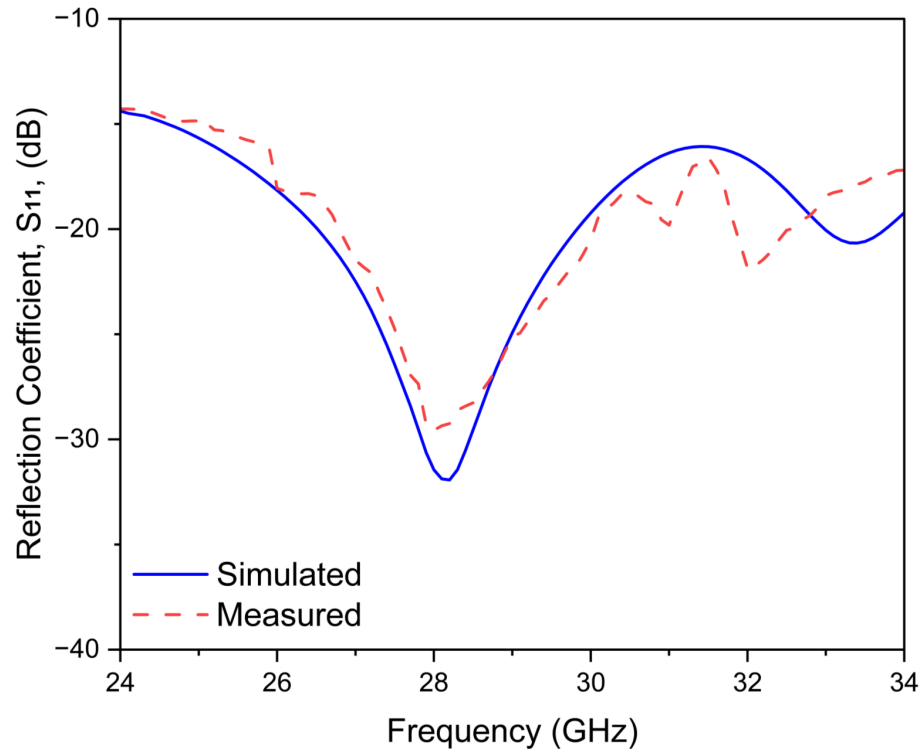


Figure 3.10: Reflection coefficient of the simulated and measured proposed LP annular ring antenna.

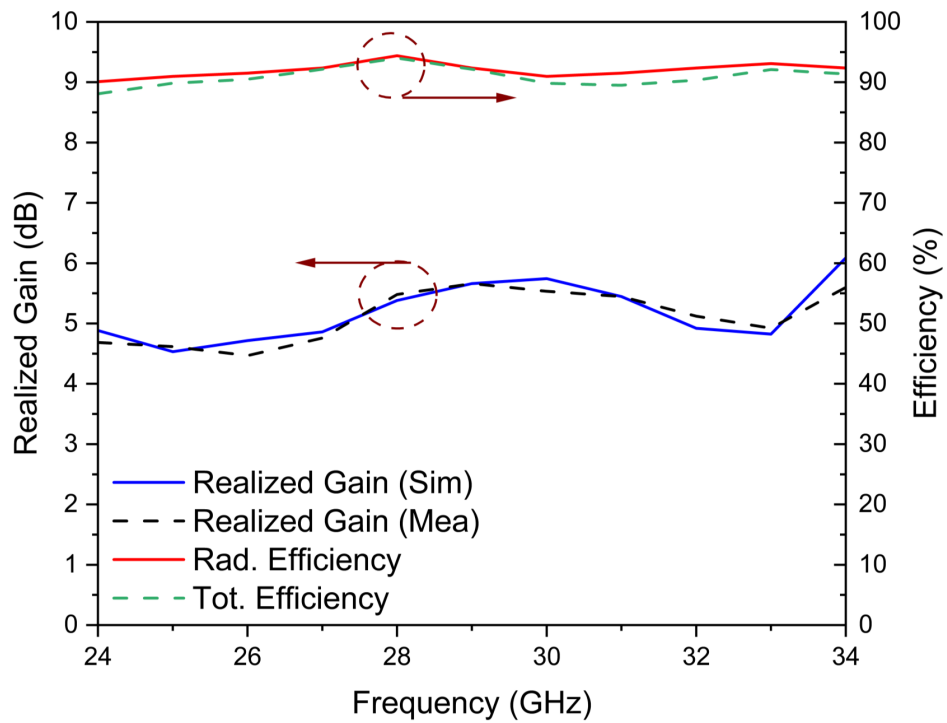


Figure 3.11: Simulated and measured gain and efficiency for the proposed LP antenna.

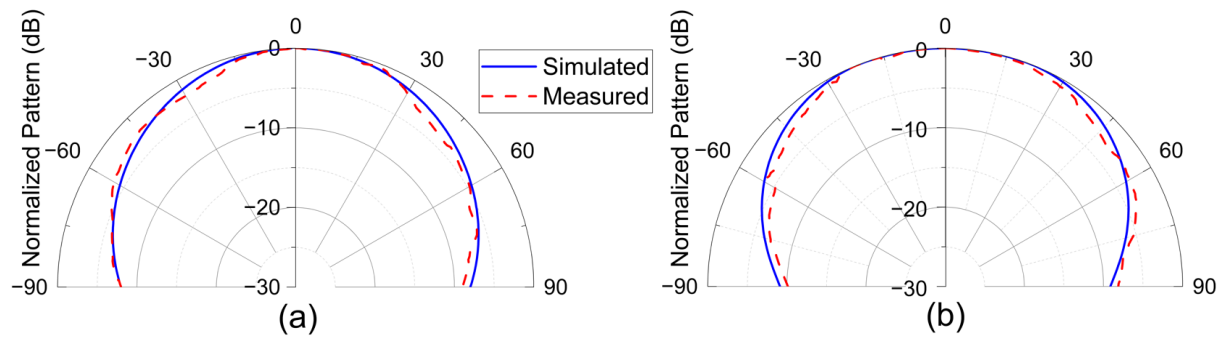


Figure 3.12: Simulated and measured radiation pattern of the proposed LP annular ring antenna (a)  $\phi = 0^\circ$  and (b)  $\phi = 90^\circ$ .

Table 3.3: Comparison of the proposed LP design with other similar works.

| Ref.       | Freq (GHz) | layers | Volume ( $mm^3$ ) | Effi. % | IBW%  | Polarization |
|------------|------------|--------|-------------------|---------|-------|--------------|
| [8]        | 28         | 3      | 263.8             | 89      | 10    | LP           |
| [119]      | 28         | 1      | 409.7             | 85      | 26.9  | LP           |
| [121]      | 27         | 3      | 381.2             | N/A     | 18.5  | LP           |
| [122]      | 25.3       | 2      | 321.2             | N/A     | 20.6  | LP           |
| [125]      | 28         | 3      | 219.8             | 70      | 27.1  | LP           |
| Prop. work | 28         | 1      | 228.23            | 94      | 35.71 | LP           |

## 3.5 Annular Ring Patch Antenna Array

The proposed single-element annular ring patch antenna successfully provides the wide impedance bandwidth required for 5G V2X applications. However, to further enhance the antenna's performance, particularly in overcoming the atmospheric attenuation that mmWave frequencies experience, it is necessary to increase the antenna's gain. To achieve this, the single element is developed into a 9-element series-fed array. This array configuration not only improves gain but also maintains the wide impedance bandwidth achieved with the single element, making the antenna suitable for long-range, high-performance communication in future V2X environments. The following presents the design steps for the series-fed LP patch antenna array, with a focus on its development, simulation, and experimental results.

### 3.5.1 Design and Analysis of the Antenna Array

The design of a series-fed LP patch antenna array has been developed from the single element proposed in section 3.4.1. The design and simulation of the array are carried out using CST Microwave Studio 2023. The antenna is fabricated on a Rogers RT-duroid 5880 substrate, chosen for its dielectric constant of 2.2 and thickness of 0.787 mm. The

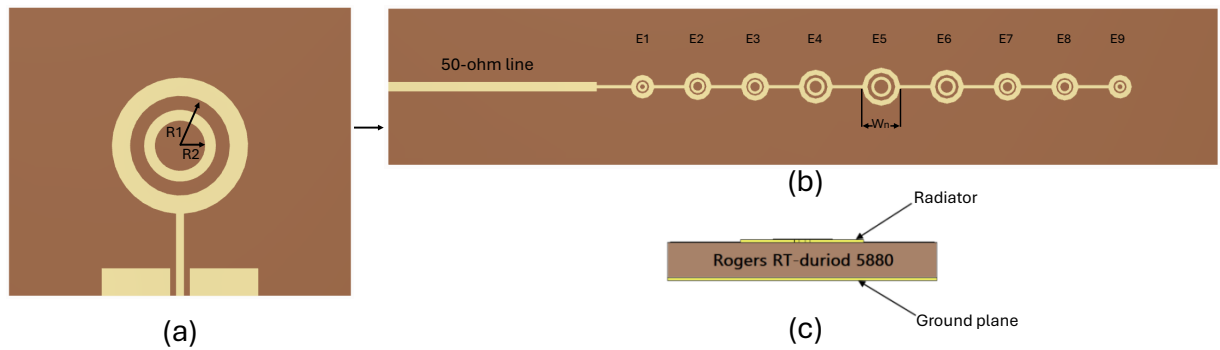


Figure 3.13: Structure of the proposed antenna array (a) single-element top view (b) array top view (c) side view.

foundational configuration of the series-fed array being analyzed in this study is depicted in Fig. 3.13 (b). This design consists of a 9-element array, arranged symmetrically around the central element (e.g., element 1 mirrors element 9, element 2 mirrors element 8, etc.). The design process commences with the central element, identified as element 5, whose dimensions correspond to those shown in Fig. 3.13 (a). Subsequent to this, the widths of the remaining array patches are calculated using an aperture scaling method aimed at achieving the desired SLLs. The Dolph-Chebyshev weighting technique is employed to optimize the trade-off between beamwidth and SLLs. The element weights derived from the Dolph-Chebyshev method are presented in Table 3.4 [134]. To implement this tapering, each element's weight,  $D_n$ , is multiplied by the width of the central element to determine the dimensions of the other patches. This results in a series of elements with varying widths,  $W_n$ , as shown in Fig. 3.13 (b). The elements are spaced at half-wavelength intervals [135], requiring precise inter-element feed connectivity to maintain an input impedance of  $50 \Omega$  for each patch. The application of the Dolph-Chebyshev weighting to the array's design not only standardizes the input impedance across all elements but also optimizes the array's performance in terms of SLLs and beamwidth. This approach ensures that the series-fed patch antenna array meets the stringent requirements of 5G V2X applications, providing both precision and reliability. In addition, the widths of the inter-element feedlines are varied to maintain impedance matching along the series path, taking into account the differences in patch size introduced by the tapering. While the length of each segment remains at half-wavelength to preserve phase coherence, the feedline widths were optimized in the simulation to ensure efficient power transfer. The resulting feedline dimensions used in the array design are listed in Table 3.5.

### 3.5.2 Simulation Analysis

The series-fed patch antenna array design is developed based on the single-element configuration shown in Fig. 3.13. During the development of the series-fed array, particular

Table 3.4: The Dolph-Chebyshev approach for 9-element array weights.

| Element 1,<br>Element 9 | Element 2,<br>Element 8 | Element 3,<br>Element 7 | Element 4,<br>Element 6 | Element 5 |
|-------------------------|-------------------------|-------------------------|-------------------------|-----------|
| 0.601                   | 0.615                   | 0.812                   | 0.950                   | 1.0       |

Table 3.5: Optimized feedline widths between adjacent elements.

| Feed       | 1 to 2<br>8 to 9 | 2 to 3<br>7 to 8 | 3 to 4<br>6 to 7 | 4 to 5<br>5 to 6 |
|------------|------------------|------------------|------------------|------------------|
| Width (mm) | 0.32             | 0.36             | 0.33             | 0.38             |

focus is placed on ensuring that the simulated  $S_{11}$  achieves a wide impedance bandwidth, which is essential for supporting a broad range of mmWave applications, including 5G V2X communications. The  $S_{11}$  simulation results for both the single-element and series-fed array designs are presented in Fig. 3.14, demonstrating a broad impedance bandwidth of 35.17% (24 to 34 GHz).

The series-fed antenna array is also analyzed with the primary objective of increasing the gain obtained from the single element. For mmWave frequencies, high gain is crucial to mitigating atmospheric attenuation. A proven method to enhance gain in antenna arrays is by increasing the number of elements [136]. The proposed design progresses through two stages, as shown in Fig. 3.15, with the corresponding realized gain depicted in Fig. 3.16. A 9-element series-fed LP patch antenna array is selected for its ability to achieve a high realized gain. As seen in Fig. 3.16, the 9-element design attains a realized gain of 16.6 dBi at 28 GHz, while the 7-element design achieves a realized gain of 14.5 dBi. Notably, the inter-element feeds and the design approach remain consistent in both configurations. Furthermore, the surface current distribution at 28 GHz is illustrated in Fig. 3.17, highlighting the current flow along the proposed series-fed antenna array.

### 3.5.3 Measurement Results and Discussion

To validate the design, the series-fed LP patch antenna array is fabricated, and measurements are conducted to compare with the simulation results. The antenna is fabricated on a Rogers RT-duroid 5880 substrate, which has a dielectric constant of 2.2 and a thickness of 0.787 mm. The  $S_{11}$  of the proposed series-fed LP patch antenna array is measured using a mmWave vector network analyzer. The results, as illustrated in Fig. 3.18, confirm that the measured  $S_{11}$  achieves the desired wide impedance bandwidth, meeting the design's objectives. A strong agreement between the simulated and measured results further validates the accuracy of the simulation.

The series-fed antenna array is also evaluated with the goal of increasing the gain. However, achieving a high realized gain must be balanced with maintaining low SLLs

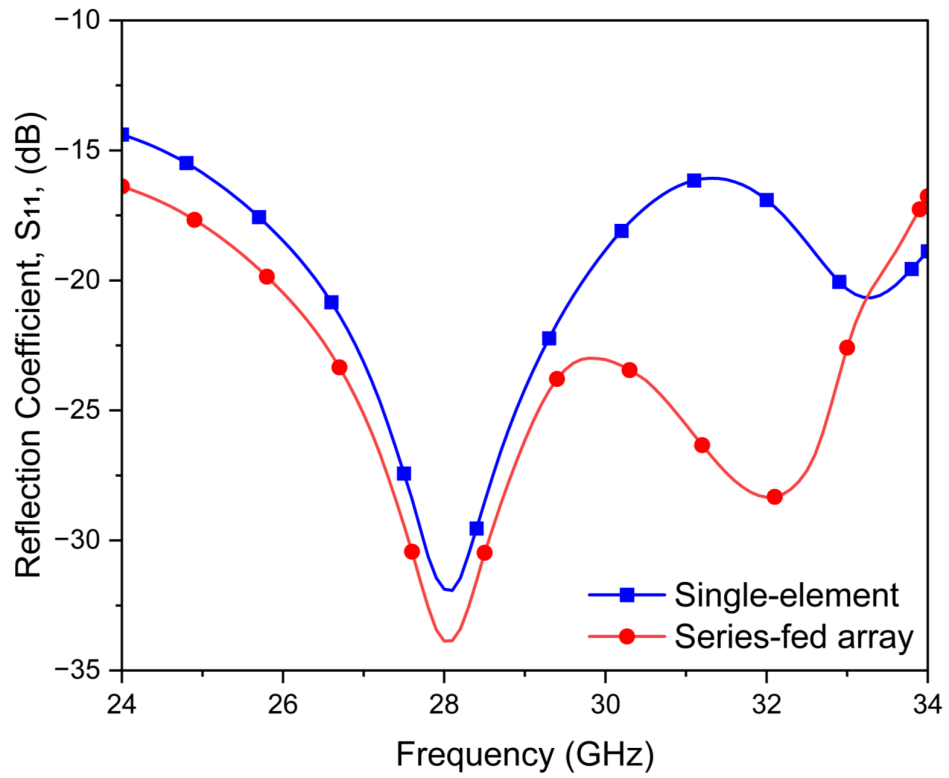


Figure 3.14: Reflection coefficient of the simulated proposed LP antenna array.

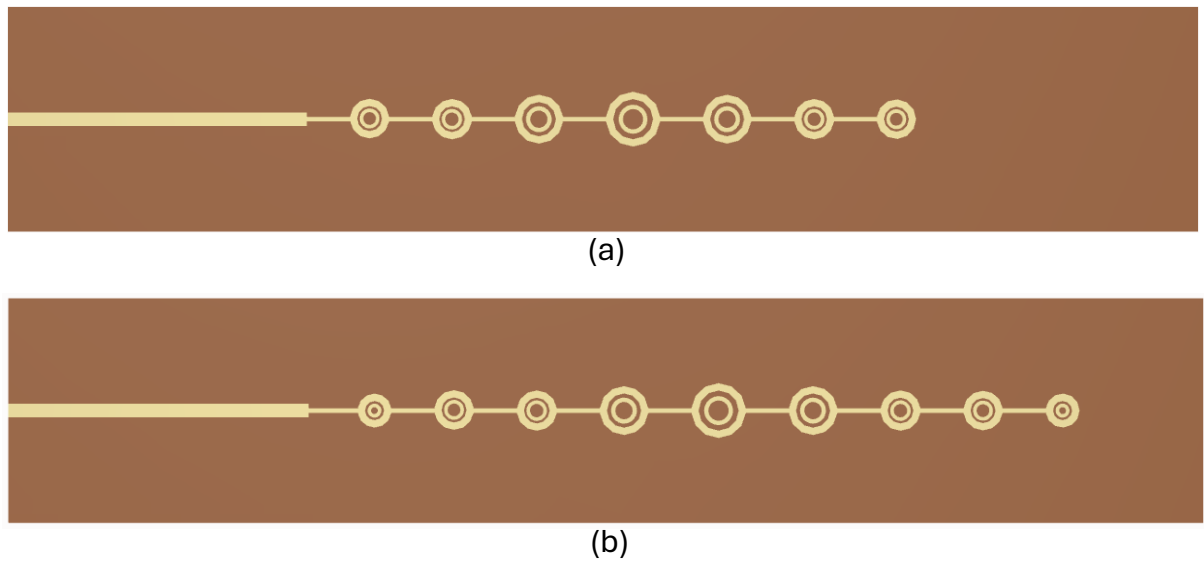


Figure 3.15: Evolution of the proposed LP antenna array (a) 7-element (b) 9-element.

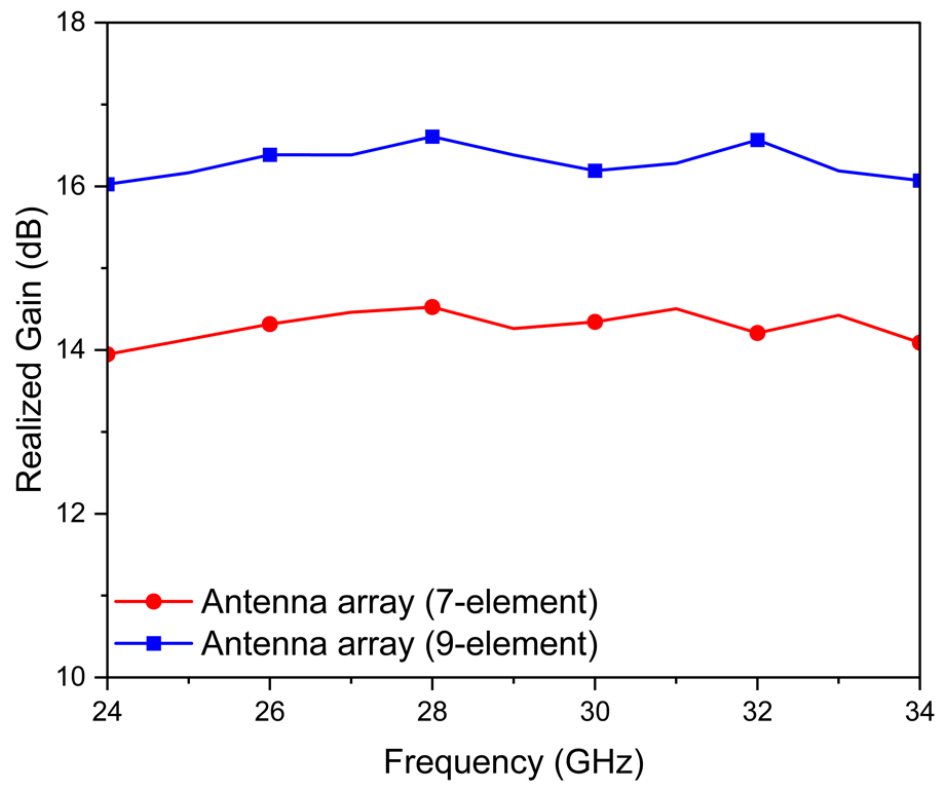


Figure 3.16: Evolution of the gain for the proposed LP antenna array.

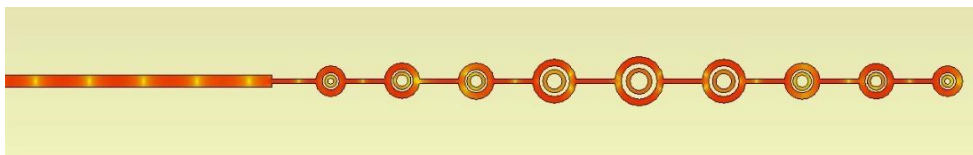


Figure 3.17: Current distribution of the proposed LP antenna array.

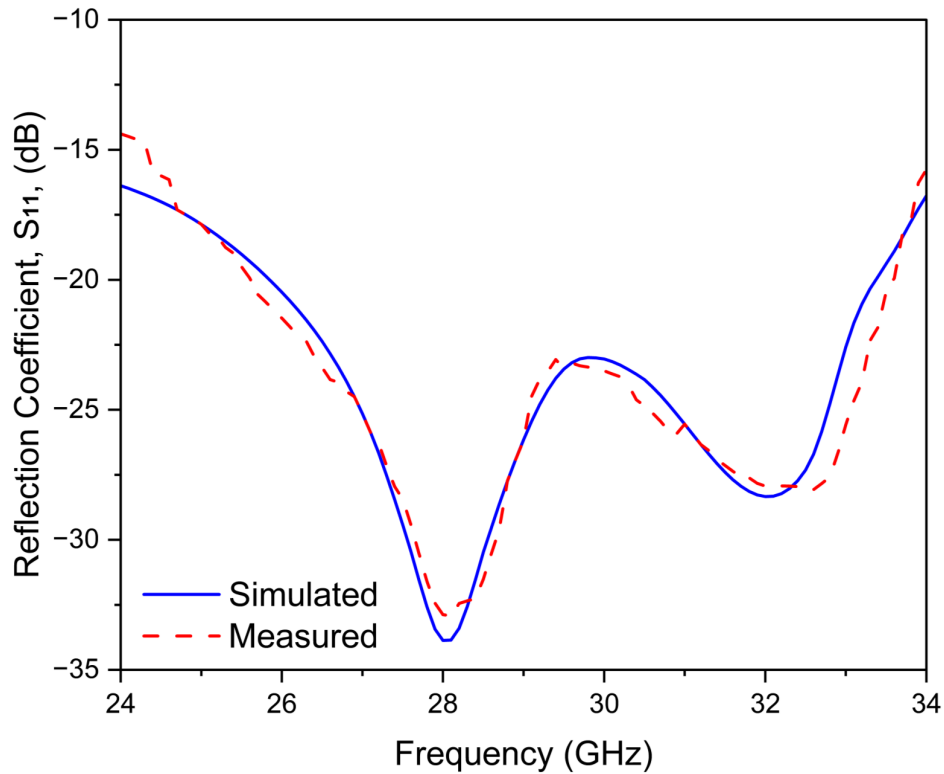


Figure 3.18: Reflection coefficient of the simulated and measured proposed LP antenna array.

to ensure a focused and strong main lobe. As discussed in 3.5.1, the Dolph-Chebyshev weighting method is applied to optimize the SLLs. The gain, SLLs, and radiation pattern are measured to validate the simulation results. The measurement setup, depicted in Fig. 3.19, is arranged in an open space within an indoor lab using the Rohde & Schwarz ATS800B CATR benchtop OTA system for far-field mmWave measurements. The results, shown in Fig. 3.20, demonstrate a high realized gain of 16.6 dBi and a low SLLs exceeding -17 dB at 28 GHz. Additionally, Fig. 3.21 compares the radiation patterns obtained from simulations and measurements in both the E and H planes (at 0° and 90°, respectively). The strong correlation between these results reaffirms the reliability of the simulation process.

### 3.6 Summary

In this chapter, the design, simulation, and experimental validation of LP designs for 5G V2X applications were presented. The work began with the development of a rectangular patch antenna; however, its narrow impedance bandwidth limited its practicality for 5G V2X applications. To address this limitation, the design was modified to an annular ring patch antenna, optimized to achieve a wider impedance bandwidth of 35.17%. While

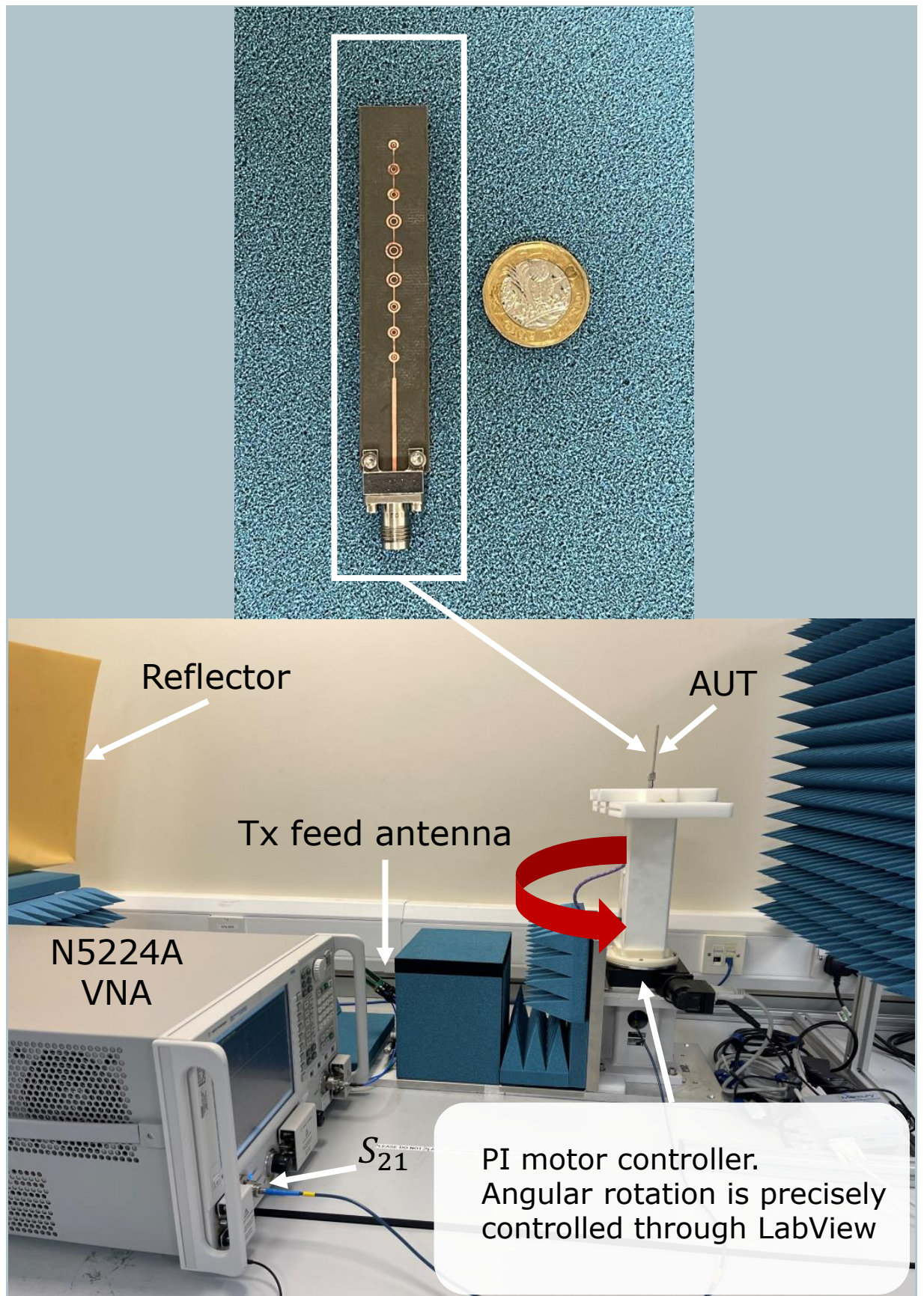


Figure 3.19: Measurement system and the LP antenna array prototype.

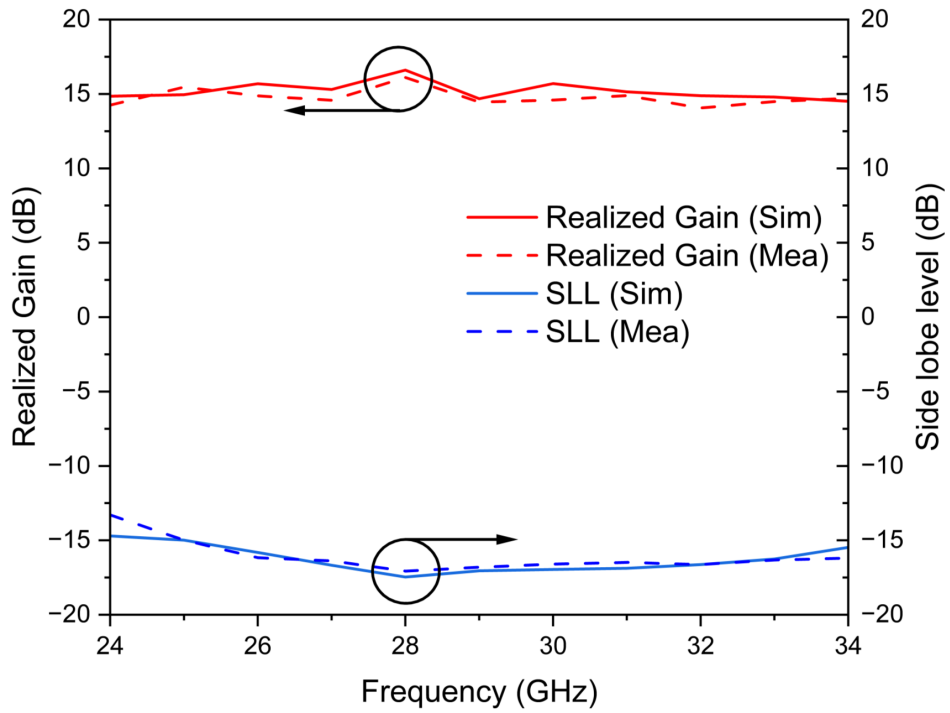


Figure 3.20: Simulated and measured realized gain and SLLs results as a function of the frequency.

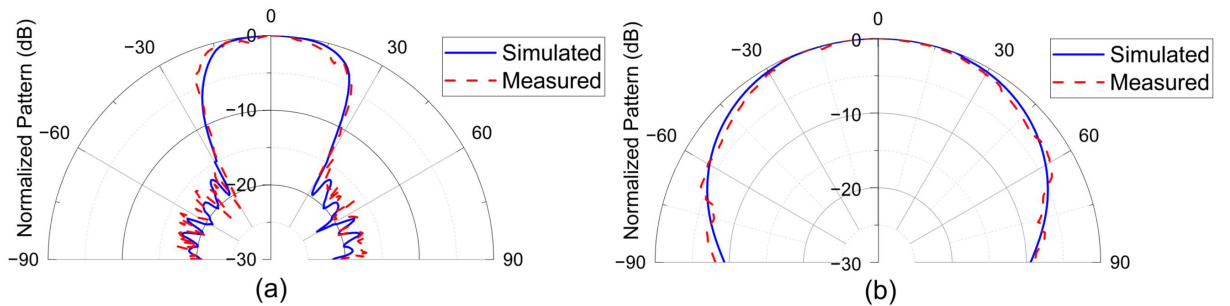


Figure 3.21: Simulated and measured radiation pattern of the proposed LP antenna array (a)  $\phi = 0^\circ$  and (b)  $\phi = 90^\circ$ .

the annular ring design provided sufficient bandwidth, its single-element configuration lacked the high gain necessary to overcome the atmospheric attenuation challenges at mmWave frequencies. To enhance gain, a series-fed 9-element LP patch antenna array was designed and analyzed. The array demonstrated a high realized gain of 16.6 dBi while maintaining the wide impedance bandwidth and achieving low SLLs of -17 dB through the application of the Dolph-Chebyshev weighting method, ensuring a focused main lobe. The antennas were subsequently fabricated and validated through measurements, showing close agreement with simulated results. Despite these advancements, the static nature of the beam limited its adaptability in dynamic vehicular environments, motivating the development of beamsteering capabilities in the following chapter.

# Chapter 4

## Beamsteering Antenna

In this chapter, the focus shifts from the series-fed 9-element LP patch antenna array developed in Chapter 3 to the beamsteering capabilities aimed at achieving efficient beam steering for 5G V2X applications. Building upon the wide impedance bandwidth and high gain achieved in the previous chapter, the development of a phased array is introduced to enhance the antenna's ability to steer radiation beams. The beamsteering antenna design presented in this chapter allows for the antenna to cover a  $360^\circ$  area around the vehicle, supporting versatile vehicular communication needs. The primary objective, aligned with  $O\beta$ , is to implement phased array technology to achieve precise beam steering and improved coverage. This chapter details the design progression from the 9-element series-fed array introduced in 3.5 to a 2x9 and 4x9 series-fed array, culminating in a phased array with four ports. The design methodology, simulation results, and analysis of the beamsteering capabilities are presented, demonstrating the antenna's potential to meet the requirements of 5G V2X communication systems.

### 4.1 Introduction

In 5G V2X communication systems, achieving high gain and efficient coverage is critical to overcoming atmospheric attenuation and ensuring reliable connectivity in dynamic environments. MPAs are frequently employed to enhance antenna performance by increasing the number of elements, which effectively boosts gain while mitigating signal loss at mmWave frequencies. Compared to other configurations, such as waveguides, MPAs experience higher dielectric and conductor losses, but their compact size, simplicity, and ease of integration make them attractive for automotive applications [137]. The choice of feeding technique, whether series or parallel, plays a crucial role in determining the array's efficiency, compactness, and SLLs. While parallel-fed arrays are known for their higher losses and bulkier structures, series-fed arrays offer a more compact design with low SLLs, making them suitable for reducing interference and improving signal quality in wireless

communication and sensor applications [138].

Beamsteering is an essential aspect of 5G V2X applications, enabling antennas to adapt to specific coverage needs in diverse environments. For instance, scenarios such as trackside installations or intersections may require different beam coverage, while vehicles may not always need full 360° coverage and, depending on the communication needs, could require only 90° or 180° coverage to ensure efficient connectivity. Beamsteering, achieved through phased array design, is crucial in addressing these varying demands. Phased arrays enable the precise steering of radiation beams, allowing for dynamic coverage across different angles. Numerous studies have explored beamsteering techniques using various antenna designs, including magneto-electric dipoles [139], dielectric resonators [140], monopoles [141], and patch antennas [142]. However, many of these designs face challenges such as limited beamsteering ranges, increased structural complexity, and higher fabrication costs.

## 4.2 Contributions

This chapter makes several key contributions to the field of 5G V2X communications, focusing on the development of phased array beamsteering capabilities to achieve precise beam steering and enhanced coverage. The work presented in this chapter addresses challenges related to dynamic vehicular communication environments, where adaptable beam steering is crucial for ensuring reliable connectivity. By advancing phased array designs, this chapter demonstrates how beam steering can be utilized to address the coverage challenges in 5G V2X networks, with suggestions for achieving flexible 360° coverage depending on the communication system and practical deployment. Through a combination of design progression, optimization, and validation, the proposed beamsteering capabilities significantly improve antenna performance in real-world scenarios. The key contributions of this chapter are:

- Design and analysis of a 2x9 series-fed LP patch antenna array, providing enhanced gain while maintaining wide impedance bandwidth, offering a step towards phased array performance.
- Development of a 4x9 series-fed LP patch antenna array, further improving gain and demonstrating the scalability of the antenna design for more robust communication needs.
- Implementation of a beamsteering phased array with four ports, capable of dynamic beam steering, providing flexible coverage solutions ranging for 90°, 180°, 270°, and 360°, depending on vehicular communication requirements.

The organization of this chapter is as follows: The first section presents the design and analysis of the 2x9 series-fed LP patch antenna array. Next, the second section introduces

the 4x9 series-fed array, which further enhances gain performance. Finally, the phased array design is developed and analyzed, providing a flexible solution for beam steering and coverage. The chapter concludes with a summary of the results and their implications for 5G V2X communications.

### 4.3 2x9 series-fed LP patch antenna array

The proposed 9-element LP patch antenna array, introduced in 3.5, successfully provides the increased gain required to mitigate atmospheric attenuation at mmWave frequencies. However, to further enhance the antenna's performance and offer different gain levels for a range of 5G V2X applications, the 9-element antenna array is developed into a 2x9 series-fed LP patch antenna array. This array configuration not only improves gain but also retains the benefits of the series-fed technique, including a compact configuration and low SLLs, which are essential for minimizing interference. The following presents the design steps for the 2x9 series-fed LP patch antenna array, with a focus on its development, simulation, and experimental results.

#### 4.3.1 Design and Analysis of 2x9 Antenna Array

The design of the 2x9 series-fed LP patch antenna array is an extension of the 9-element LP patch antenna array introduced in section 3.5. The design and simulation of this array are conducted using 2023 CST Microwave Studio. The configuration of the 2x9 array, as shown in Fig. 4.1, consists of 18 elements arranged in two parallel rows. The overall dimensions of the antenna array are 80 mm in length and 20 mm in width. A series-fed array technique is employed, utilizing tapering to simplify the feeding network and contribute to low SLLs. To further optimize the balance between beamwidth and SLLs, the Dolph-Chebyshev weighting method is applied, with the element weights derived from this method presented in Table 3.4. To implement the tapering, the width of each patch element is adjusted by multiplying the weight ( $D_n$ ) of each element by the width of the central element, resulting in a series of elements with varying widths, as shown in Fig. 4.1. The elements are spaced at half-wavelength intervals to ensure accurate inter-element connectivity and maintain a  $50 \Omega$  input impedance across the array. The application of the Dolph-Chebyshev weighting not only ensures consistent impedance matching across all elements but also optimizes the overall array performance in terms of beamwidth and SLLs. This design meets the high-performance demands of 5G V2X applications by offering precision, reliability, and robust performance in challenging communication environments.

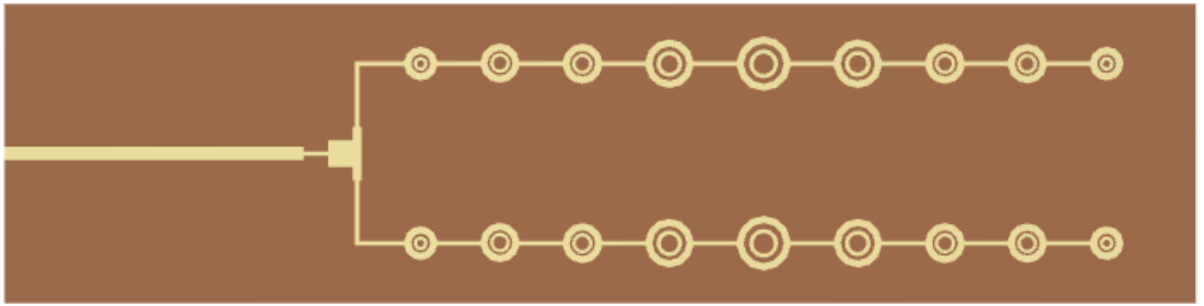


Figure 4.1: Structure of the proposed 2x9 series-fed antenna array.

### 4.3.2 Simulation Results

The 2x9 series-fed LP patch antenna array is developed based on the 9-element series-fed configuration introduced in section 3.5, with the goal of providing higher gain to meet the demands of 5G V2X applications. Increasing gain is crucial for mmWave applications, as it helps counteract atmospheric attenuation by strengthening the received signal. Throughout the development of the 2x9 series-fed array, particular attention is given to ensuring that the simulated  $S_{11}$  achieves a wide impedance bandwidth, which is critical for supporting a broad range of mmWave applications, including 5G V2X communications. The  $S_{11}$  simulation results for the 2x9 series-fed LP patch antenna array is presented in Fig. 4.2, demonstrating an impedance bandwidth of 35.17% (24 to 34 GHz).

In addition to achieving a wide impedance bandwidth, the primary objective of developing the 2x9 series-fed array is to increase the realized gain compared to the 9-element series-fed LP patch antenna array. Achieving higher gain is essential for enhancing the performance of mmWave antennas in 5G V2X applications, where overcoming signal loss due to atmospheric attenuation is a key challenge. By increasing the number of elements from 9 to 18, the design is optimized to achieve a more focused and powerful radiation pattern. As shown in Fig. 4.3, the proposed 2x9 array achieves a realized gain of 17.9 dBi, a significant improvement over the 9-element array, making it a highly effective solution for environments where high gain is required to maintain reliable communication. This improved gain performance directly contributes to enhancing the overall effectiveness of the antenna for long-range communication in challenging vehicular environments.

### 4.3.3 Experimental Discussion

To validate the performance of the 2x9 series-fed LP patch antenna array, the design is fabricated on a Rogers RT-duroid 5880 substrate with a dielectric constant of 2.2 and a thickness of 0.787 mm. The  $S_{11}$  of the array is measured using a mmWave vector network analyzer, and as illustrated in Fig. 4.4, the measured results confirm the wide impedance bandwidth of 35.17% (24 to 34 GHz), consistent with the design objectives. The strong

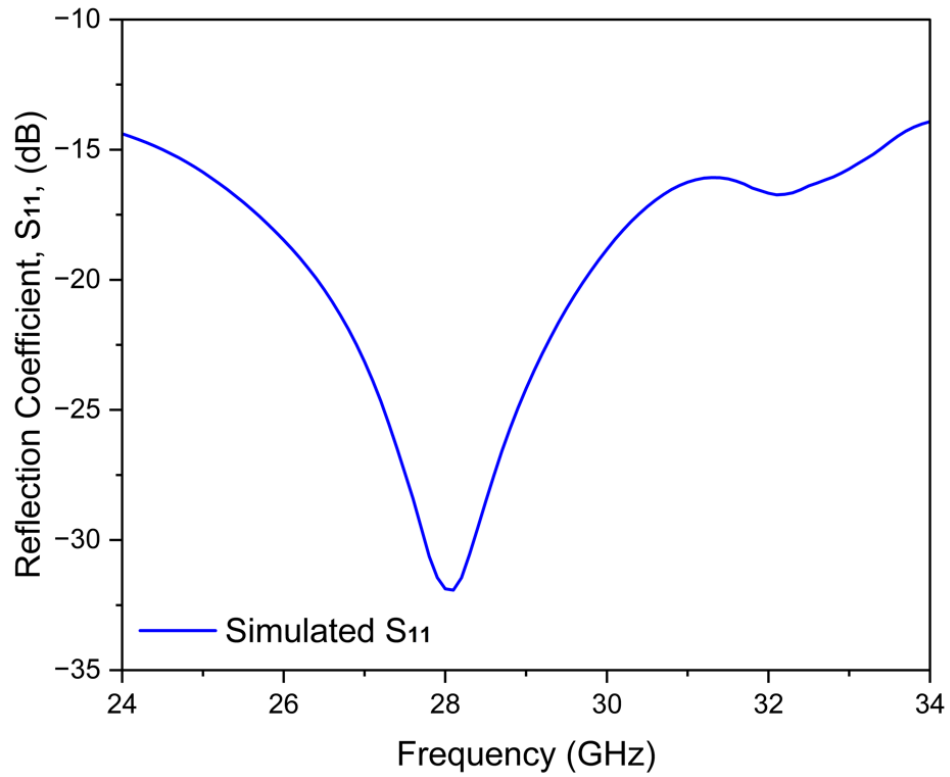


Figure 4.2: Reflection coefficient of the simulated proposed 2x9 LP antenna array.

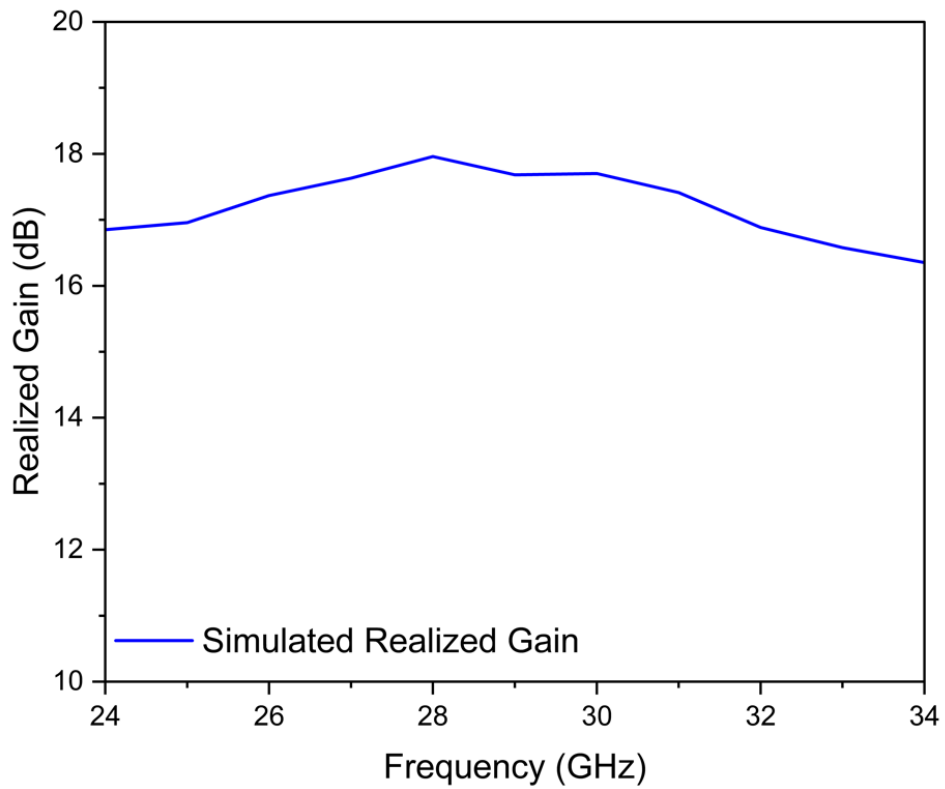


Figure 4.3: Realized gain of the simulated proposed 2x9 LP antenna array.

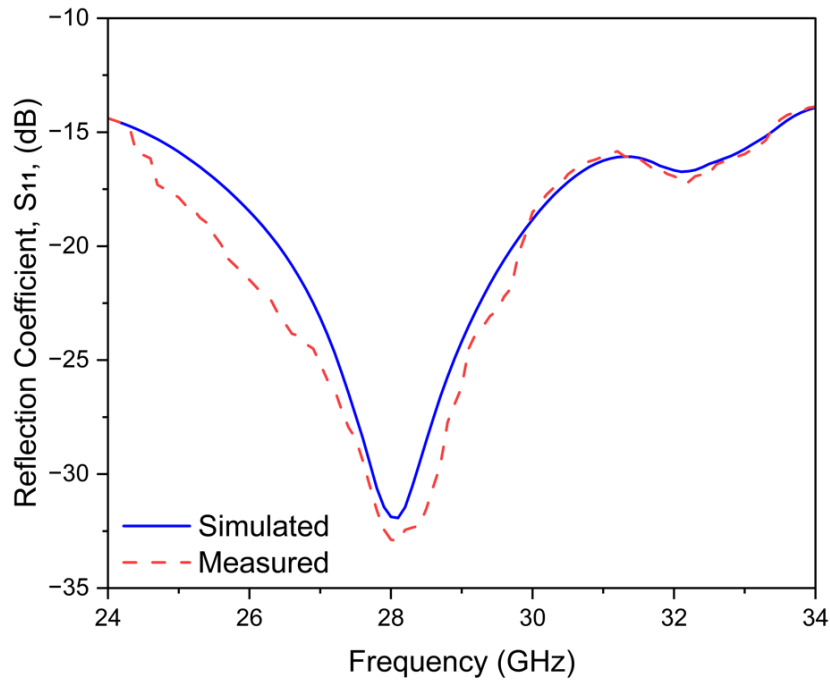


Figure 4.4: Reflection coefficient of the simulated and measured proposed 2x9 LP antenna array.

agreement between the simulated and measured  $S_{11}$  results further validates the accuracy of the simulation.

In addition to bandwidth validation, the 2x9 series-fed antenna array is also evaluated to verify the expected increase in gain. Both the gain and radiation pattern are measured to compare with the simulation results. The measurement setup, shown in Fig. 4.5, is arranged in an indoor lab using the Rohde & Schwarz ATS800B CATR benchtop OTA system for far-field mmWave measurements. As seen in Fig. 4.6, the array achieves a realized gain of 17.9 dBi, confirming that the design meets the gain requirements. Furthermore, Fig. 4.7 compares the radiation patterns obtained from both simulations and measurements in the E and H planes (at  $0^\circ$  and  $90^\circ$ , respectively), and demonstrates a beamwidth of  $26^\circ$ . Moreover, the design achieves sidelobe levels of  $-16$  dB. The close correlation between the simulated and measured results affirms the reliability of the simulation process, confirming the accuracy of the design for real-world 5G V2X applications.

The development and validation of the 2x9 series-fed LP patch antenna array highlight key advancements in antenna performance for 5G V2X applications. The design achieves a wide impedance bandwidth of 35.17% and a realized gain of 17.9 dBi, effectively enhancing signal strength to overcome atmospheric attenuation. Through comprehensive simulation and experimental validation, the array demonstrates reliable performance, offering high gain and wide bandwidth, making it a strong candidate for high-performance vehicular

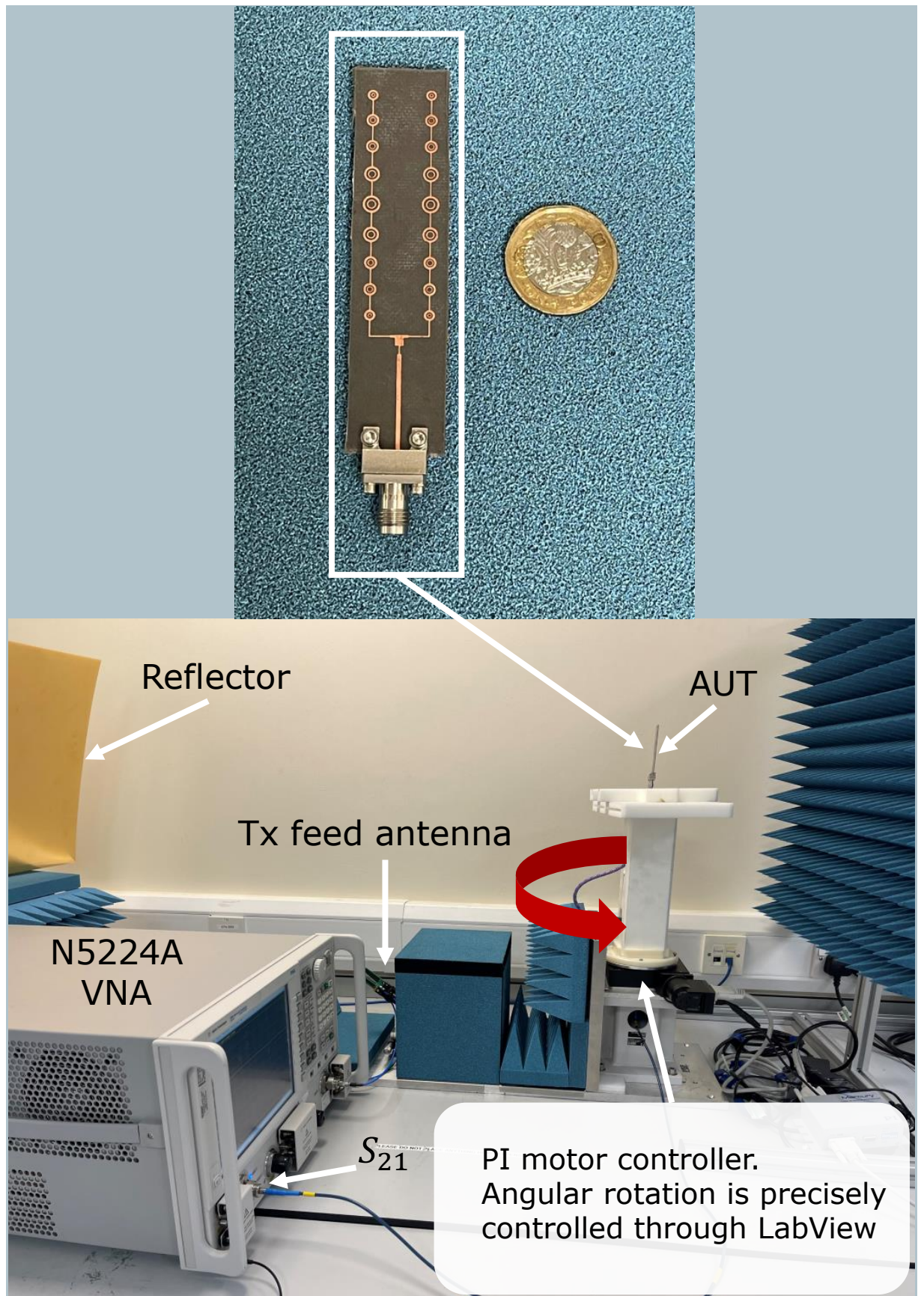


Figure 4.5: Measurement system and the 2x9 LP antenna array prototype.

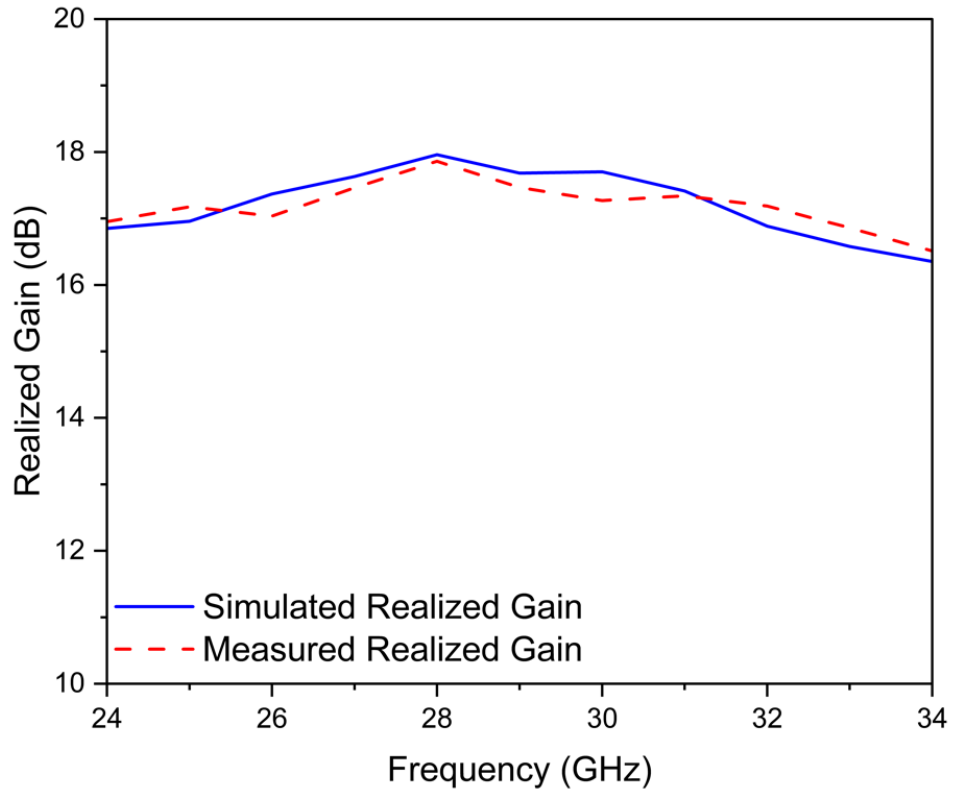


Figure 4.6: Simulated and measured realized gain results of the proposed 2x9 LP antenna array.

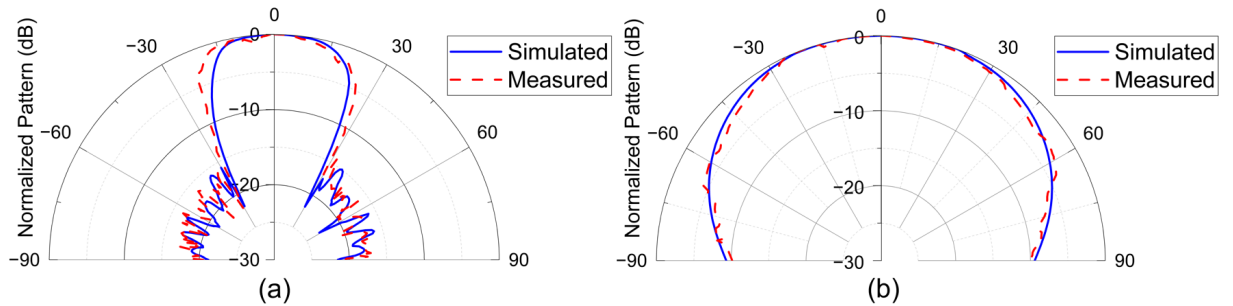


Figure 4.7: Simulated and measured radiation pattern of the proposed 2x9 LP antenna array (a)  $\phi = 0^\circ$  and (b)  $\phi = 90^\circ$ .

communication systems. These contributions expand the capabilities of the series-fed array design, supporting flexible and robust solutions for a variety of 5G V2X applications.

## 4.4 4x9 series-fed LP patch antenna array

Building on the success of the 2x9 series-fed LP patch antenna array, which demonstrated enhanced gain and wide impedance bandwidth, this section focuses on further improving the array's performance by developing it into a 4x9 series-fed LP patch antenna array. The motivation for this development is to achieve even higher gain, which is essential for overcoming greater atmospheric attenuation and supporting long-range communication in 5G V2X applications. By increasing the number of elements in the array, the 4x9 series-fed LP patch antenna array offers an optimized design capable of delivering stronger signals and more robust performance. The following presents the design progression, simulation results, and experimental validation for the 4x9 series-fed LP patch antenna array.

### 4.4.1 4x9 Antenna Array Configuration

The design of the 4x9 series-fed LP patch antenna array follows the same principles used in the development of the 9-element and 2x9 series-fed arrays, with the goal of achieving higher gain to meet the demands of 5G V2X applications. The configuration of the 4x9 array, as illustrated in Fig. 4.8, consists of 36 elements arranged in four parallel rows, with overall dimensions of 80 mm in length and 50 mm in width. The series-fed technique is employed, as it not only simplifies the feeding network but also contributes to maintaining a compact design while ensuring precise impedance matching across all elements. This technique is particularly effective in optimizing the balance between beamwidth and SLLs, which are critical for minimizing interference and achieving focused radiation patterns in high-frequency applications. The elements of the 4x9 array are spaced at half-wavelength intervals, ensuring that the array maintains an input impedance of  $50 \Omega$ , essential for consistent signal performance and connectivity between each patch. By expanding the number of elements to 36, this design is optimized for increased gain, enhancing the antenna's ability to overcome atmospheric attenuation at mmWave frequencies. The series-fed approach, combined with the optimized arrangement of elements, allows the antenna array to deliver a focused radiation pattern while keeping SLLs low, further improving its performance in high-demand environments like 5G V2X.

### 4.4.2 Simulation Analysis of 4x9 Antenna Array

The 4x9 series-fed LP patch antenna array is developed as an extension of the 2x9 series-fed array, with the primary goal of providing higher gain while maintaining the wide

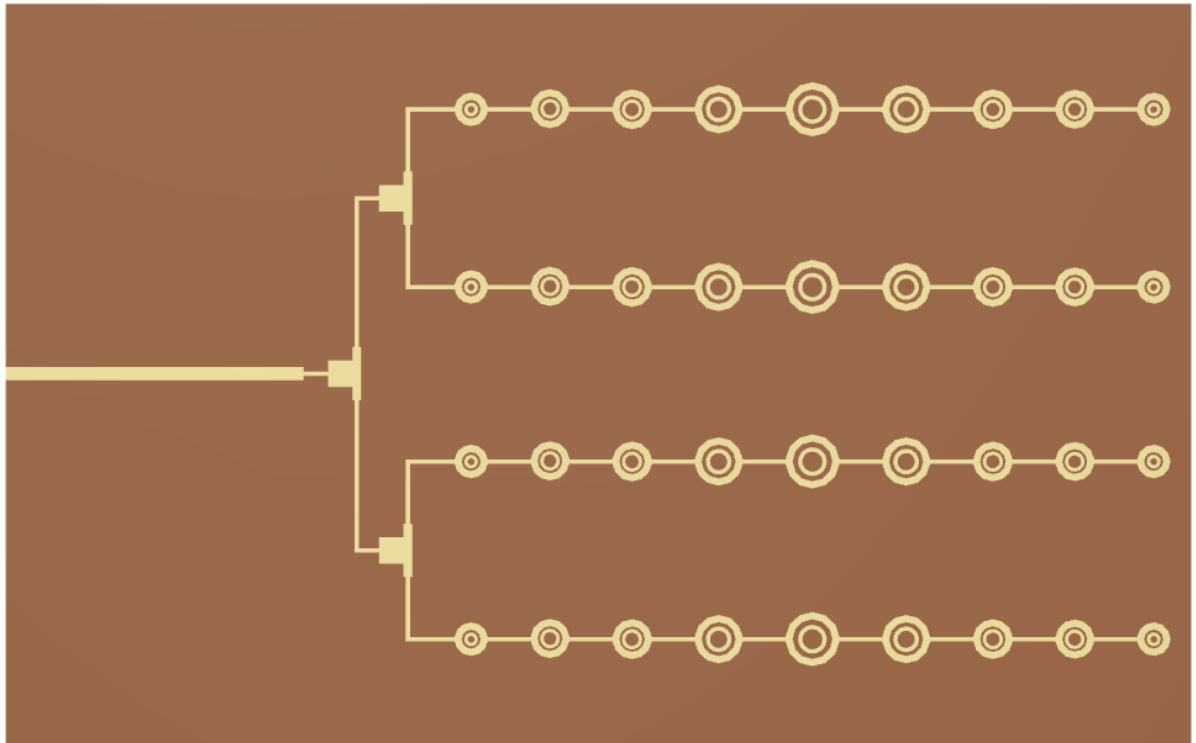


Figure 4.8: Structure of the proposed 4x9 series-fed antenna array.

impedance bandwidth critical for 5G V2X applications. During the simulation, particular focus is placed on ensuring that the  $S_{11}$  covers the desired bandwidth. As shown in Fig. 4.9, the simulated  $S_{11}$  demonstrates a wide impedance bandwidth of 35.17%, ranging from 24 to 34 GHz. This result is consistent with the performance of the previous 2x9 array, ensuring that the bandwidth requirements are met for a variety of mmWave applications in 5G networks.

In addition to the bandwidth performance, the primary objective of this array is to achieve a higher realized gain to improve signal strength and counteract atmospheric attenuation. By increasing the number of elements from 18 to 36, the array's design is optimized to deliver stronger and more focused radiation. As illustrated in Fig. 4.10, the simulated realized gain of the 4x9 series-fed LP patch antenna array reaches 21.1 dBi, a significant improvement over the 2x9 array's gain of 17.9 dBi. This gain enhancement makes the 4x9 array particularly suited for long-range communication and high-performance requirements in 5G V2X environments, where overcoming signal loss due to atmospheric attenuation is critical.

### 4.4.3 Experimental Validation

The performance of the 4x9 series-fed LP patch antenna array is validated through fabrication and experimental measurements. The array is fabricated on a Rogers RT-

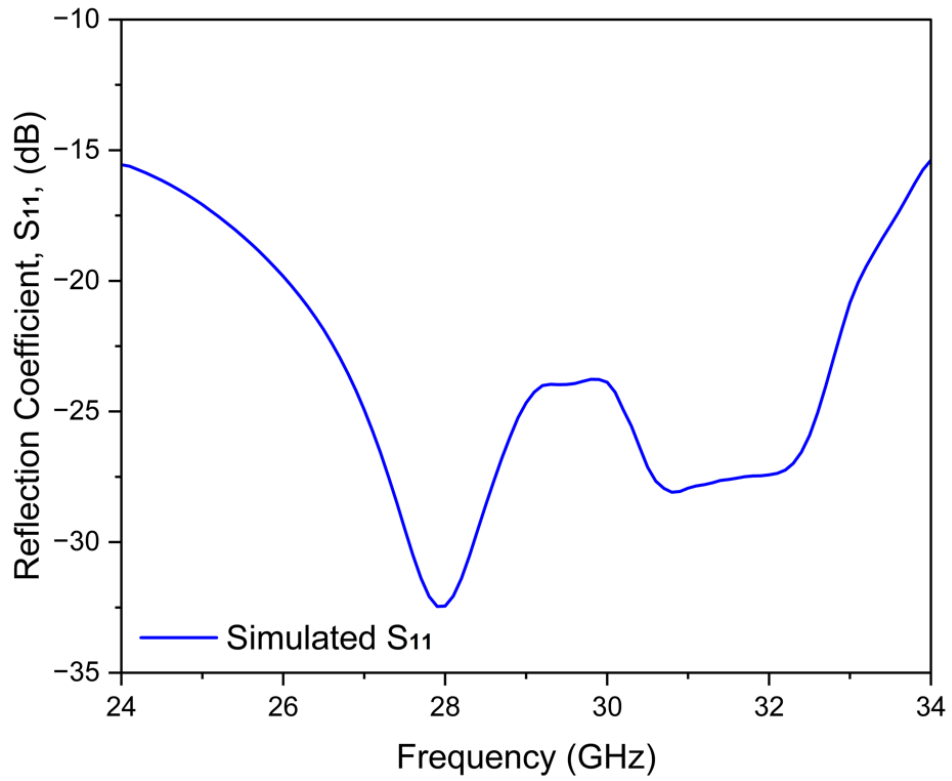


Figure 4.9: Reflection coefficient of the simulated proposed 4x9 LP antenna array.

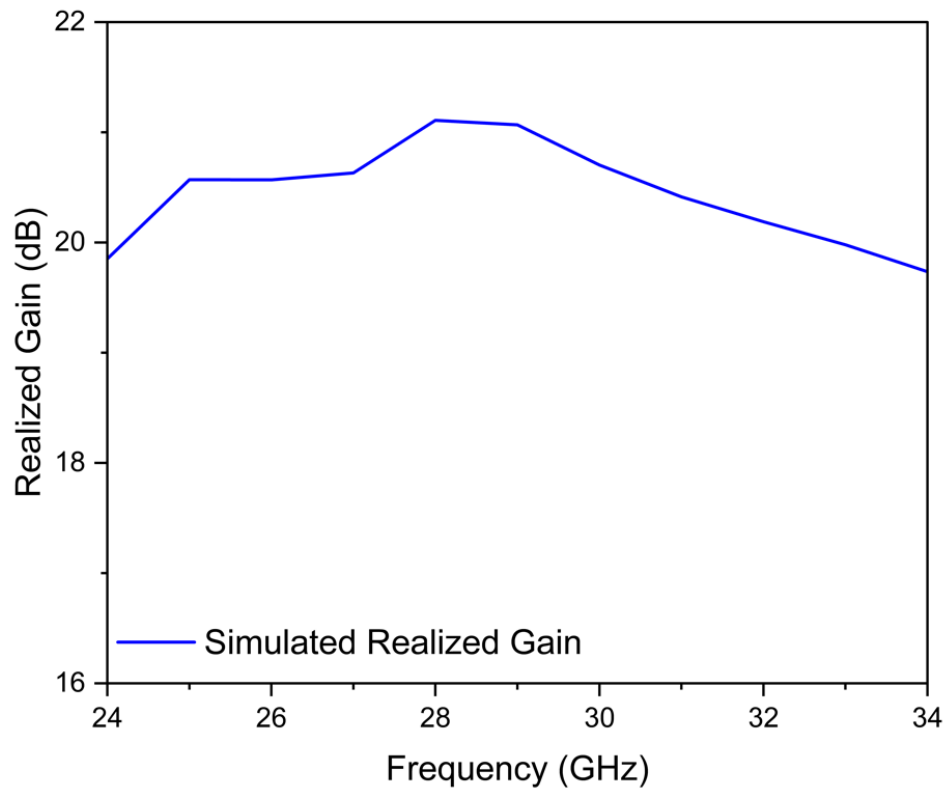


Figure 4.10: Realized gain of the simulated proposed 4x9 LP antenna array.

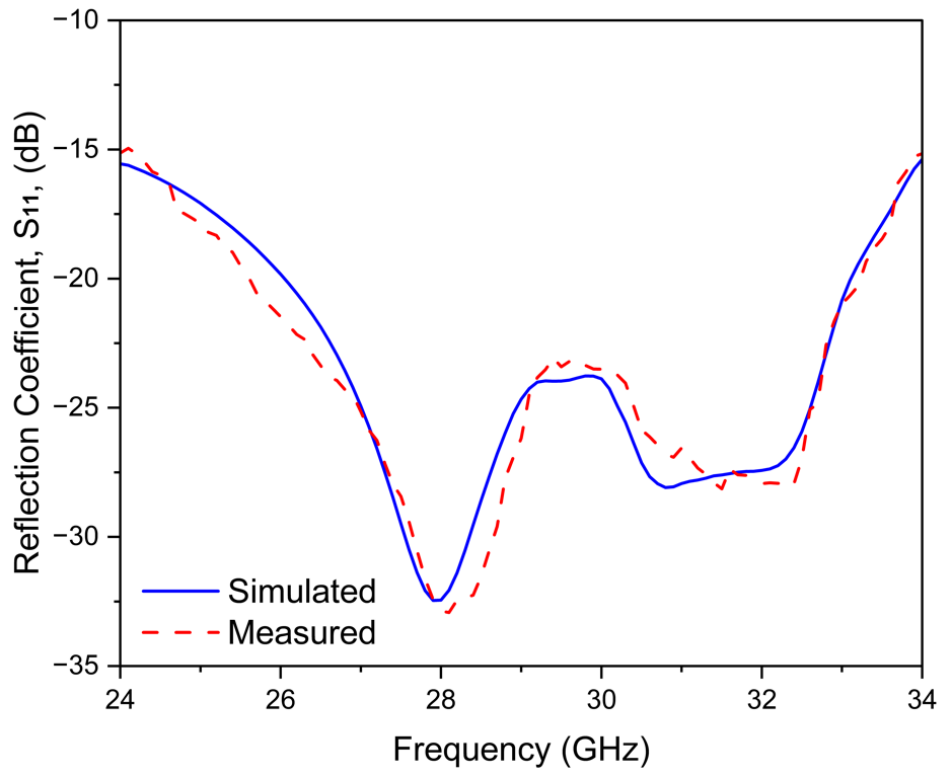


Figure 4.11: Reflection coefficient of the simulated and measured proposed 4x9 LP antenna array.

duroid 5880 substrate, with a dielectric constant of 2.2 and a thickness of 0.787 mm. The  $S_{11}$  of the antenna is measured using a mmWave vector network analyzer. As shown in Fig. 4.11, the measured results confirm a wide impedance bandwidth of 35.17% (24 to 34 GHz), aligning with the design objectives. The strong agreement between the simulated and measured  $S_{11}$  results further confirms the accuracy of the design's simulation.

Beyond bandwidth validation, the 4x9 series-fed antenna array is further evaluated to assess the anticipated gain improvement. Both the gain and radiation pattern are measured and compared against the simulation results. The measurement setup, shown in Fig. 4.12, is arranged in an indoor lab using the Rohde & Schwarz ATS800B CATR benchtop OTA system for far-field mmWave measurements. As seen in Fig. 4.13, the array achieves a realized gain of 21.1 dBi, meeting the expected gain improvements. Additionally, Fig. 4.14 compares the radiation patterns obtained from both simulations and measurements in the E and H planes (at  $0^\circ$  and  $90^\circ$ , respectively), and demonstrates a beamwidth of  $16^\circ$ . Moreover, the design achieves sidelobe levels of  $-15.5$  dB. The strong correlation between these results further confirms the reliability of the simulation process and ensures the design's accuracy in real-world 5G V2X applications.

The successful development of the 4x9 series-fed LP patch antenna array demonstrate its ability to deliver a wide impedance bandwidth and high realized gain of 21.1 dBi,

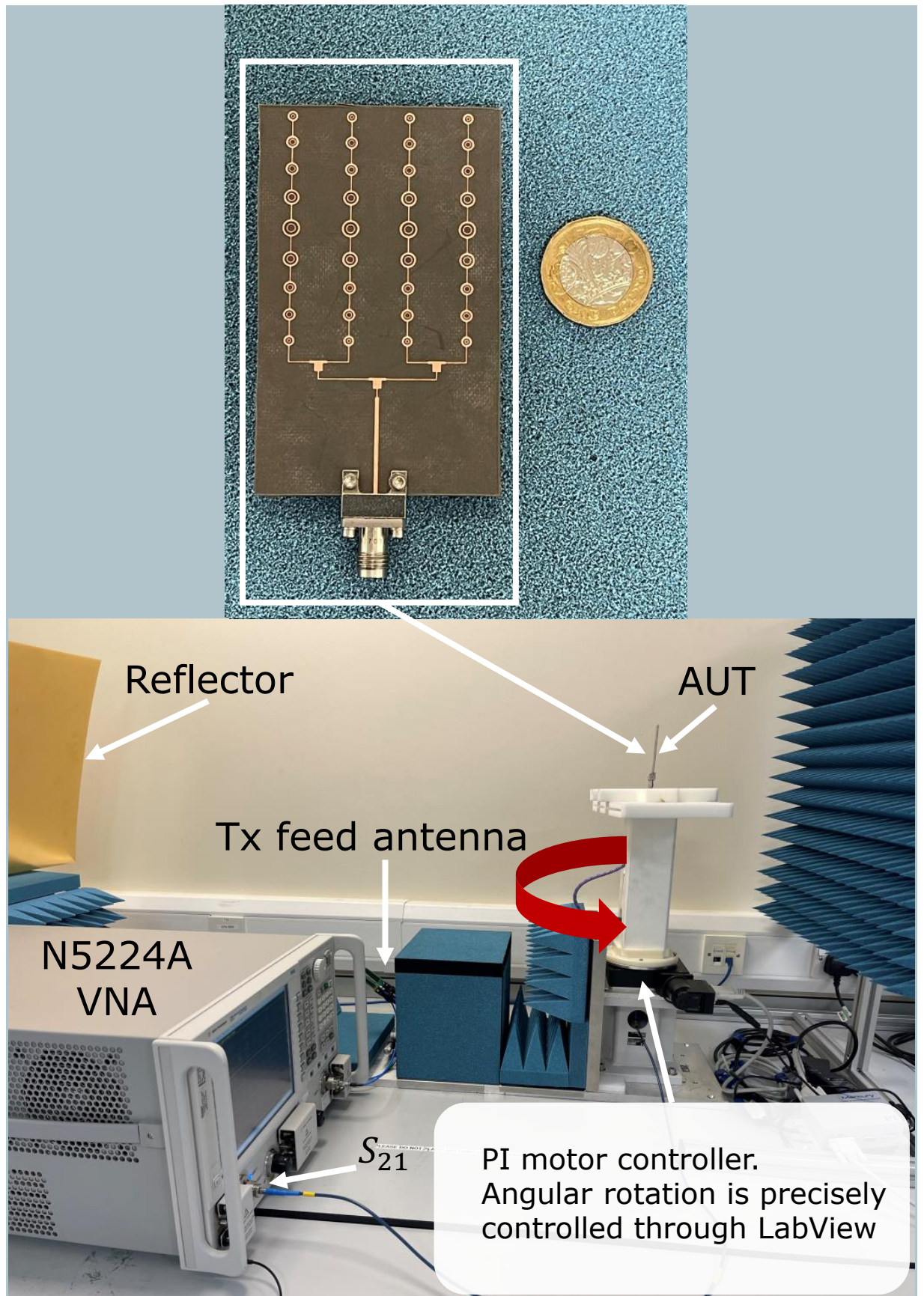


Figure 4.12: Measurement system and the 4x9 LP antenna array prototype.

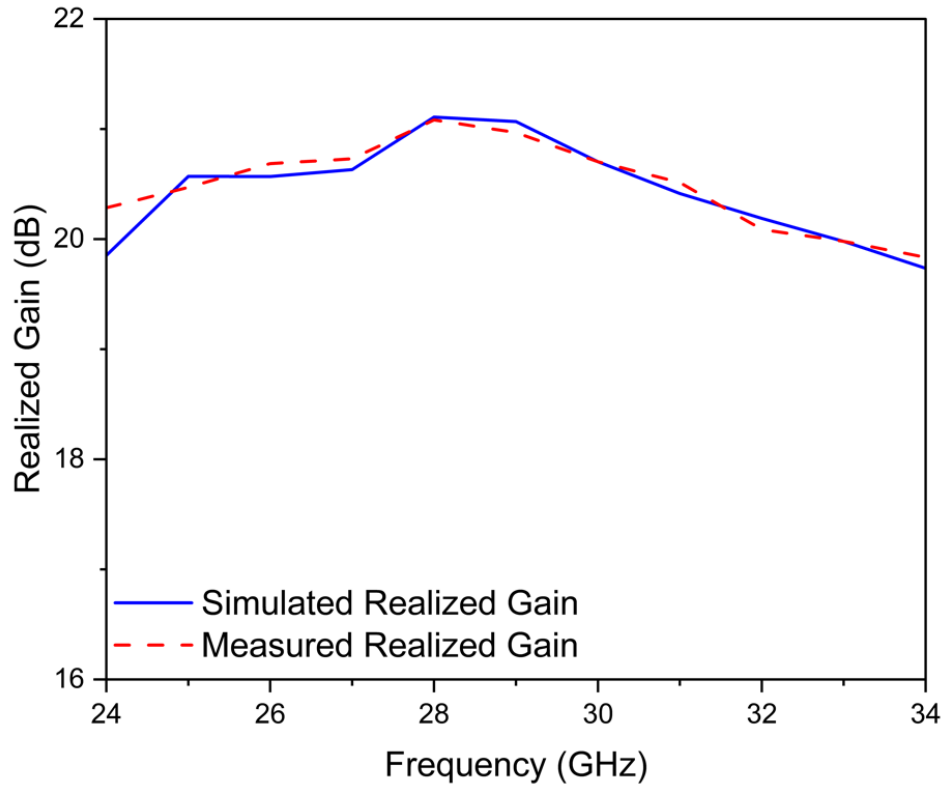


Figure 4.13: Simulated and measured realized gain of the proposed 4x9 LP antenna array.

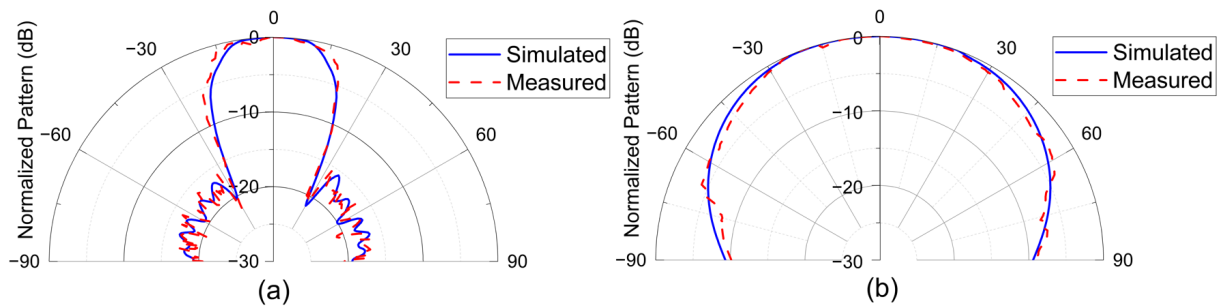


Figure 4.14: Simulated and measured radiation pattern of the proposed 4x9 LP antenna array (a)  $\phi = 0^\circ$  and (b)  $\phi = 90^\circ$ .

making it an excellent solution for overcoming atmospheric attenuation. The robust performance, verified through simulation and experimental testing, showcases the array's potential for enhancing signal strength and range in demanding vehicular communication systems. This validation reinforces the design's suitability for high-performance 5G V2X applications, where reliable long-range communication is critical.

## 4.5 Phased Array with Beamsteering Capabilities

Building on the foundation of the 4x9 series-fed LP patch antenna array, this section introduces beamsteering capabilities by developing the design into a phased array with four ports. Beamsteering is critical for 5G V2X applications, enabling the antenna to dynamically adjust its coverage to meet the communication requirements of moving vehicles. The phased array design allows the beam to be steered across  $\pm 39^\circ$ , providing a total coverage of  $\pm 90^\circ$  from a single unit. With the addition of four ports for phased array operation, the antenna retains the performance benefits of the 4x9 design while offering the flexibility needed for beamsteering. Additionally, a proposed structure utilizing four phased array units can achieve full  $360^\circ$  coverage, which is essential for comprehensive communication in 5G V2X environments.

### 4.5.1 An Overview

Beamsteering is a crucial feature in phased array antenna design, especially for 5G V2X applications, where flexible and dynamic coverage is essential. By steering the antenna's radiation pattern, the phased array can adapt to varying vehicular environments and provide targeted coverage where needed. While there are several approaches to achieving beamsteering, this work prioritizes simplicity and efficiency. To this end, a four-port phased array design is selected, offering a practical method for steering the beam while keeping the structure streamlined.

In this design, each of the four ports is assigned a phase shift, which controls the direction of the beam. By carefully adjusting the phase delay between the ports, the phased array can steer the beam across  $\pm 39^\circ$ , resulting in a total coverage of  $\pm 90^\circ$  when combined with the antenna's inherent beamwidth. The choice of a four-port configuration is deliberate, as it simplifies the implementation of beamsteering without the need for complex feed networks or additional hardware. This design strikes a balance between performance and practicality, ensuring that the antenna can meet the demanding requirements of 5G V2X communications while maintaining a simple structure.

The coverage requirements of 5G V2X applications demand adaptable solutions, leading to the evolution of the proposed series-fed patch antenna array into a beamsteerable phased array, as shown in Fig. 4.15. This enhancement allows the array to accommodate

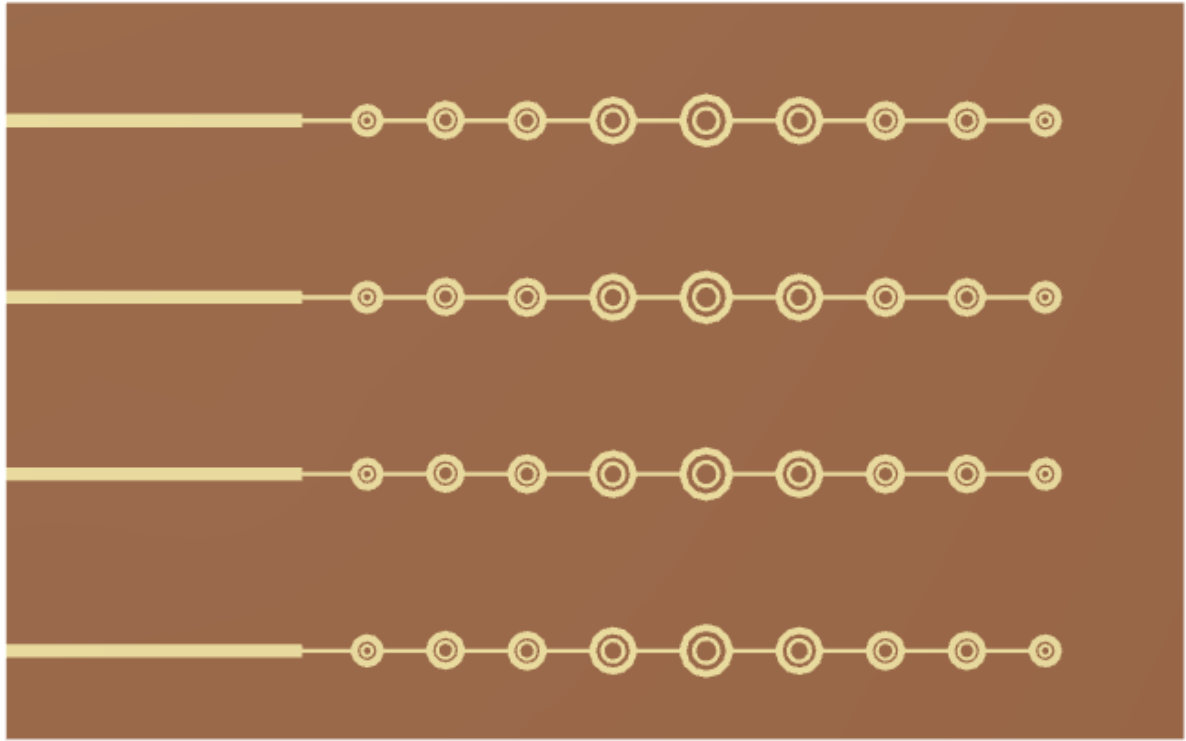


Figure 4.15: Structure of the proposed series-fed phased antenna array.

various coverage needs. For example, a track-side access point may require  $180^\circ$  coverage rather than  $360^\circ$ , and the phased array design presented here is configurable to support  $90^\circ/180^\circ/270^\circ/360^\circ$  beam coverage. This adaptability is achieved by utilizing up to four array units, each providing  $90^\circ$  sector coverage, ensuring optimal communication coverage tailored to the specific requirements of 5G V2X environments.

#### 4.5.2 Simulation Results of the Proposed Phased Antenna Array

The performance of the proposed phased antenna array is first evaluated by analyzing the simulated  $S_{11}$ , which confirms that the design maintains a wide impedance bandwidth, essential for supporting the full frequency range required in 5G V2X applications. The  $S_{11}$  simulation results, illustrated in Fig. 4.16, show that the phased array achieves an impedance bandwidth of 35.17% (24 to 34 GHz), indicating that the antenna operates efficiently across the entire frequency range. This result ensures that the antenna design meets the wide bandwidth requirements for reliable communication in 5G V2X applications.

In addition to the impedance bandwidth, the beamsteering capability of the proposed phased array is evaluated through simulations in CST 2023 by applying different phase shifts to the signals in segments P1 to P4. Beam steering is theoretically determined by the equation [143]

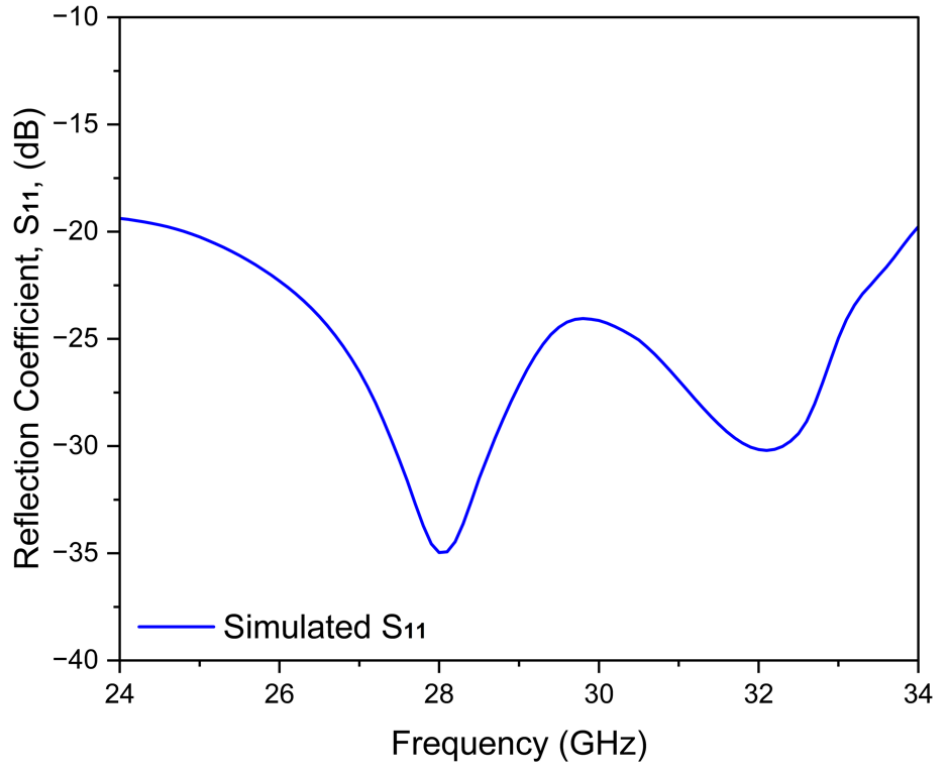


Figure 4.16: Reflection coefficient of the simulated proposed phased antenna array.

$$\Delta\phi = \frac{2\pi d}{\lambda} \sin(\theta_s), \quad (4.1)$$

where  $\Delta\phi$  is the phase shift for the  $n$ -th element,  $d$  is the distance between array elements,  $\lambda$  is the wavelength, and  $\theta_s$  is the desired steering angle. The phase shifts applied to P1/P2/P3/P4 are  $0^\circ/0^\circ/0^\circ/0^\circ$  for a  $0^\circ$  beam,  $49^\circ/17^\circ/131^\circ/98^\circ$  for a  $-39^\circ$  beam, and  $98^\circ/131^\circ/17^\circ/49^\circ$  for a  $+39^\circ$  beam. The resulting beamsteering performance, illustrated in Fig. 4.17, shows the array achieving a steering range of  $\pm 39^\circ$  at peak gain, with coverage extending to  $\pm 45^\circ$  within the beamwidth range and supporting a  $360^\circ$  beamforming structure. The phased array demonstrates consistent steering across its range, ensuring minimal loss in gain and SLLs performance. This level of control is crucial for real-world 5G V2X applications, where precise beamsteering is needed to adapt to dynamic coverage scenarios, such as intersections or highways.

### 4.5.3 Experimental Validation and Discussion

To validate the simulation results, the series-fed phased antenna array is fabricated and measured. The  $S_{11}$  of the phased array is measured using a mmWave vector network analyzer, and as shown in Fig. 4.18, the measured results confirm a wide impedance bandwidth of 35.17% (24 to 34 GHz), which aligns well with the simulated  $S_{11}$  results,

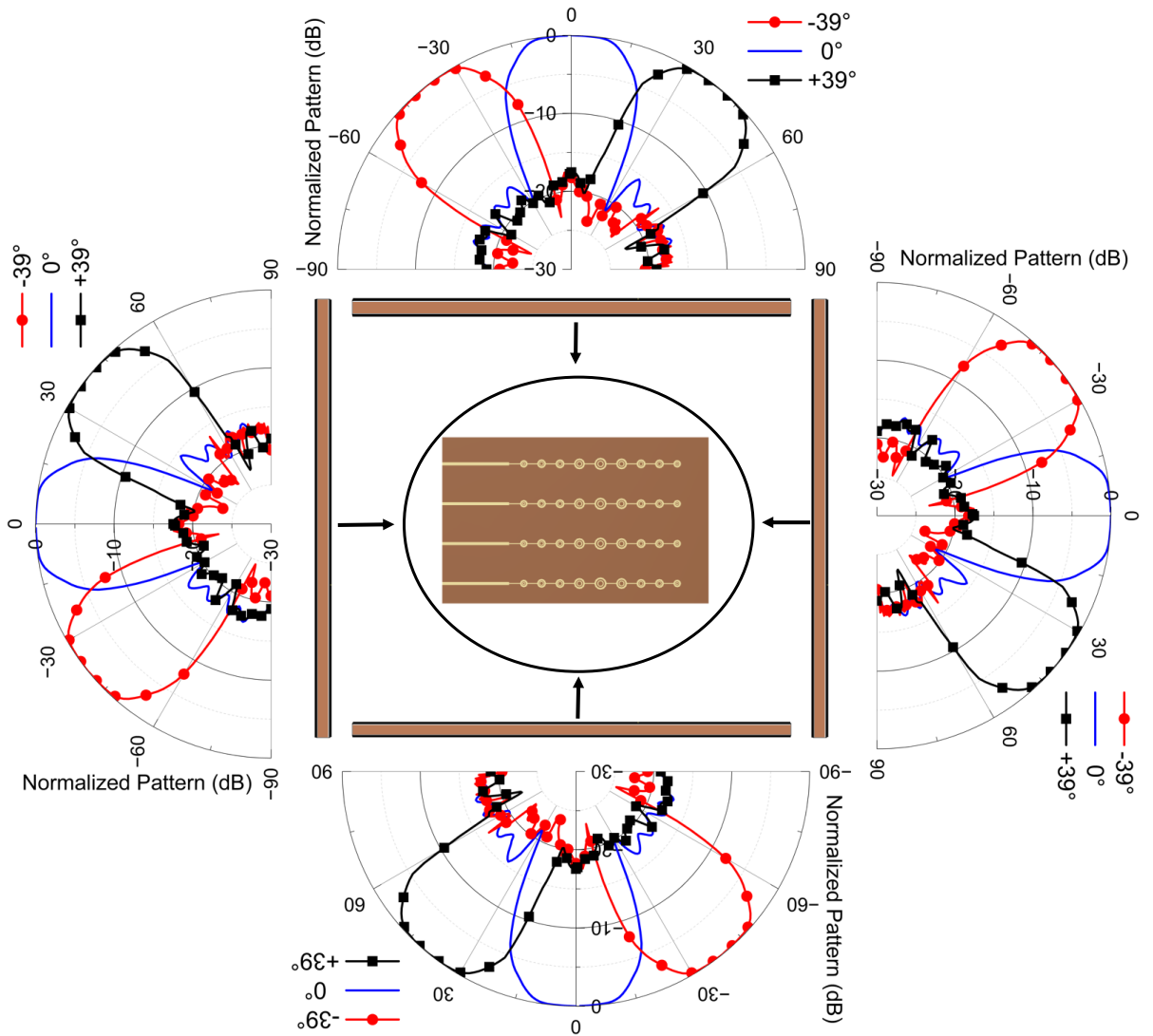


Figure 4.17: The proposed series-fed phased antenna array and its corresponding simulated radiation pattern results.

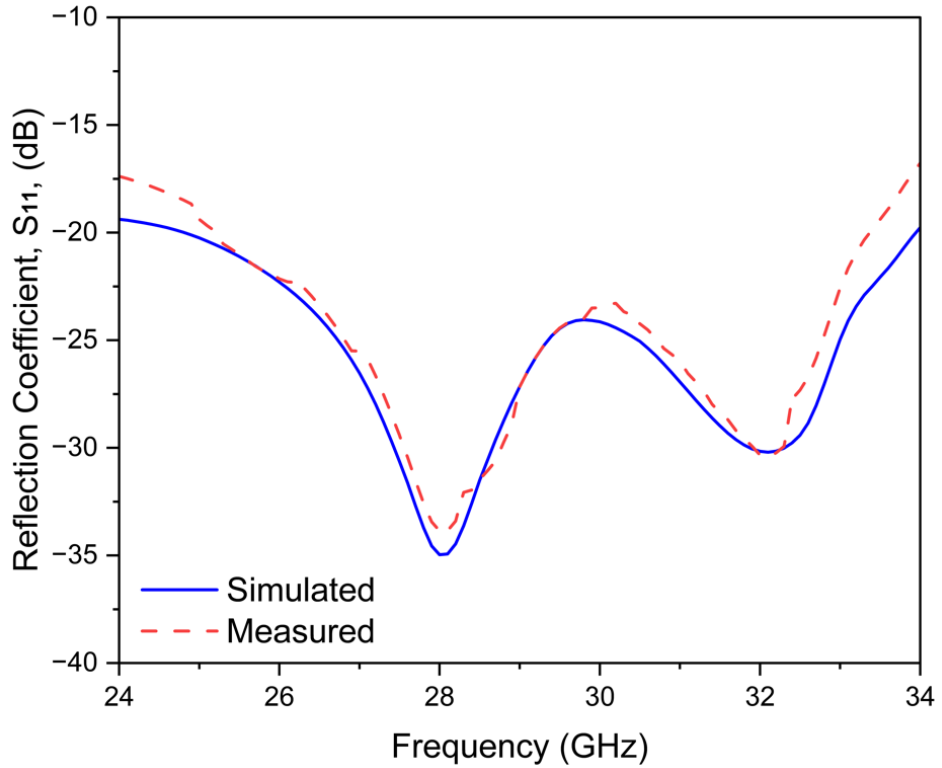


Figure 4.18: Reflection coefficient of the simulated and measured proposed phased array.

verifying that the phased array maintains efficient operation across the entire frequency range required for 5G V2X applications. The strong agreement between the simulated and measured  $S_{11}$  results further supports the accuracy of the design.

The beamsteering radiation pattern and gain are measured using the TMYTEK beamforming system, designed for precise mmWave antenna testing. The TMYTEK beamforming system is an integrated mmWave testing platform that includes a phased array front-end module, baseband interface, and control software. It allows programmable control over the phase of each antenna port through a user-friendly software interface, enabling real-time beamsteering without manual reconfiguration. The system supports a wide frequency range and is well-suited for rapid prototyping and validation of 5G phased array antennas. In this setup, the TMYTEK system was used to provide four-port phase-shifted excitation to the antenna under test (AUT), enabling dynamic control of the beam direction by programming specific phase differences between the ports. Radiation pattern measurements are conducted in an anechoic chamber, where the beam is steered across different angles, and the radiated power is recorded using a calibrated receiver. The gain of the AUT is calculated by comparing the received power from the AUT with the reference antenna, using the following equation [144]

$$G_{\text{AUT}} = G_{\text{ref}} + 10 \log_{10} \left( \frac{P_{\text{AUT}}}{P_{\text{ref}}} \right), \quad (4.2)$$

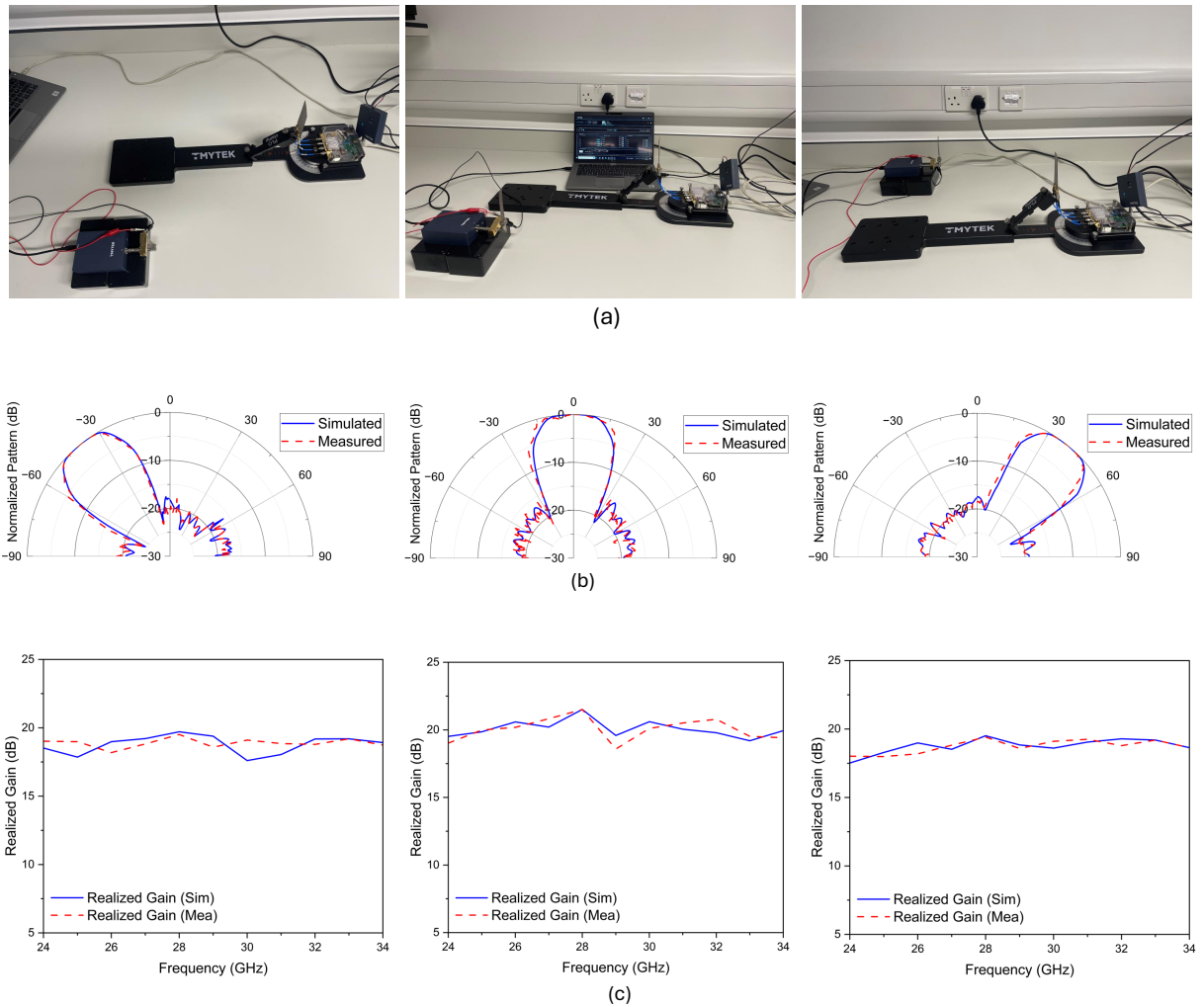


Figure 4.19: Experimental validation of the proposed phased antenna array. (a) Measurement system and the prototype. (b) Simulated and measured radiation pattern. (c) Simulated and measured realized gain.

where  $G_{\text{ref}}$  is the gain of the reference antenna,  $P_{\text{AUT}}$  is the power received from the AUT, and  $P_{\text{ref}}$  is the power received from the reference antenna. Fig. 4.19 shows the measurement system and the measured beam angles of  $-39^\circ$ ,  $0^\circ$ , and  $+39^\circ$ , revealing the phased array's precise beamsteering ability with minimal degradation in gain across the steering range. This confirms the design's robustness for consistent performance at varying angles.

Additionally, Table 4.1 highlights how the proposed design outperforms existing state-of-the-art solutions, offering superior realized gain while maintaining lower implementation complexity. The design successfully balances high performance and cost-efficiency, making it an attractive option for 5G V2X applications requiring dynamic coverage and reduced interference.

Table 4.1: Comparison of the proposed work with other similar works.

| Ref.       | Freq (GHz) | No. of layers | Gain | Steering range |
|------------|------------|---------------|------|----------------|
| [14]       | 28         | 7             | 22   | $\pm 55^\circ$ |
| [13]       | 28         | 1             | 7.95 | $\pm 18^\circ$ |
| [15]       | 28         | 3             | 13.2 | $\pm 22^\circ$ |
| [145]      | 27         | 3             | 11.6 | $\pm 39^\circ$ |
| Prop. work | 28         | 1             | 21.5 | $\pm 39^\circ$ |

## 4.6 Summary

This chapter focused on advancing the design of LP patch antennas for 5G V2X applications by developing beamsteering capabilities. The design was extended to a 2x9 and 4x9 series-fed LP patch antenna array, achieving higher realized gain while continuing to offer the wide impedance bandwidth required for 5G V2X applications. The 2x9 array demonstrated an enhanced realized gain of 17.9 dBi, while the 4x9 array further increased the realized gain to 21.1 dBi, both maintaining the wide impedance bandwidth. While these arrays provided improved directional control, their fixed beam direction posed limitations in highly dynamic vehicular environments, where the communication link must adapt rapidly to changing conditions. To overcome this limitation, a phased array with four ports was introduced to enable dynamic beamsteering, allowing flexible beam control over  $\pm 39^\circ$  per unit. A proposed structure using four phased array units achieved full  $360^\circ$  coverage, which supported multiple configurations of  $90^\circ$ ,  $180^\circ$ , and  $270^\circ$ , depending on the communication needs. The phased array's performance was validated through simulation and experimental testing, demonstrating high realized gain and precise beamsteering capabilities. Although this chapter addressed the challenge of adaptability, it was limited to LP designs. This motivated the exploration of CP antennas, developed from LP antenna, in the next chapter to enhance signal stability and mitigate polarization mismatches in complex vehicular environments.

# Chapter 5

## Circularly Polarized Antenna Design

The preceding chapters have focused on the designing and development of LP antennas, demonstrating their capability to meet the high-performance demands of 5G V2X communications through wide impedance bandwidth, increased gain, and beamsteering techniques. However, CP antennas offer significant advantages for mmWave band applications, particularly in improving signal stability and mitigating polarization mismatches in dynamic vehicular environments. In this chapter, techniques are introduced to transform the single-element LP patch antenna into a CP antenna, achieving wide impedance bandwidth and wide axial ratio essential for 5G V2X communication requirements. After validating the performance of the CP single element, the design is further developed into a 9-element series-fed CP patch antenna array to enhance gain while maintaining the circular polarization benefits. This work aligns with *O4*, focusing on advancing antenna designs to support robust and reliable communication in next-generation vehicular networks.

### 5.1 Introduction

CP antennas are gaining increasing recognition for their ability to address key challenges in mmWave communications, particularly for 5G V2X applications. One of the main advantages of CP antennas is their resilience to polarization mismatches and multipath interference, which are common issues in dynamic environments like vehicular networks [146]. A wide variety of CP antenna designs have been explored in the literature, including microstrip patch antennas [147], cavity-backed slot antennas [148], and magneto-electric dipole antennas [149], [150]. These designs have significantly contributed to improving both impedance and AR bandwidths, which are critical for CP antenna performance. However, many existing configurations often involve complex structures, leading to increased fabrication costs and difficulty in implementation.

For future V2X communication systems, where high data rates and reliable connectivity

are essential, there is a growing need for CP antennas that offer a balance between performance and simplicity. Wide impedance bandwidth and wide AR bandwidth are essential requirements for maintaining reliable signal transmission, even in environments prone to reflection and scattering [151]. This chapter introduces a technique to transform the single-element LP patch antenna developed in previous chapters into a CP antenna, achieving both wide impedance bandwidth and AR bandwidth to meet the stringent demands of future vehicular networks.

To further enhance the antenna's performance, particularly in increasing gain while maintaining wide impedance bandwidth, the CP single element is developed into a 9-element series-fed CP patch antenna array. This array configuration improves gain while retaining the advantages of circular polarization, making the design suitable for long-range, high-performance communication in 5G V2X environments. By arranging the elements in a series-fed configuration, the array not only increases gain but also ensures consistent polarization and beam stability across the operational frequency band, addressing the demanding requirements of vehicular communication systems [152].

## 5.2 Contributions

This chapter presents significant advancements in CP antenna design, focusing on the development of efficient, cost-effective solutions to meet the unique demands of 5G V2X communication systems. CP antennas offer substantial benefits over LP antennas, particularly in mitigating polarization mismatches and enhancing signal stability in dynamic vehicular environments. The work addresses key challenges related to achieving wide impedance bandwidth, wide AR bandwidth, and high gain, all critical for maintaining reliable communication in the mmWave band. By employing innovative techniques, including the incorporation of air gaps and cross-stubs, the proposed CP antenna designs successfully achieve both wide impedance and AR bandwidths, positioning them as ideal candidates for high-performance applications in 5G V2X networks. These designs also address the complexity and cost issues typically associated with mmWave antennas, offering practical solutions that maintain performance while reducing implementation challenges. Through simulation, fabrication, and experimental validation, the chapter demonstrates how the proposed designs meet the stringent requirements of next-generation vehicular communication systems, making meaningful contributions to the field. The contributions of this work can be summarized as follow:

- Design of a CP single-element antenna: A novel CP antenna is generated by applying the air gap technique to an LP annular ring patch antenna, achieving an AR bandwidth of 6.42%. This design also maintains a wide impedance bandwidth of 35.71%, ensuring consistent performance across the operational frequency range.

- AR bandwidth enhancement: To overcome the limitation of AR narrowband, the cross-stubs technique is applied to the LP antenna, resulting in an AR bandwidth of 20.35%.
- Development of a 9-element series-fed CP patch antenna array: The single-element CP antenna is extended into a series-fed array, achieving a realized gain of 15.2 dBi and low SLLs exceeding -17 dB. This array configuration enhances gain and beam stability while maintaining the benefits of circular polarization.

The organization of this chapter is as follows: The first section covers the development of the CP single-element antenna, including the techniques used to achieve wide impedance and AR bandwidths. The subsequent sections detail the design progression to a 9-element series-fed CP antenna array, focusing on gain improvement and polarization consistency. Finally, the chapter concludes with the simulation and experimental validation results, comparing the proposed designs against existing solutions to demonstrate their suitability for 5G V2X communication environments.

## 5.3 Circularly Polarized Patch Antenna

In the pursuit of optimizing antenna performance for 5G V2X applications, CP antennas have garnered significant attention due to their ability to mitigate polarization mismatches and enhance signal stability in dynamic vehicular environments. This section focuses on the development of a single-element CP patch antenna, which leverages two distinct techniques to achieve circular polarization: the air-gaps technique and the cross-stubs technique. These approaches are implemented to achieve wide AR bandwidth and wide impedance bandwidth, both of which are crucial for maintaining reliable communication across the mmWave band. By building upon the design principles established in the LP patch antenna in 3.4.1, the following subsections detail the design configuration, simulation, and measurement analysis of the proposed CP patch antenna.

### 5.3.1 Antenna Configuration and Analysis

#### Air-Gaps Technique

The structure of the proposed CP patch antenna is shown in Fig. 5.1 (a). The parameter values for the LP patch antenna, which is introduced in 3.4.1, have been predetermined and remain fixed. The distinguishing feature between the LP and CP patch antennas is the inclusion of air gaps in the annular ring of the LP patch antenna, which are essential for generating CP. The dimensions of these air gaps are defined by the angles  $\phi_1$  and  $\phi_2$ . Adjusting the width and position of these gaps enables the achievement of the

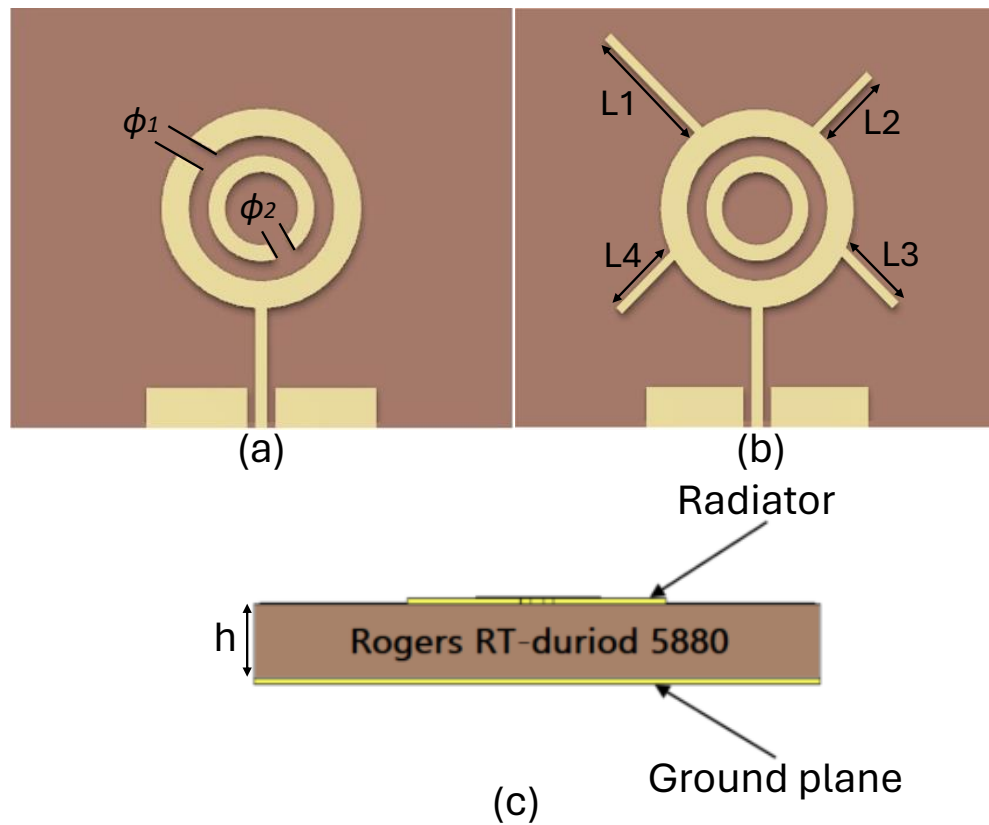


Figure 5.1: Structure of the circularly polarized antenna (a) air-gaps (b) cross-stubs (c) side view.

desired AR. Repeated simulations have demonstrated that modifications in the width of the gap angles significantly affect the AR, indicating their critical role in optimizing CP performance. Accordingly, the parameters  $\phi_1$  and  $\phi_2$  are adjusted based on optimization results to enhance CP performance, being set to  $270^\circ$  and  $70^\circ$ , respectively. The work in [153] theoretically demonstrated that by introducing a gap of a specific width and position in a loop antenna equipped with a coaxial probe, it is possible to excite a traveling-wave current distribution on the loop. This excitation is crucial for achieving CP. This principle guided the adjustment of the air gaps in this design to optimize the CP patch antenna's performance. To clarify the underlying design methodology, the air gaps disrupt the current distribution symmetry along the ring, leading to the excitation of two orthogonal modes. When these modes are properly phase-shifted, typically by  $90^\circ$ , circular polarization is achieved. In this design, the angular positioning and widths of the gaps were optimized to ensure these orthogonal components are equal in magnitude and in quadrature phase, a requirement for effective CP generation.

### Cross-Stubs Technique

The designs presented in this study aim to provide a wide AR bandwidth. Due to the limitations of the AR band using the air-gaps technique, the cross-stubs technique is employed to achieve an extensive AR bandwidth. The structure of the suggested stubs antenna, shown in Fig. 5.1 (b), features four orthogonally aligned linear stubs arms connected to an outer annular ring [154]. These stubs, labeled as  $L_1$ ,  $L_2$ ,  $L_3$ , and  $L_4$ , have identical widths ( $W_s$ ) and are strategically positioned to enhance the matching and generate the required phase shift for achieving CP. Adjustments in the lengths and placements of these stubs enable the attainment of CP. Positioned at angles of  $45^\circ$ ,  $135^\circ$ ,  $225^\circ$ , and  $315^\circ$  relative to the feedline, these four distinctively narrow stubs contribute to a wide AR bandwidth. The study conducted a detailed parametric analysis of these stubs, setting their widths at 0.16 mm and lengths at 2.08 mm, 1.34 mm, 1.08 mm, and 1.41 mm, respectively. Simulations analysis are conducted using CST studio software to achieve the desired outcomes. To clarify the mechanism, the orthogonal stubs introduce asymmetry and localized current paths that support the generation of two orthogonal modes. By fine-tuning their lengths, the required  $90^\circ$  phase difference is achieved between these modes, resulting in circular polarization. Moreover, unlike the air-gaps technique, which provides a narrow axial ratio bandwidth, the cross-stubs enable stronger and more distributed coupling to the outer ring. This facilitates a broader range of phase and amplitude conditions that maintain CP over a wider frequency band, thereby significantly enhancing the axial ratio bandwidth.

### 5.3.2 Simulation Analysis of CP Antennas

The simulation  $S_{11}$  for both CP designs is maintained similarly to the LP, as shown in Fig. 5.2, covering a wide impedance bandwidth of 35.17% (24 to 34 GHz). This demonstrates the antenna design's capability to support a broad range of mmWave applications, including 5G V2X communications, with the CP design further enhancing this capability by offering superior multipath interference mitigation and maintaining signal integrity across a wide bandwidth. To achieve circular polarization, the LP antenna design is modified using two techniques. Initially, air gaps are inserted into both the outer and inner annular rings, as depicted in Fig. 5.1 (a), effectively generating CP. This modification results in an AR bandwidth of 6.42% (AR < 3 dB within 27.2 - 29 GHz), as illustrated in Fig. 5.3. To address the AR bandwidth limitation present in the air gaps technique, the cross-stubs technique is subsequently applied, significantly expanding the AR bandwidth to 20.35% (AR < 3 dB within 26.4 - 32.1 GHz), as presented in Fig. 5.3. This adaptation of the LP design to meet CP requirements underscores the adaptability and potential of the antenna for 5G V2X applications.

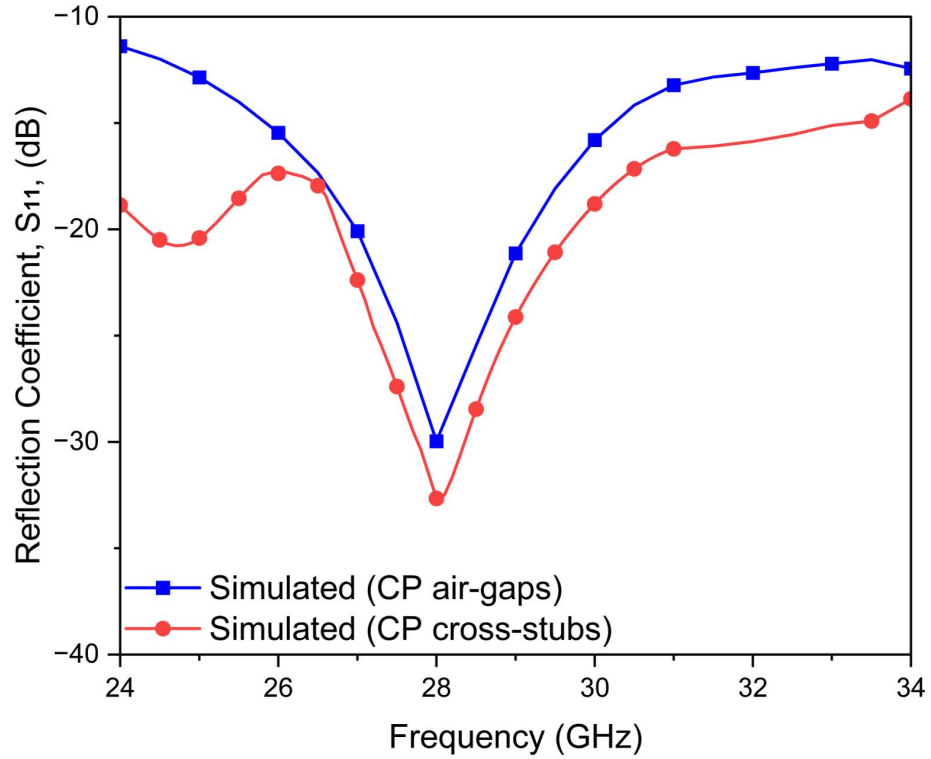


Figure 5.2: Simulated reflection coefficient of the proposed CP antennas.

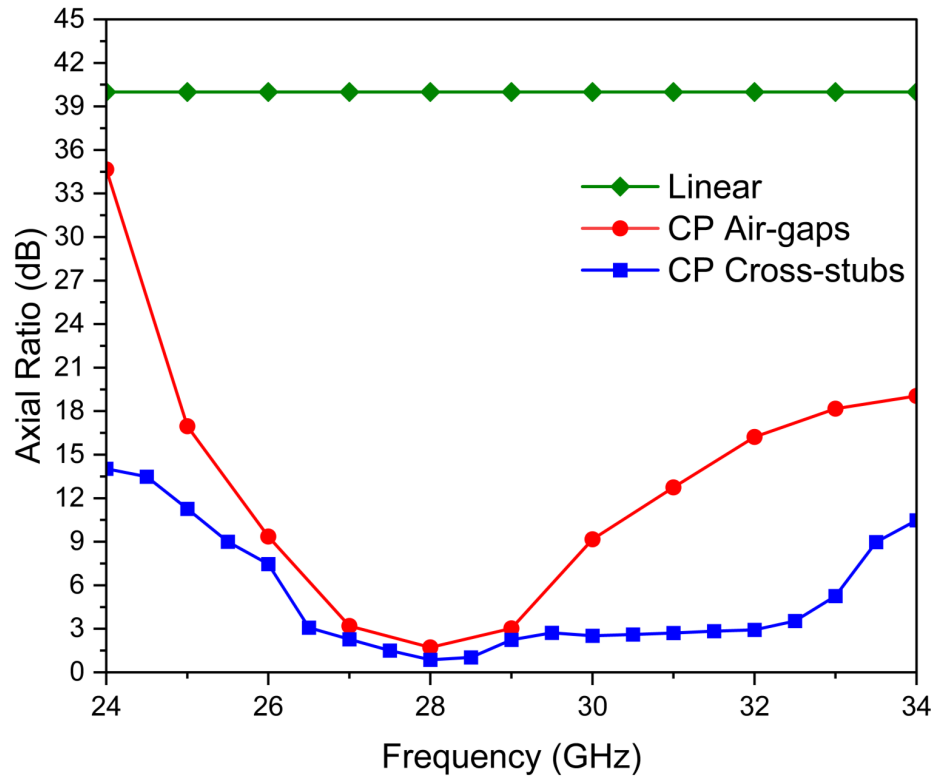


Figure 5.3: Axial ratio in the process of the CP antennas evolution.

### 5.3.3 Experimental Validation and Discussion

The proposed CP patch antennas have been fabricated using PCB technology and subsequently measured to validate the simulated results, as illustrated in Fig. 5.4. The antennas are fabricated on a Rogers RT-duroid 5880 substrate, maintaining dimensions identical to those of the proposed LP patch antenna design. The  $S_{11}$  is measured using a mmWave VNA and a  $50 \Omega$  coaxial cable. The AR bandwidth, gain, and radiation pattern are measured using a far-field mmWave measurement system, specifically the Rohde & Schwarz ATS800B, a CATR benchtop OTA system.

The  $S_{11}$  for the proposed antennas, both simulated and measured, are depicted in Fig. 5.5. These antennas exhibit a wide impedance bandwidth covering from 24 GHz to 34 GHz (35.71%), confirming the effectiveness of the simplified antenna design in achieving extensive bandwidth for 5G V2X applications. Furthermore, there is a notable correlation between the  $S_{11}$  results obtained from simulations and measurements.

Fig. 5.6 illustrates the AR for the developed CP antennas, determined through both simulation and measurement. With an AR below 3 dB, the antenna incorporating the air-gaps technique achieves a CP bandwidth of 6.42% across the range of 27.2 GHz to 29 GHz. Additionally, utilizing the cross-stubs technique, the antenna secures an AR bandwidth of 20.35%, covering from 26.4 GHz to 32.1 GHz. The strong correlation between the simulated and actual AR measurements further reinforces the precision of the proposed antennas' performance.

Radiation efficiency and realized gains, both simulated and measured, for the CP antennas are depicted in Fig. 5.7. The air-gaps technique achieves a peak realized gain of 5.5 dBi, whereas the cross-stubs technique results in a realized gain of 5.7 dBi, each measured at a frequency of 28 GHz. Additionally, the antennas demonstrate a radiation efficiency of 94%.

The radiation patterns of the proposed CP antennas at 28 GHz are shown in Fig. 5.8, obtained using a far-field mmWave measurement system. Simulations and measurements of the antenna's radiation are conducted on both the E and H planes at  $0^\circ$  and  $90^\circ$ , respectively. The proposed CP antennas radiate a left-hand circularly polarized (LHCP) pattern with a high cross-polarization of -30 dB. A strong alignment between simulated and actual measurement results substantiates the effectiveness of the design approach, with the observed slight variations attributable to common fabrication tolerances and experimental setup discrepancies. These findings not only validate the antenna's design but also emphasize the robustness of the simple structures in achieving superior performance for 5G V2X applications.

Table 5.1 compares the proposed CP designs against state-of-the-art works, focusing on complexity and cost. Existing literature showcases mmWave band designs achieving wide impedance bandwidth and AR band through complex, multi-layered structures. In

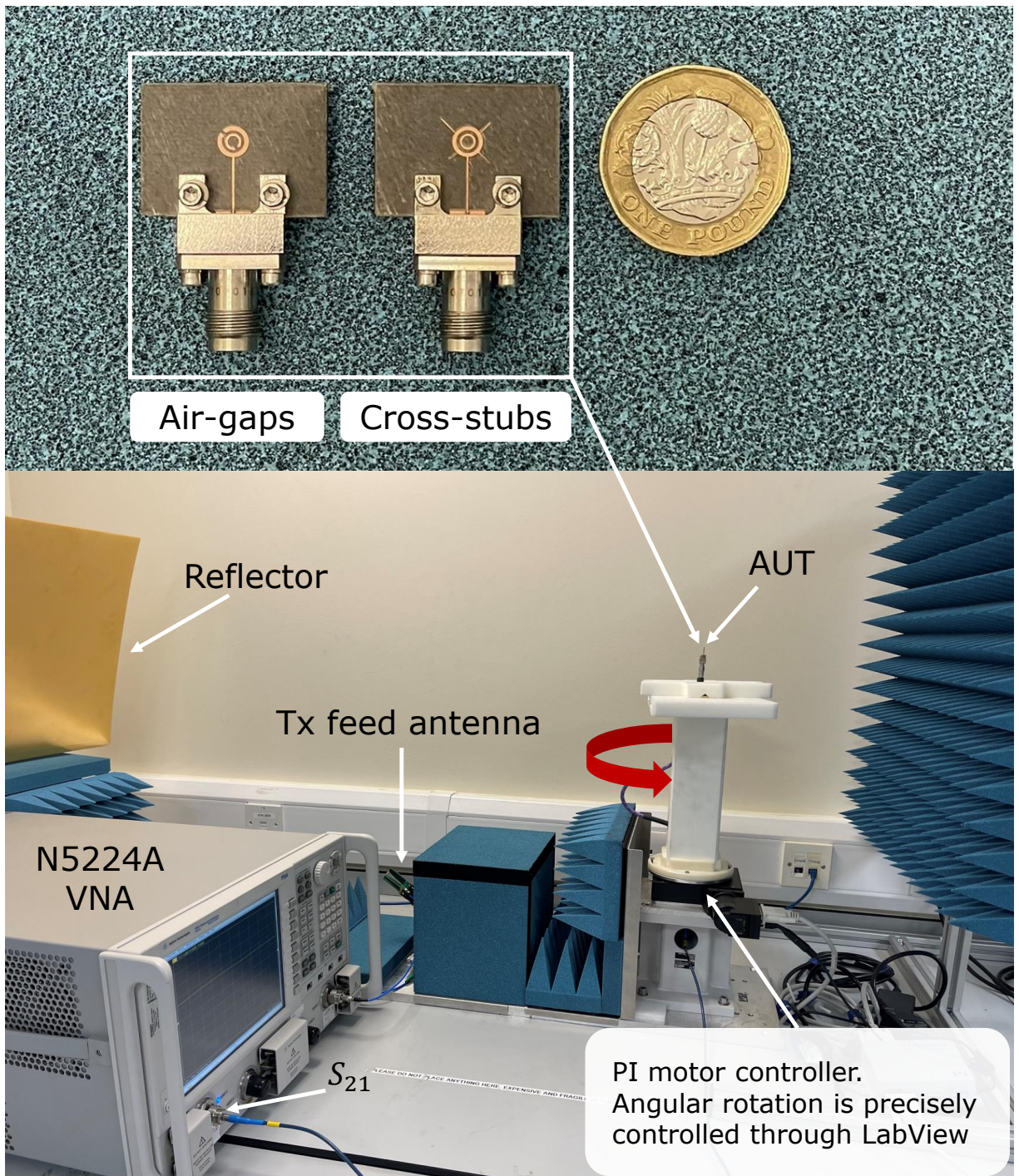


Figure 5.4: Measurement system and the CP antennas prototype.

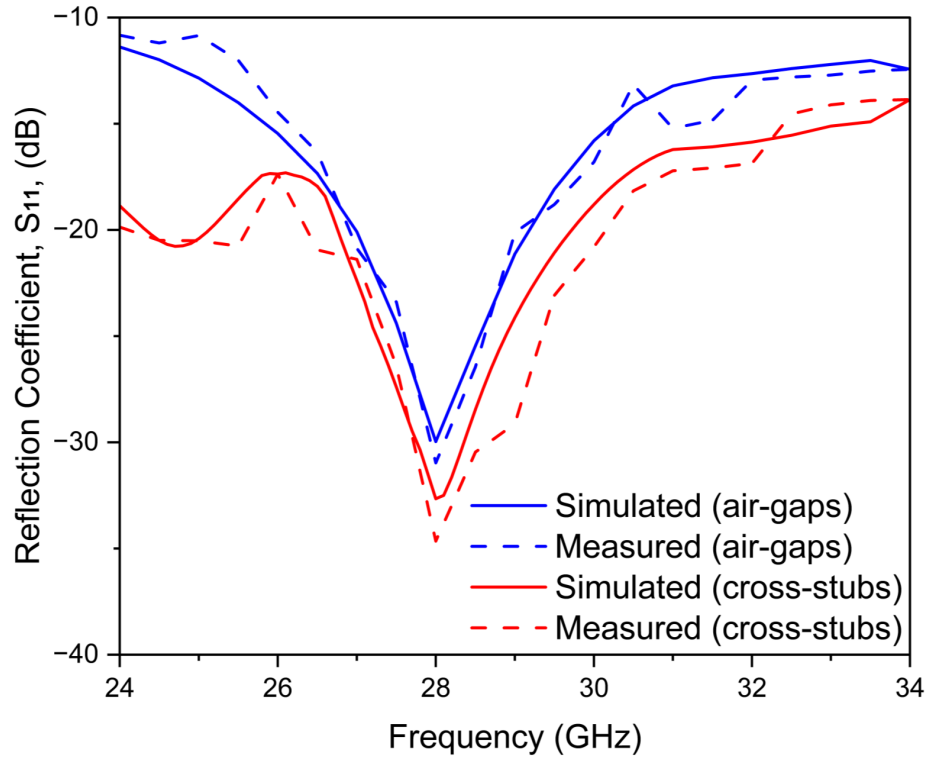


Figure 5.5: Reflection coefficient of the simulated and measured CP antennas.

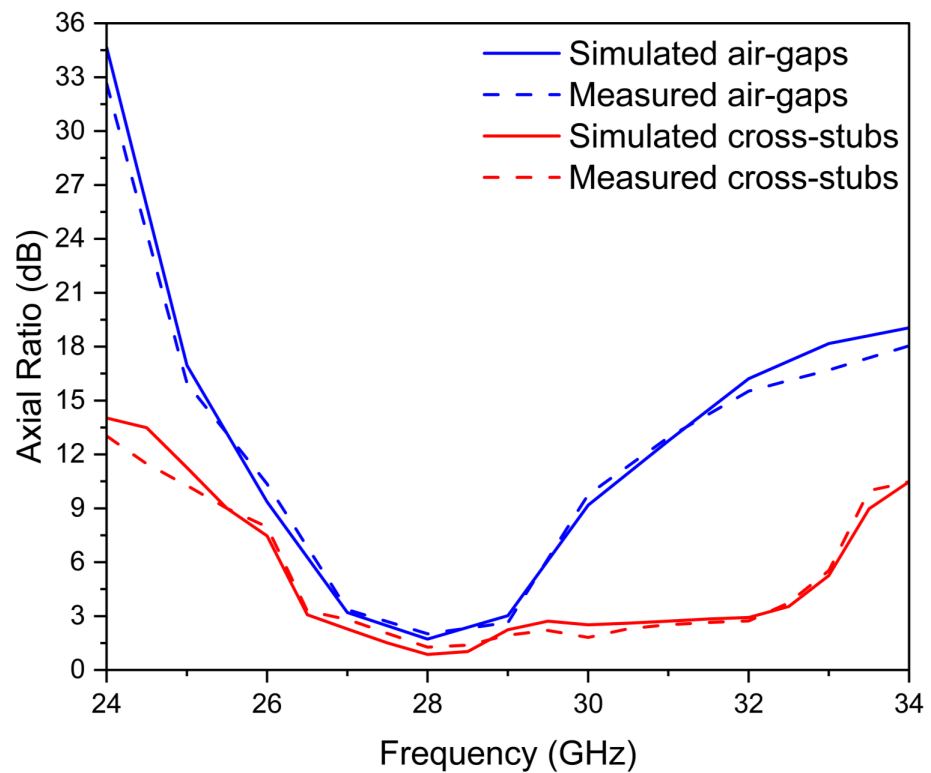


Figure 5.6: Simulated and measured AR of the proposed CP antennas.

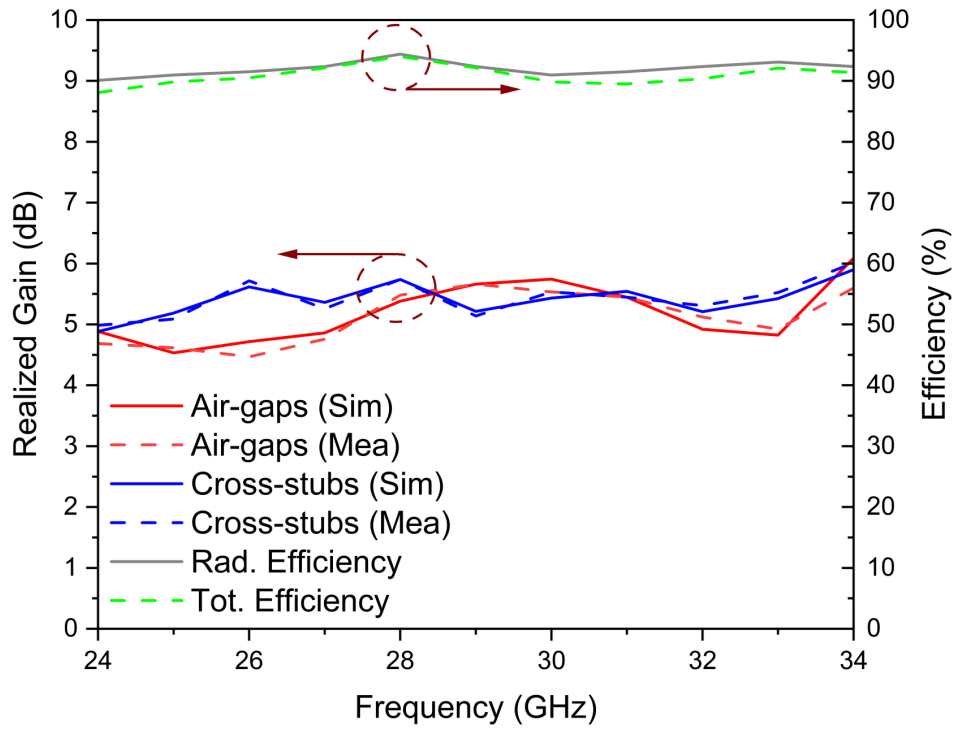


Figure 5.7: Simulated and measured gain and efficiency for the proposed CP antennas.

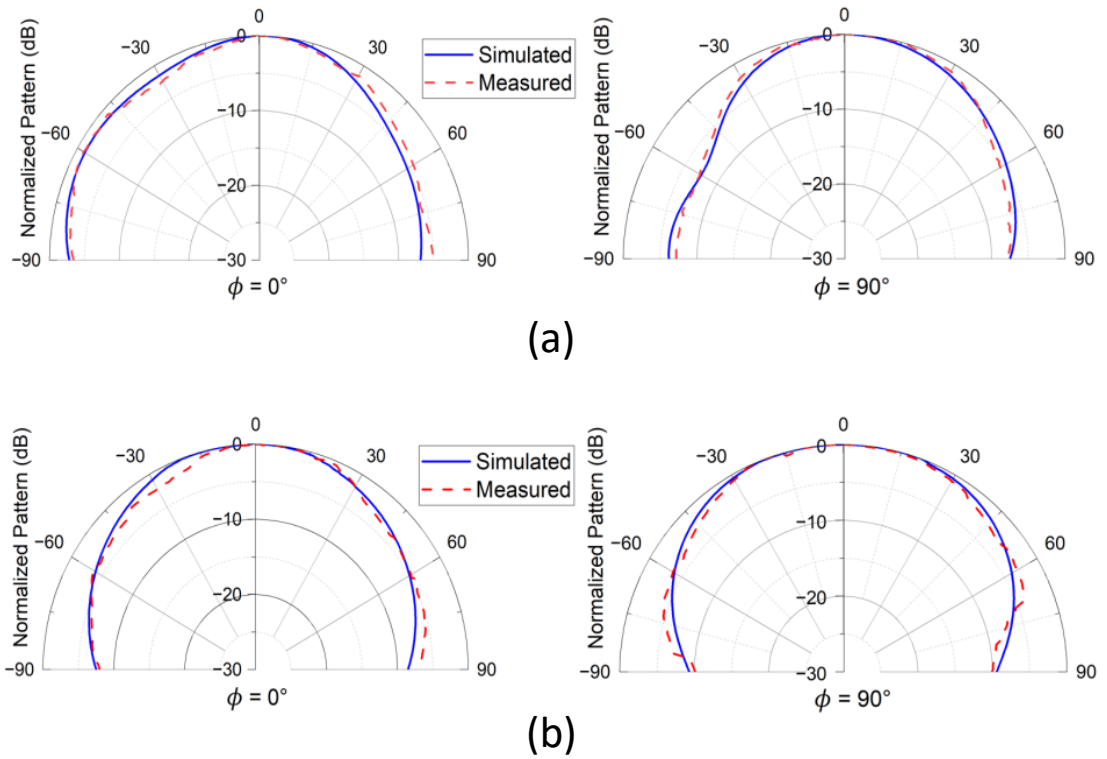


Figure 5.8: Simulated and measured radiation pattern of CP antennas (a) air-gaps and (b) cross-stubs.

Table 5.1: Comparison of the proposed CP design with other closely related works.

| Ref.       | Freq (GHz) | No. of layers | Volume ( $mm^3$ ) | IBW%  | AR%   |
|------------|------------|---------------|-------------------|-------|-------|
| [147]      | 27         | 3             | 971.24            | 29.6  | 7.14  |
| [124]      | 27.5       | 1             | 246.88            | 8.12  | 4.2   |
| [150]      | 28         | 2             | 950               | 24.6  | 18.1  |
| [155]      | 28         | 1             | 631.68            | 5.05  | 2.5   |
| [156]      | 28         | 4             | 556.22            | 10.89 | 8.57  |
| Prop. work | 28         | 1             | 228.23            | 35.71 | 20.35 |

contrast, the proposed designs simplify the approach. By integrating the air-gaps and the cross-stubs techniques into the low-profile LP annular ring patch antenna, the designs achieve high performance with a single layer and a straightforward feeding mechanism. This innovation underscores the design's ease of fabrication and leads to reduced costs, presenting a practical yet effective solution in 5G V2X antenna design.

## 5.4 Circularly Polarized Patch Antenna Array

The single-element CP patch antenna successfully achieves wide impedance bandwidth and an extended axial ratio bandwidth, meeting the requirements for 5G V2X applications. However, for enhanced performance, particularly to mitigate the effects of atmospheric attenuation in mmWave frequencies, increasing the antenna's gain becomes crucial. To accomplish this, the single element is further developed into a 9-element series-fed CP patch antenna array. This array configuration not only enhances the realized gain but also retains the benefits of circular polarization, ensuring stable and reliable communication in dynamic vehicular environments. The following section presents the design, simulation, and experimental validation of the 9-element series-fed CP patch antenna array.

### 5.4.1 Antenna Configuration and Analysis

The proposed 9-element series-fed CP patch antenna array is illustrated in Fig. 5.9. The array configuration consists of nine elements symmetrically arranged around the central element (for example, element 1 mirrors element 9, and element 2 mirrors element 8, etc.), ensuring balanced radiation and consistent performance. The design process starts with the central element, labeled as element 5, which maintains the same dimensions established for the CP single element, as shown in Fig. 5.1 (b). To further enhance performance, the widths of the remaining array patches are calculated using an aperture scaling method specifically aimed at optimizing SLLs. A Dolph-Chebyshev weighting technique is applied in this design, which effectively manages the trade-off between beamwidth and SLLs,

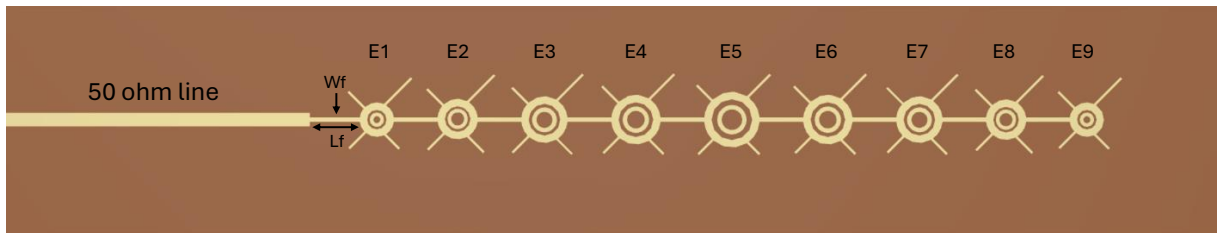


Figure 5.9: Structure of the proposed series-fed CP patch antenna array.

key factors in ensuring optimal array performance. The element weight values derived from the Dolph-Chebyshev method are presented in Table 3.4. The tapering technique involves multiplying the weights of the individual elements,  $D_n$ , by the width of the central element, allowing precise determination of the widths for the remaining patches. This method results in a series of patches with varying widths,  $W_n$ , as illustrated in Fig. 5.9. The elements are spaced at half-wavelength intervals [135], a critical parameter that guarantees accurate inter-element feed connectivity and maintains the necessary input impedance of 50 ohms for each patch. The feedline dimensions,  $L_f$  and  $W_f$ , are set at 3.3 mm and 0.3 mm, respectively, which helps to standardize the array's input impedance at 50 ohms. A thin feedline with an impedance of 100 ohms is used across the array to differentiate it from the patch elements and to ensure efficient impedance matching. By incorporating the Dolph-Chebyshev weighting, this design not only standardizes the input impedance across all elements but also optimizes critical performance metrics, such as beamwidth and SLLs. The resulting series-fed CP patch antenna array successfully meets the requirements of mmWave applications, offering high precision, stable performance, and enhanced reliability, making it well-suited for next-generation communication systems.

#### 5.4.2 Simulation Analysis of Series-Fed CP Antenna Array

The design of the proposed series-fed CP antenna array is analyzed with the objective of increasing the gain of the single element. The mmWave band necessitates high gain to overcome atmospheric attenuation. Enhancing the gain of an antenna array is commonly achieved by increasing the number of its elements [136]. The proposed design is developed in two stages, as illustrated in Fig. 5.10, with the corresponding realized gains presented in Fig. 5.11. A 9-element series-fed CP patch antenna array is carefully selected and optimized for its ability to provide a high realized gain and maintain stable performance across the operational frequency range. As depicted in Fig. 5.11, the 9-element design achieves a realized gain of 15.2 dBi at 28 GHz, whereas the 7-element design has a realized gain of 12.9 dBi. Notably, the interconnecting feeds and the approach method are consistent in both designs. Moreover, the surface current at 28 GHz is shown in Fig. 5.12, illustrating the distribution along the proposed series-fed antenna array.

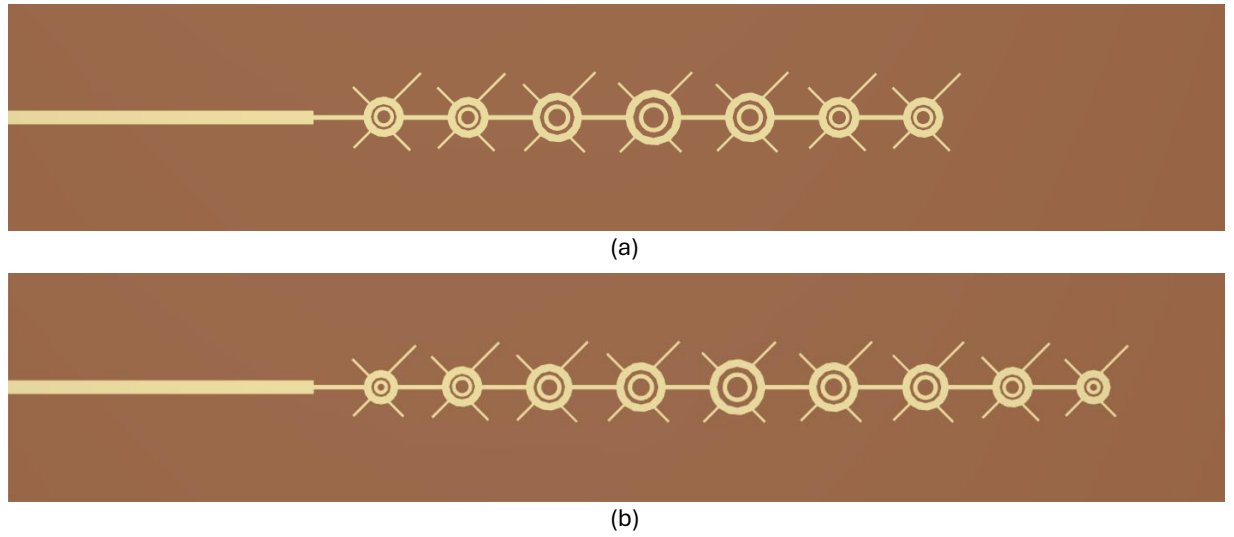


Figure 5.10: Evolution of the proposed CP antenna array (a) 7-element (b) 9-element.

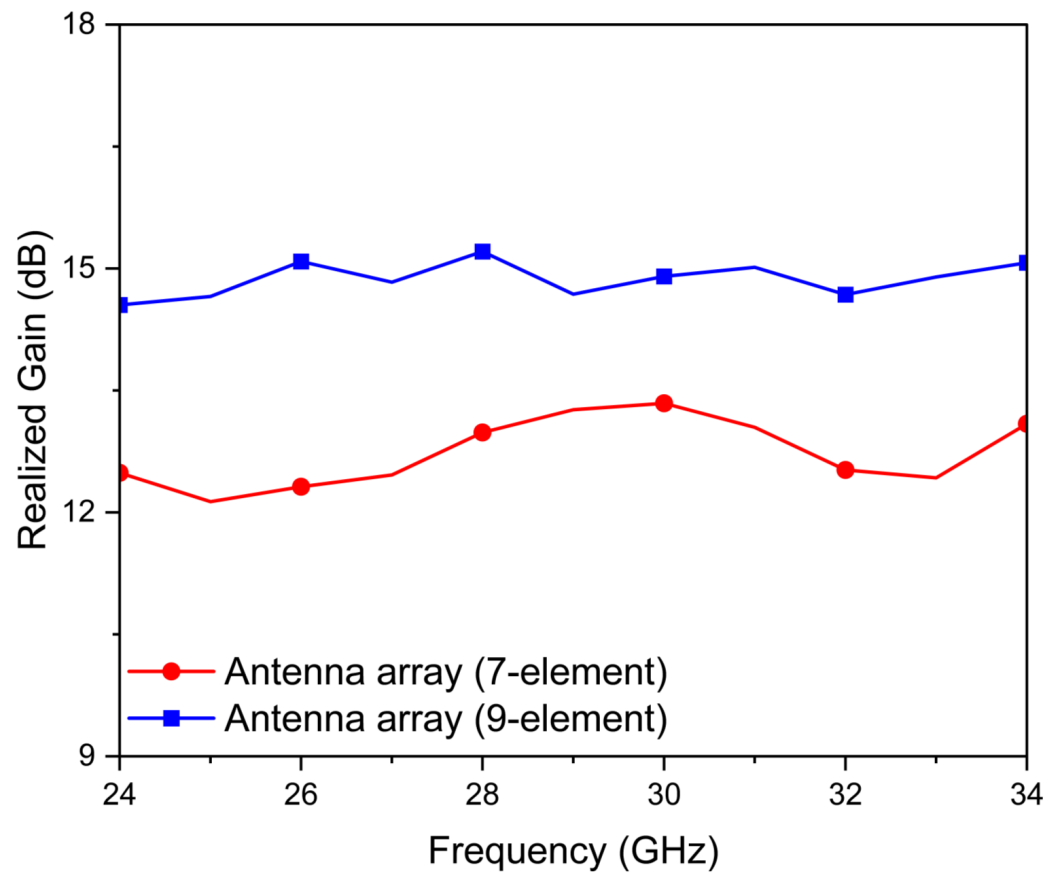


Figure 5.11: Evolution of the simulated gain for the proposed antenna array.

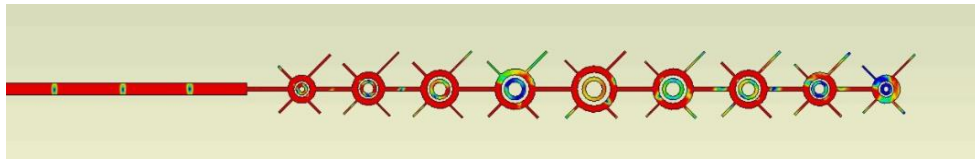


Figure 5.12: Current distribution of the proposed CP antenna array.

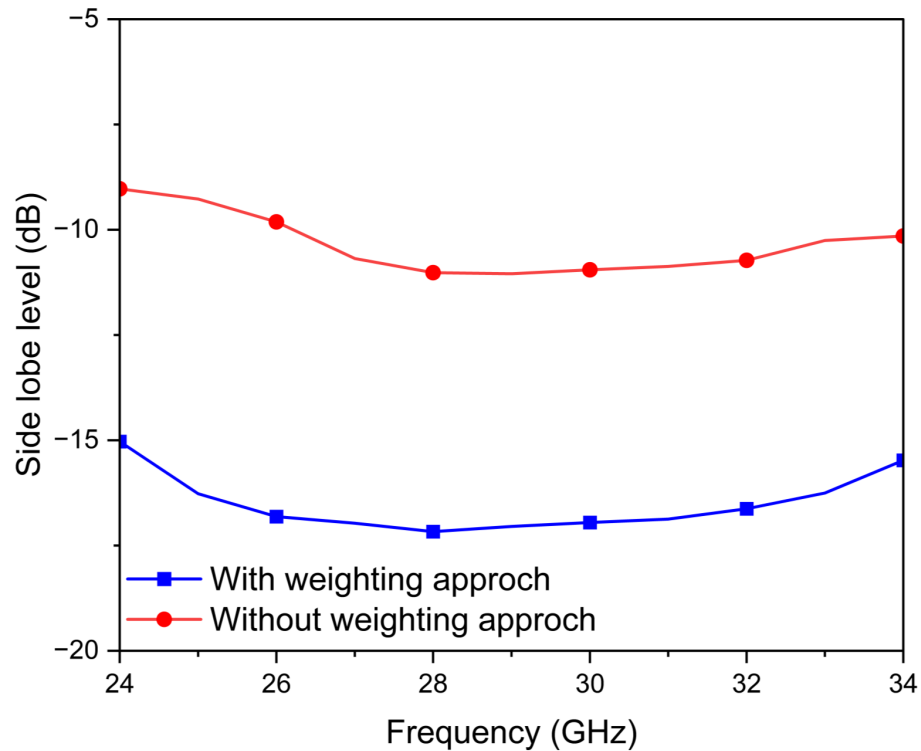


Figure 5.13: Sidelobe levels of the proposed CP antenna array.

As mentioned earlier, the Dolph-Chebyshev weighting approach is chosen to achieve SLLs. Fig. 5.13 illustrates the difference in SLLs achieved with and without applying this approach. By employing the Dolph-Chebyshev weighting method, the SLLs are significantly improved, reaching values exceeded  $-17$  dB. Conversely, when all patches are uniform in size, the SLLs are less optimal, around  $-11$  dB.

The design and simulation analysis reveal that the proposed series-fed CP antenna array, particularly the 9-element configuration, marks a significant step forward in enhancing mmWave system performance. By integrating the Dolph-Chebyshev weighting approach, it not only elevates the array's gain to  $15.2$  dBi but also refined the sidelobe levels to exceed  $-17$  dB. These achievements in high gain and low sidelobe level significantly bolster 5G V2X communications' reliability and reduce latency. High gain improves signal quality and reach, while optimized sidelobes minimize interference, ensuring faster, more stable connections.

### 5.4.3 Experimental Validation and Discussion

To verify the accuracy of simulation results, the designed series-fed CP patch antenna array is fabricated and subsequently measured. The antenna array is fabricated on a Rogers RT-duroid 5880 substrate, characterized by a dielectric constant of 2.2 and a thickness of 0.787 mm. Fig. 5.14 illustrates the setup for the measurements and a prototype of the innovative antenna. The gain, sidelobe levels, and radiation pattern of the antenna are measured using the far-field mmWave measurement system, specifically the Rohde & Schwarz ATS800B CATR benchtop OTA system. An OTA measurement setup is arranged in an open space within an indoor lab for assessing the antenna's far-field radiation pattern, sidelobe levels, and gain, as depicted in Fig. 5.14.

Fig. 5.15 displays the  $S_{11}$ , while Fig. 5.16 illustrates the AR for the proposed antenna array, each evaluated through both simulation and measurement. The antenna design is optimized to achieve a wide bandwidth, resulting in 10 GHz for  $S_{11}$  and 5.5 GHz for AR. These outcomes demonstrate a high degree of congruence between the simulated and experimental results, affirming the reliability of the simulation process.

The simulated and measured results for the realized gain and sidelobe levels are depicted in Fig. 5.17. An observed measured peak realized gain of 15.2 dBi at a frequency of 28 GHz corresponds closely to the simulation result. The antenna achieves its lowest sidelobe levels at -17 dB at 28 GHz, with levels remaining greater than -14 dB throughout its operational bandwidth. Furthermore, Fig. 5.18 illustrates the comparison between the radiation patterns obtained through simulations and measurements on the E and H planes (at  $0^\circ$  and  $90^\circ$ , respectively). The outcomes from both the simulation and measurement results closely align with each other.

Table 5.2 compares the proposed series-fed CP patch antenna array with existing designs, emphasizing simplicity, gain, and sidelobe levels. The proposed array design not only achieves the high gain necessary for overcoming mmWave atmospheric attenuation but does so with a streamlined, single-layer structure that reduces implementation complexity. Many existing designs rely on multi-layered configurations or intricate feeding mechanisms to achieve similar performance, which often increases fabrication challenges and costs. In contrast, the proposed design employs a straightforward series-fed network and a single-layer patch configuration, simplifying the fabrication process without compromising performance. Furthermore, it maintains excellent sidelobe performance, essential for minimizing interference and enhancing signal clarity. This combination of features underscores the array's suitability for advanced mmWave applications, such as 5G V2X communications.

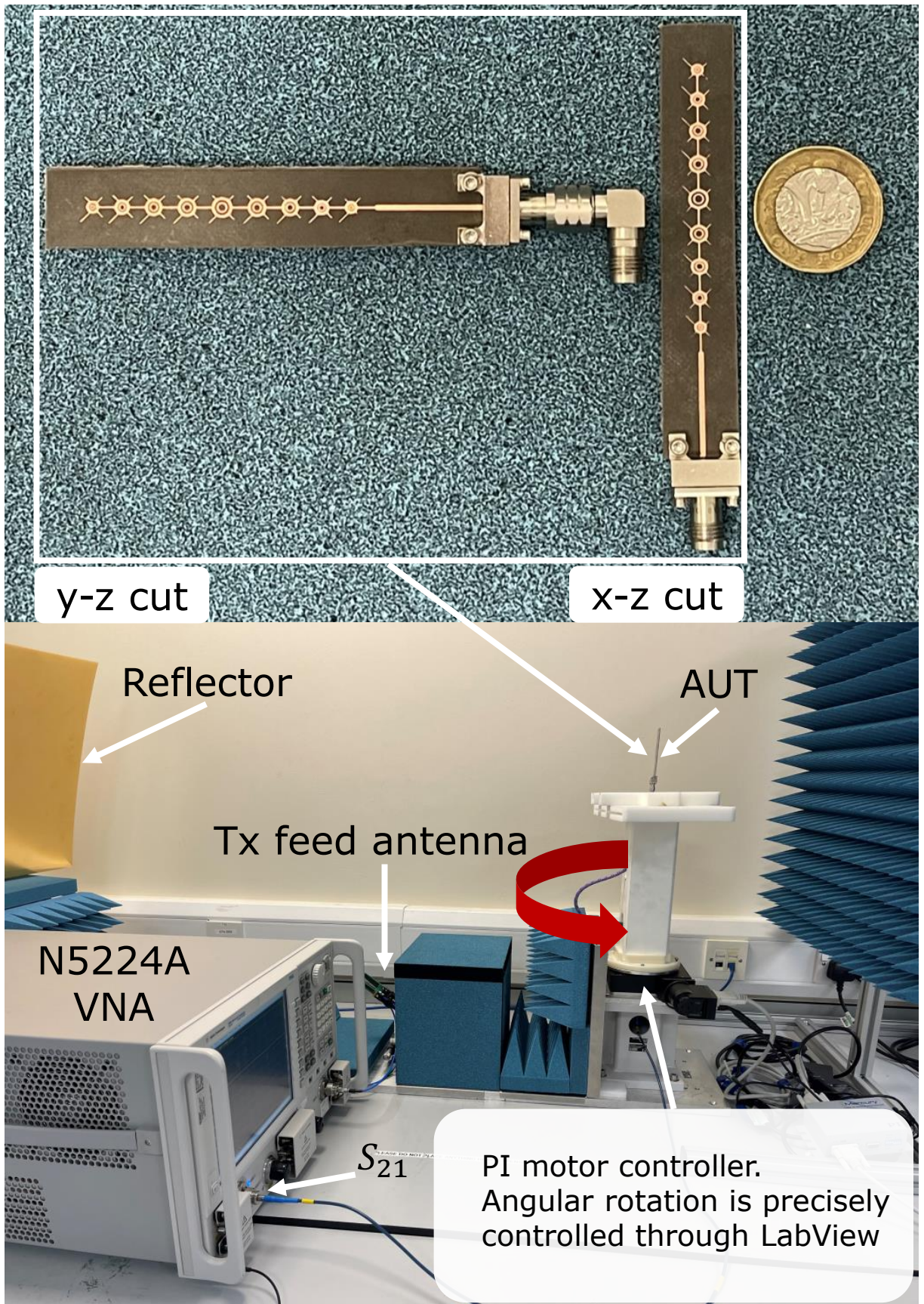


Figure 5.14: Measurement system and the CP antenna array prototype.

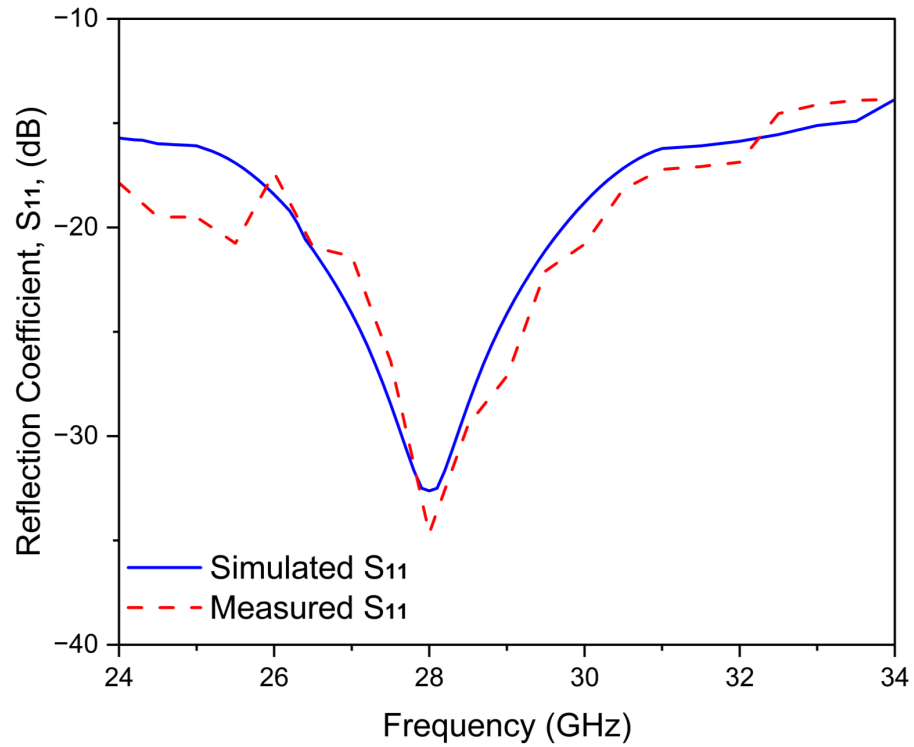


Figure 5.15: Simulated and measured  $S_{11}$  of the proposed CP antenna array.

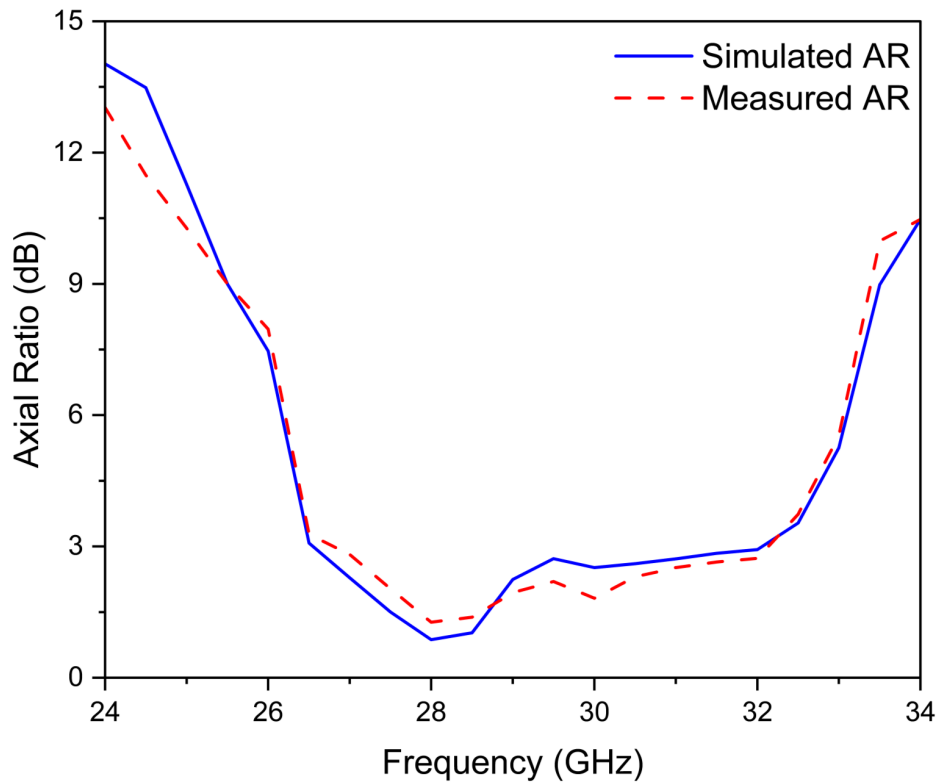


Figure 5.16: Simulated and measured AR of the proposed CP antenna array.

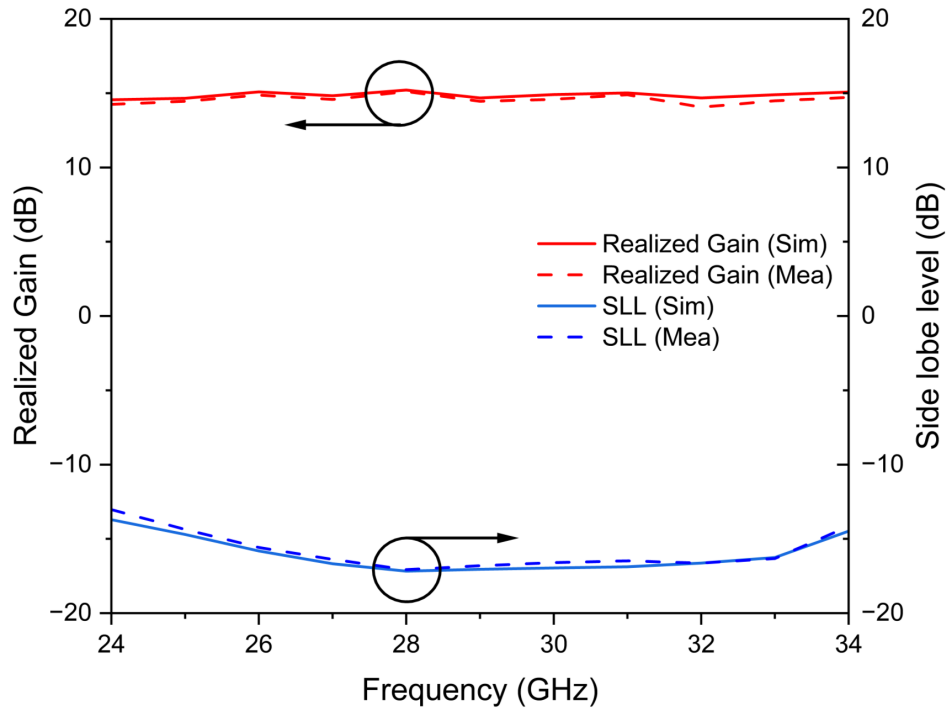


Figure 5.17: Simulated and measured realized gain and SLLs of the proposed CP antenna array.

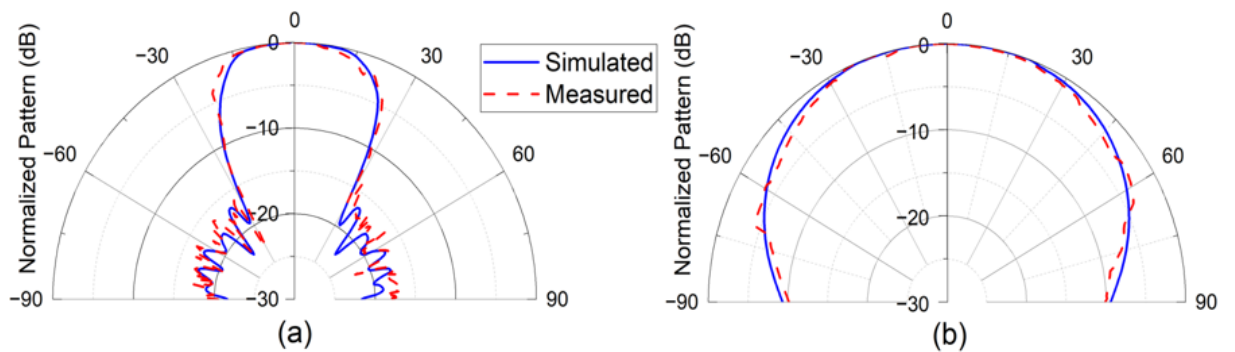


Figure 5.18: Simulated and measured radiation pattern of the proposed CP antenna array (a)  $\phi = 0^\circ$  and (b)  $\phi = 90^\circ$ .

Table 5.2: Comparison of the proposed CP array design with other similar works.

| Ref.       | Freq (GHz) | No. of layers | Volume ( $mm^3$ ) | Gain (dBi) | SLLs (dB) |
|------------|------------|---------------|-------------------|------------|-----------|
| [157]      | 28         | 4             | 1385              | 11.65      | -         |
| [126]      | 27         | 1             | 829.28            | 12.8       | -11.8     |
| [158]      | 28         | 1             | 5120              | 5          | -         |
| [159]      | 28         | 1             | 1463.4            | 10.9       | -18.8     |
| [160]      | 32.5       | 1             | 1050              | 10.95      | -15       |
| [161]      | 28         | 1             | 150               | 10.7       | -15       |
| [162]      | 28         | 3             | 1476.5            | 15.08      | -23.7     |
| Prop. work | 28         | 1             | 944.4             | 15.2       | -17       |

## 5.5 Summary

This chapter presented the design and development of CP antennas for 5G V2X communications, addressing the critical need for enhanced signal stability and mitigation of polarization mismatches in dynamic vehicular environments. Initially, a single-element CP patch antenna was developed using two techniques: the air-gap method, which achieved an AR bandwidth of 6.42%, and the cross-stubs method, which significantly expanded the AR bandwidth to 20.35%. Both techniques ensured a wide impedance bandwidth of 35.17%, essential for supporting the broad range of mmWave applications inherent to V2X communications. However, the single-element design lacked the gain necessary to overcome atmospheric attenuation at mmWave frequencies, limiting its effectiveness in long-range vehicular communication scenarios. Building upon this foundation, the chapter progressed to the development of a 9-element series-fed CP patch antenna array, which enhanced the antenna's realized gain to 15.2 dBi while maintaining low SLLs exceeding -17 dB. This array configuration not only increased gain but also preserved the advantages of circular polarization, ensuring robust and reliable long-range communication in 5G V2X environments. Comprehensive simulation and experimental validation confirmed the alignment between simulated and measured results, demonstrating the effectiveness of the proposed CP antenna designs in achieving high realized gain, wide AR and impedance bandwidths, and excellent SLLs performance. These advancements underscored the potential of the series-fed CP patch antenna array as a practical and efficient solution for next-generation vehicular communication systems, enhancing reliability and reducing interference in future communication networks.

# Chapter 6

## Conclusions and Future Works

The following conclusion summarizes the main findings of the research conducted throughout this thesis, highlighting the key contributions in antenna design and their significance for 5G V2X communication systems. Additionally, potential avenues for future research are discussed, outlining how the work presented here can be further expanded and enhanced.

### 6.1 Concluding Remarks

Chapter 3 introduced novel LP antenna designs for 5G V2X communications, focusing on achieving wide impedance bandwidth, high gain, and low SLLs to meet the stringent requirements of next-generation vehicular communication systems. The research began with the design of a rectangular patch antenna, which highlighted limitations in impedance bandwidth. To overcome these challenges, the design was improved by transitioning to an optimized annular ring patch antenna, achieving an impressive impedance bandwidth of 35.17%. Additionally, a 9-element series-fed LP patch antenna array was developed to enhance gain and mitigate atmospheric attenuation challenges associated with mmWave communications. Both simulation and experimental validation confirmed that the array achieved a realized gain of 16.6 dBi, with low SLLs of -17 dB. The combination of wide impedance bandwidth, high realized gain, and compact design demonstrated the effectiveness of the proposed solution, positioning it as a practical and efficient option for 5G V2X applications.

In Chapter 4, the LP patch antenna design was further extended to develop phased arrays capable of beamsteering for 5G V2X applications. This chapter presented the design and optimization of 2x9 and 4x9 series-fed LP antenna arrays, both of which maintained the wide impedance bandwidth necessary for reliable 5G communication. The 2x9 array demonstrated a realized gain of 17.9 dBi, while the 4x9 array increased the realized gain to 21.1 dBi. Building on these designs, a phased array with four ports

was developed, providing dynamic beamsteering over  $\pm 39^\circ$  per unit, enabling flexible beam control based on vehicular communication requirements. A proposed structure of four phased array units allowed for full  $360^\circ$  coverage, ensuring robust performance in highly dynamic vehicular environments. Results, validated through both simulation and experimental testing, confirmed the design's effectiveness in achieving high realized gain, beamsteering capability, and low SLLs, positioning the phased array as a flexible and reliable solution for 5G V2X applications.

In Chapter 5, the focus shifted to addressing the challenges related to polarization mismatches and signal stability in dynamic vehicular environments through the development of CP antennas. Building on the LP annular ring patch antenna design, a single-element CP patch antenna was introduced, utilizing innovative techniques such as air gaps and cross-stubs to achieve wide AR and impedance bandwidths. The air-gap method resulted in an AR bandwidth of 6.42%, while the cross-stubs technique significantly expanded the AR bandwidth to 20.35%. Both designs maintained a wide impedance bandwidth of 35.17%, ensuring compatibility with mmWave frequencies required for 5G V2X communications. The CP design was further extended into a 9-element series-fed CP patch antenna array, enhancing the realized gain to 15.2 dBi while maintaining low SLLs exceeding -17 dB. This CP array effectively addressed the critical need for high gain and stable communication links in dynamic vehicular environments, offering a robust solution for next-generation 5G V2X communication systems. Comprehensive validation through simulation and measurement demonstrated the practicality and effectiveness of the proposed CP antenna designs.

Overall, this thesis has made substantial contributions to advancing antenna technology for 5G V2X communications by addressing critical challenges related to wide impedance bandwidth, high gain, polarization mismatches, and beamsteering. Through comprehensive design, simulation, and experimental validation of innovative antenna solutions, this research provides practical, high-performance designs that meet the stringent requirements of next-generation vehicular networks. The thesis successfully developed solutions for both LP and CP antenna configurations, with significant improvements in impedance bandwidth, gain, and polarization stability, ensuring reliable communication in the highly dynamic and interference-prone environments of 5G V2X applications. Additionally, the integration of phased array beamsteering techniques enhances the flexibility and adaptability of the antenna systems, allowing for scalable and configurable coverage tailored to various vehicular communication scenarios. These advancements not only demonstrate real-world applicability through rigorous simulation and experimental validation but also offer the potential to shape 5G V2X deployments by providing robust, scalable, and cost-effective antenna designs. By addressing the complex challenges of mmWave communications, this thesis lays the groundwork for more reliable

and efficient vehicular communication networks, contributing to the wider adoption and successful implementation of 5G V2X technologies on a large scale. The findings and methodologies presented in this work are expected to support future innovations in antenna design, driving progress in autonomous driving, smart transportation, and other advanced vehicular communication systems.

## 6.2 Future Work

While this thesis has successfully addressed several key challenges in antenna design for 5G V2X communications, there remain numerous opportunities for further research and exploration. The following research directions offer promising avenues to extend and enhance the findings presented in this thesis, contributing to the continued advancement of antenna technology for next-generation vehicular communication systems.

### 6.2.1 Advanced Antenna Materials and Fabrication Techniques

The designs presented in this thesis have been successfully validated using conventional microstrip patch antenna technology; however, future research could explore the use of advanced materials and fabrication techniques to further enhance antenna performance. One promising avenue is the investigation of glass substrates, which offer considerable benefits for vehicular applications due to their transparency, low dielectric loss, and ease of integration into vehicle structures, such as windshields or windows. Glass substrates could enable seamless antenna integration, reducing visual clutter and enhancing the aesthetics of the vehicle, while maintaining high-performance communication capabilities. In addition, advanced materials like liquid crystal polymers, flexible substrates, and metamaterials have demonstrated significant potential to improve antenna efficiency, bandwidth, and mechanical flexibility in dynamic vehicular environments. Incorporating these materials into the designs of LP and CP antennas, as well as phased arrays, could lead to the development of more compact, lightweight, and versatile antennas. Further research into advanced fabrication methods, such as 3D printing, could also open new possibilities for cost-effective and scalable production of custom antenna designs, offering greater flexibility in both design and performance. These novel approaches could push the boundaries of antenna technology, making the designs even more suitable for next-generation vehicular systems and 5G V2X communications.

## 6.2.2 Optimizing Phased Array Design for Enhanced Beamsteering

The phased array designs presented in this thesis have successfully demonstrated dynamic beamsteering capabilities, offering flexible coverage suitable for various vehicular communication scenarios. However, future work can explore further optimizations, particularly in enhancing the precision and control of beamsteering angles to improve communication reliability in environments like dense urban intersections or highways. One avenue of exploration is refining the phased array configurations to allow more accurate and seamless beam directionality while minimizing any losses in gain or increasing sidelobe levels. By focusing on precise control of the phase shifts across the four-port antenna system, more efficient steering can be achieved without adding complexity to the overall system.

Additionally, there is potential to investigate the use of conformal phased arrays, which can be integrated into the curved surfaces of modern vehicles. These conformal arrays could allow antennas to be placed more naturally within the vehicle's structure, such as on windshields or vehicle bodies, improving not only the aerodynamic design but also providing uninterrupted 360° coverage with optimal beamsteering. This approach would retain the simplicity of the current design philosophy while enhancing the ability of the antenna to provide reliable and wide-angle beamsteering across various vehicular orientations.

Another future direction could involve optimization of the four-port phased array design to achieve even wider beam coverage with minimal interference or beam distortions. By refining the geometry and arrangement of antenna elements, improvements in gain and beam control can be realized without adding significant structural complexity. Continued advancements in phased array technology can therefore lead to antennas that are both compact and highly adaptable, ensuring consistent high-performance communication in next-generation 5G V2X networks.

## 6.2.3 Further Enhancement of CP Antenna Arrays

The CP antennas developed in this thesis have demonstrated excellent performance in terms of AR bandwidth, impedance bandwidth, and gain. However, future work could focus on further optimizing these designs for specific applications, such as autonomous driving, where reliable communication in challenging environments is essential. One potential avenue for further research is to develop the 9-element series-fed CP antenna array into larger configurations, such as 2x9 and 4x9 arrays, to offer higher realized gain CP antennas. This would mirror the progression demonstrated with the LP arrays in this thesis, allowing CP antennas to achieve even more robust performance in terms of gain and

beamsteering. Additionally, comparative analysis revealed that the 9-element series-fed LP array offers a higher gain than the 9-element CP array, which suggests that further investigation is needed to understand and address this discrepancy. Research could focus on improving the gain of the CP arrays without compromising their other key performance characteristics.

Moreover, while the CP antenna designs introduced in this thesis already maintain a simple and efficient structure, future research could further enhance their practicality by refining the current designs. This includes investigating alternative methods to maintain or even improve performance without increasing complexity. For example, optimizing the feeding network to reduce loss or exploring more efficient fabrication techniques could provide more seamless integration into vehicular systems. Additionally, as CP antennas play a crucial role in mitigating polarization mismatches, future research could explore how to expand the applicability of these designs to other frequency ranges or more challenging vehicular environments. By focusing on optimizing gain, bandwidth, and overall efficiency while preserving the simplicity of the design, future work can ensure that CP antennas continue to meet the evolving demands of next-generation V2X applications.

# Bibliography

- [1] K. Sjoberg, P. Andres, T. Buburuzan, and A. Brakemeier, “Cooperative intelligent transport systems in Europe: Current deployment status and outlook,” *IEEE Veh. Technol. Mag.*, vol. 12, no. 2, pp. 89–97, Jun. 2017.
- [2] M. Bonato, *et al.*, “Assessment of SAR in road-users from 5G-V2X vehicular connectivity based on computational simulations,” *Sensors*, vol. 22, no. 17, p. 6564, Aug. 2022.
- [3] W. Anwar, S. Dev, A. Kumar, N. Franchi, and G. Fettweis, “PHY abstraction techniques for V2X enabling technologies: Modeling and analysis,” *IEEE Trans. Veh. Technol.*, vol. 70, no. 2, pp. 1501–1517, Feb. 2021.
- [4] T. S. Rappaport, *et al.*, “Millimeter wave mobile communications for 5G cellular: It will work!” *IEEE access*, vol. 1, pp. 335–349, May. 2013.
- [5] A. N. Uwaechia and N. M. Mahyuddin, “A comprehensive survey on millimeter wave communications for fifth-generation wireless networks: Feasibility and challenges,” *IEEE Access*, vol. 8, pp. 62 367–62 414, Apr. 2020.
- [6] M. U. Khan, M. S. Sharawi, and R. Mittra, “Microstrip patch antenna miniaturisation techniques: a review,” *IET Microw. Antennas Propag.*, vol. 9, no. 9, pp. 913–922, Jun. 2015.
- [7] S. S. Gao, Q. Luo, and F. Zhu, *Circularly polarized antennas*. John Wiley & Sons, 2013.
- [8] J. Kim and J. Oh, “Liquid-crystal-embedded aperture-coupled microstrip antenna for 5G applications,” *IEEE Antennas Wireless Propag. Lett.*, vol. 19, no. 11, pp. 1958–1962, Nov. 2020.
- [9] S. Targonski, R. Waterhouse, and D. Pozar, “Design of wide-band aperture-stacked patch microstrip antennas,” *IEEE Trans. Antennas Propag.*, vol. 46, no. 9, pp. 1245–1251, Sep. 1998.

- [10] W. Liu, Z. N. Chen, and X. Qing, "Metamaterial-based low-profile broadband mushroom antenna," *IEEE Trans. Antennas Propag.*, vol. 62, no. 3, pp. 1165–1172, Mar. 2014.
- [11] R. Chopra and G. Kumar, "Series-fed binomial microstrip arrays for extremely low sidelobe level," *IEEE Trans. Antennas Propag.*, vol. 67, no. 6, pp. 4275–4279, Jun. 2019.
- [12] A. Sabban, "Microstrip antenna arrays," in *Microstrip Antennas*. InTech Croatia, 2011, pp. 361–384.
- [13] H. Zahra, *et al.*, "A simple monopole antenna with a switchable beam for 5G millimeter-wave communication systems," *Electronics*, vol. 10, no. 22, p. 2870, 2021.
- [14] G. Scalise, *et al.*, "Dual-polarized magneto-electric dipole for 5G 28 GHz phased array applications," *IEEE Open J. Antennas Propag.*, 2023.
- [15] W. Shao, B. Yang, H. Kamada, and N. Shinohara, "Aperture-coupled beam-scanning patch array with parasitic elements using a reconfigurable series-fed phase-shifting structure," *IEEE Antennas Wireless Propag. Lett.*, vol. 22, no. 7, pp. 1617–1621, 2023.
- [16] C. A. Balanis, *Antenna theory: analysis and design*. John Wiley & sons, 2016.
- [17] I. Singh, V. Tripathi *et al.*, "Micro strip patch antenna and its applications: a survey," *Int. J. Comp. Tech. Appl.*, vol. 2, no. 5, pp. 1595–1599, 2011.
- [18] J. Hao, J. Ren, X. Du, J. H. Mikkelsen, M. Shen, and Y. Z. Yin, "Pattern-reconfigurable yagi-uda antenna based on liquid metal," *IEEE Antennas Wireless Propag. Lett.*, vol. 20, no. 4, pp. 587–591, 2021.
- [19] K.-R. Xiang, F.-C. Chen, Q. Tan, and Q.-X. Chu, "Design of novel printed filtering dipole antennas," *IEEE Trans. Antennas Propag.*, vol. 69, no. 5, pp. 2537–2545, 2020.
- [20] Y. He, X. Zhao, L. Zhao, Z. Fan, J.-K. Wang, L. Zhang, C. Ni, and W.-J. Wu, "Design of broadband double-ridge horn antenna for millimeter-wave applications," *IEEE Access*, vol. 9, pp. 118 919–118 926, 2021.
- [21] I. Lau, S. Ekpo, M. Zafar, M. Ijaz, and A. Gibson, "Hybrid mmwave-Li-Fi 5G architecture for reconfigurable variable latency and data rate communications," *IEEE Access*, vol. 11, pp. 42 850–42 861, 2023.

- [22] M. Rao and K. Sarabandi, "A tunable, high-gain, very low-profile composite monopole antenna for low-frequency applications," *IEEE Trans. Antennas Propag.*, vol. 66, no. 7, pp. 3286–3294, 2018.
- [23] P. Mathur, R. Augustine, M. Gopikrishna, and S. Raman, "Dual MIMO antenna system for 5G mobile phones, 5.2 GHz wlan, 5.5 GHz WiMAX and 5.8/6 GHz WiFi applications," *IEEE Access*, vol. 9, pp. 106 734–106 742, 2021.
- [24] S. Gao, L. Chang, A. Zhang, Y. Li, and Z. Zhang, "Small-volume microstrip patch antennas exactly covering Wi-Fi 6 bands of 2.4–2.5 GHz and 5.15–5.85 GHz," *IEEE Trans. Antennas Propag.*, vol. 71, no. 7, pp. 5739–5748, 2023.
- [25] J. Khan, S. Ullah, F. A. Tahir, F. Tubbal, and R. Raad, "A sub-6 GHz MIMO antenna array for 5G wireless terminals," *Electronics*, vol. 10, no. 24, p. 3062, 2021.
- [26] F. T. Dagefu, J. Choi, B. M. Sadler, and K. Sarabandi, "A survey of small, low-frequency antennas: Recent designs, practical challenges, and research directions," *IEEE Antennas Propag. Mag.*, vol. 65, no. 1, pp. 14–26, 2021.
- [27] R. Wu, G.-H. Wen, Y. Liu, and F.-C. Chen, "A broadband filtering antenna array for sub-6 GHz base station applications," *IEEE Antennas Wireless Propag. Lett.*, 2023.
- [28] J. de Dieu Ntawangaheza, L. Sun, Z. Xie, Y. Pang, Z. Zheng, and G. Rushingabigwi, "A single-layer low-profile broadband metasurface antenna array for sub-6 GHz 5G communication systems," *IEEE Trans. Antennas Propag.*, vol. 69, no. 4, pp. 2061–2071, 2020.
- [29] P. P. Mercier, S. Bandyopadhyay, A. C. Lysaght, K. M. Stankovic, and A. P. Chandrakasan, "A sub-nW 2.4 GHz transmitter for low data-rate sensing applications," *IEEE J. Solid-State Circuits*, vol. 49, no. 7, pp. 1463–1474, 2014.
- [30] J. Guo, H. Bai, A. Feng, Y. Liu, Y. Huang, and X. Zhang, "A compact dual-band slot antenna with horizontally polarized omnidirectional radiation," *IEEE Antennas Wireless Propag. Lett.*, vol. 20, no. 7, pp. 1234–1238, 2021.
- [31] X. Wang, L. Kong, F. Kong, F. Qiu, M. Xia, S. Arnon, and G. Chen, "Millimeter wave communication: A comprehensive survey," *IEEE Commun. Surv. Tutor.*, vol. 20, no. 3, pp. 1616–1653, 2018.
- [32] B. P. Shariff, T. Ali, P. R. Mane, and P. Kumar, "Array antennas for mmwave applications: A comprehensive review," *IEEE Access*, vol. 10, pp. 126 728–126 766, 2022.

- [33] M. Hussain, E. Mousa Ali, S. M. R. Jarchavi, A. Zaidi, A. I. Najam, A. A. Alotaibi, A. Althobaiti, and S. S. Ghoneim, “Design and characterization of compact broadband antenna and its MIMO configuration for 28 GHz 5G applications,” *Electronics*, vol. 11, no. 4, p. 523, 2022.
- [34] X.-C. Wang, Y.-J. Xia, J.-H. Yang, and W.-Z. Lu, “Wideband high-gain circularly polarized substrate integrated cavity antenna array for millimeter-wave applications,” *IEEE Trans. Antennas Propag.*, vol. 71, no. 1, pp. 1041–1046, 2022.
- [35] Y.-F. Tsao, A. Desai, and H.-T. Hsu, “Dual-band and dual-polarization CPW fed MIMO antenna for fifth-generation mobile communications technology at 28 and 38 GHz,” *IEEE Access*, vol. 10, pp. 46 853–46 863, 2022.
- [36] H. Al Kassir, Z. D. Zaharis, P. I. Lazaridis, N. V. Kantartzis, T. V. Yioultsis, and T. D. Xenos, “A review of the state of the art and future challenges of deep learning-based beamforming,” *IEEE Access*, vol. 10, pp. 80 869–80 882, 2022.
- [37] H. Ullah and F. A. Tahir, “A novel snowflake fractal antenna for dual-beam applications in 28 GHz band,” *IEEE Access*, vol. 8, pp. 19 873–19 879, 2020.
- [38] J. K. Ray, A. S. Biswas, S. Sil, R. Bera, S. Shome, P. Biswas, and M. Mitra, “Realization of 5G V2V communication system at 28 GHz for smart vehicle,” *Innov. Syst. Softw. Eng.*, pp. 1–19, 2022.
- [39] A. Ghosal and M. Conti, “Security issues and challenges in V2X: A survey,” *Comput. Netw.*, vol. 169, p. 107093, 2020.
- [40] A. Mohammed, S. Kamal, M. F. Ain, Z. A. Ahmad, U. Ullah, M. Othman, R. Hussin, and M. Rahman, “Microstrip patch antenna: A review and the current state of the art,” *J. Adv. Res. Dyn. Control Syst.*, vol. 11, no. 7, pp. 510–524, 2019.
- [41] H. Hong, Y. Y. Kim, R. Y. Kim, and W. Ahn, “An effective wide-bandwidth channel access in next-generation WLAN-based V2X communications,” *Appl. Sci.*, vol. 10, no. 1, p. 222, 2019.
- [42] J. Tan, T. H. Luan, W. Guan, Y. Wang, H. Peng, Y. Zhang, D. Zhao, and N. Lu, “Beam alignment in mmwave V2X communications: A survey,” *IEEE Commun. Surv. Tutor.*, 2024.
- [43] A. Belogaev, A. Elokhin, A. Krasilov, E. Khorov, and I. F. Akyildiz, “Cost-effective V2X task offloading in MEC-assisted intelligent transportation systems,” *IEEE access*, vol. 8, pp. 169 010–169 023, 2020.

- [44] Y. Segawa, S. Tang, T. Ueno, T. Ogishi, and S. Obana, “Improving performance of C-V2X sidelink by interference prediction and multi-interval extension,” *IEEE Access*, vol. 10, pp. 42 518–42 528, 2022.
- [45] O. Darboe, D. B. O. Konditi, and F. Manene, “A 28 GHz rectangular microstrip patch antenna for 5G applications,” *International Journal of Engineering Research and Technology*, vol. 12, no. 6, pp. 854–857, 2019.
- [46] K. A. Alblaihed, Q. H. Abbasi, M. A. Imran, and L. Mohjazi, “Wideband of microstrip patch antenna for 28 GHz 5G applications,” in *2023 IEEE International Symposium on Antennas and Propagation and USNC-URSI Radio Science Meeting (USNC-URSI)*. IEEE, 2023, pp. 189–190.
- [47] —, “Gain enhancement of microstrip patch antenna for 28 ghz 5g applications,” in *2022 IEEE International Symposium on Antennas and Propagation and USNC-URSI Radio Science Meeting (AP-S/URSI)*. IEEE, 2022, pp. 57–58.
- [48] R. Yadav, A. Parmar, L. Malviya, and D. Nitnaware, “28 GHz inset feed circular shaped compact patch antenna array for 5G wireless communication,” in *2021 10th IEEE International Conference on Communication Systems and Network Technologies (CSNT)*. IEEE, 2021, pp. 1–4.
- [49] K. A. Alblaihed, *et al.*, “Wideband series-fed patch antenna array with high gain and low sidelobe: Linearly and circularly polarized for 5G V2X applications,” *IEEE Open J. Antennas Propag.*, 2024.
- [50] S. Aourik, A. Errkik, J. Zbitou, A. Oukaira, and S. Khoulii, “Aperture-stacked patch antenna array with front-to-back ratio enhancement for radar application at 28 GHz,” in *2024 International Conference on Computing, Internet of Things and Microwave Systems (ICCIMS)*. IEEE, 2024, pp. 1–5.
- [51] C. Zhu, G. Xu, A. Ren, W. Wang, Z. Huang, and X. Wu, “A compact dual-band dual-circularly polarized SIW cavity-backed antenna array for millimeter-wave applications,” *IEEE Antennas Wireless Propag. Lett.*, vol. 21, no. 8, pp. 1572–1576, 2022.
- [52] K. Cuneray, N. Akcam, T. Okan, and G. O. Arican, “28/38 GHz dual-band MIMO antenna with wideband and high gain properties for 5G applications,” *Int. J. Electron. Commun.*, vol. 162, p. 154553, 2023.
- [53] N. A. Aboserwal, J. L. Salazar, J. A. Ortiz, J. D. Díaz, C. Fulton, and R. D. Palmer, “Source current polarization impact on the cross-polarization definition

- of practical antenna elements: Theory and applications,” *IEEE Trans. Antennas Propag.*, vol. 66, no. 9, pp. 4391–4406, 2018.
- [54] H. Tataria, K. Haneda, A. F. Molisch, M. Shafi, and F. Tufvesson, “Standardization of propagation models: 800 MHz to 100 GHz—a historical perspective,” *arXiv preprint arXiv:2006.08491*, 2020.
- [55] W. L. Stutzman, *Polarization in electromagnetic systems*. Artech house, 2018.
- [56] K. K. Katare, I. M. Yousaf, and B. K. Lau, “Challenges and solutions for antennas in vehicle-to-everything services,” *IEEE Commun. Mag.*, vol. 60, no. 1, pp. 52–58, 2022.
- [57] H. Chen, H. Chen, W. Che, and Q. Xue, “A wideband V2X antenna with tilted beam pattern and transparent characteristics,” *IEEE Antennas Wirel. Propag. Lett.*, 2025.
- [58] B. A. Esmail, S. Koziel, A. Pietrenko-Dabrowska, and D. Isleifson, “wideband high-gain low-profile series-fed antenna integrated with optimized metamaterials for 5G millimeter wave applications,” *Sci. Rep.*, vol. 14, no. 1, p. 185, 2024.
- [59] S. Zakariyya, B. Sadiq, R. Alao, J. Adesina, and E. Obi, “Design of an improved microstrip antenna operating at a frequency band of 28 GHz,” *arXiv preprint arXiv:2412.20400*, 2024.
- [60] S. Rawat, Y. Bisht, A. Kothari, A. Kumar, B. Negi, and A. Bartwal, “Design of 5G mm-Wave patch antenna with ultra low return loss using Rogers RT 5880,” in *2025 3rd International Conference on Device Intelligence, Computing and Communication Technologies (DICCT)*. IEEE, 2025, pp. 328–332.
- [61] M.-A. Chung, D. Udris, C.-W. Lin, and C.-W. Yang, “A 28-GHz vivaldi array antenna with power divider structure for achieving wide band and gain enhancement,” *Int. J. Antennas Propag.*, vol. 2024, no. 1, p. 9935054, 2024.
- [62] M. A. Sufian, N. Hussain, A. Abbas, J. Lee, S. G. Park, and N. Kim, “Mutual coupling reduction of a circularly polarized MIMO antenna using parasitic elements and DGS for V2X communications,” *IEEE Access*, vol. 10, pp. 56 388–56 400, 2022.
- [63] J.-N. Wang, Z.-J. Guo, and Z.-C. Hao, “A millimeter-wave planar dual-band array antenna having individually LHCP and RHCP radiation characteristics,” *IEEE Open J. Antennas Propag.*, vol. 3, pp. 768–773, 2022.
- [64] Y. Sang, J. Han, T. Zhao, P. Duan, and M. Liu, “Circularly polarized luminescence in nanoassemblies: generation, amplification, and application,” *Adv. Mater.*, vol. 32, no. 41, p. 1900110, 2020.

- [65] S. Sun, X. Li, C. Xu, Y. Li, Y. Wu, B. L. Feringa, H. Tian, and X. Ma, "Scale effect of circularly polarized luminescent signal of matter," *Natl. Sci. Rev.*, vol. 10, no. 5, p. nwad072, 2023.
- [66] T. Shu, B. Feng, L. Zhang, C. Chen, H. Chen, Y. Chen, and Q. Zhang, "Compact dual-band dual-sense circularly polarized fragmental patch antenna optimized by improved simulated-annealing-based algorithm," *IEEE Open J. Antennas Propag.*, 2024.
- [67] M. Li, L. Fang, L. Jin, and X. Bao, "A compact dual-circularly polarized patch antenna with wide axial ratio beamwidth based on square-ring coupled feeding," in *2024 IEEE MTT-S International Wireless Symposium (IWS)*. IEEE, 2024, pp. 1–3.
- [68] H. Xu, X.-C. Zhu, P. Wei, Z. Yu, and C. Liu, "Wideband circularly polarized magnetic-electric dipole antenna using shorted stub for millimeter wave endfire radiation," *Microw. Opt. Technol. Lett.*, vol. 66, no. 7, p. e34249, 2024.
- [69] J. Zhou, X. Pan, G. Cheng, L. Yang, Y. Li, and Z. Huang, "A wideband circularly polarized filtering antenna based on multi-layer structural design," *IEEE Antennas Wirel. Propag. Lett.*, 2024.
- [70] P. Li, Y. Zhang, X. Qin, K. Wei, P. Liang, and Y. Li, "Wideband widebeam circular-polarized antenna using asymmetrical Tri-dipoles for direct satellite-to-handset communication," *IEEE Trans. Antennas Propag.*, 2024.
- [71] R. R. Elsharkawy, K. F. Hussein, and A. E. Farahat, "Circularly-polarized 28 GHz antenna for next generations of communication systems," *Sci. Rep.*, vol. 15, no. 1, p. 5745, 2025.
- [72] Q.-Y. Guo, P. Chen, M. Liang, G.-H. Sun, and G.-B. Wu, "A high-gain aperture-shared dual-band circularly polarized antenna using polarizer integrated dual-functional surface," *IEEE Trans. Antennas Propag.*, 2024.
- [73] H. Nakano, T. Abe, A. Mehta, and J. Yamauchi, "Theoretical consideration of axial ratio deterioration in CP loop-shaped antennas," *IEEE Antennas Wirel. Propag. Lett.*, vol. 22, no. 5, pp. 1035–1039, 2022.
- [74] T. Liang, Z. Wang, and Y. Dong, "Estimation of axial ratio of single-port dual-mode circularly polarized antenna using reflection coefficient," *IEEE Transactions on Antennas and Propagation*, vol. 71, no. 2, pp. 1706–1715, 2022.
- [75] L. Sun, G. Ou, Y. Lu, T. Shusen, and A. Kishk, "Axial ratio bandwidth of a circularly polarized microstrip antenna," *Advancement in microstrip antennas with recent applications*, pp. 229–246, 2013.

- [76] Y. Sadovaya, D. Moltchanov, W. Mao, O. Orhan, S.-p. Yeh, H. Nikopour, S. Talwar, and S. Andreev, “Integrated access and backhaul in millimeter-wave cellular: Benefits and challenges,” *IEEE Commun. Mag.*, vol. 60, no. 9, pp. 81–86, 2022.
- [77] H. Wei, N. Deng, and M. Haenggi, “Performance analysis of inter-cell interference coordination in mm-wave cellular networks,” *IEEE Trans. Wirel. Commun.*, vol. 21, no. 2, pp. 726–738, 2021.
- [78] T. Nahar and S. Rawat, “Efficiency enhancement techniques of microwave and millimeter-wave antennas for 5G communication: A survey,” *Trans. Emerg. Telecommun. Technol.*, vol. 33, no. 9, p. e4530, 2022.
- [79] J. Kim and H. L. Lee, “High gain planar segmented antenna for mmwave phased array applications,” *IEEE Trans. Antennas Propag.*, vol. 70, no. 7, pp. 5918–5922, 2022.
- [80] Y.-T. Liu and K. W. Leung, “28 GHz substrate-integrated filtering dielectric resonator antenna array,” *IEEE Trans. Antennas Propag.*, vol. 70, no. 10, pp. 9900–9905, 2022.
- [81] S. H. Kiani, X. C. Ren, A. Bashir, A. Rafiq, M. R. Anjum, M. M. Kamal, B. U. Din, and F. Muhammad, “Square-framed T shape mmwave antenna array at 28 GHz for future 5G devices,” *Int. J. Antennas Propag.*, vol. 2021, no. 1, p. 2286011, 2021.
- [82] J. Ran, C. Jin, P. Zhang, W. Wang, and Y. Wu, “High-gain and low-loss dual-polarized antenna array with reduced sidelobe level based on gap waveguide at 28 GHz,” *IEEE Antennas Wirel. Propag. Lett.*, vol. 21, no. 5, pp. 1022–1026, 2022.
- [83] A. Ramos, T. Varum, and J. N. Matos, “A review on mutual coupling reduction techniques in mmwaves structures and massive MIMO arrays,” *IEEE Access*, 2023.
- [84] J. Khan, S. Ullah, U. Ali, F. A. Tahir, I. Peter, and L. Matekovits, “Design of a millimeter-wave MIMO antenna array for 5G communication terminals,” *Sensors*, vol. 22, no. 7, p. 2768, 2022.
- [85] M. Noor-A-Rahim, Z. Liu, H. Lee, M. O. Khyam, J. He, D. Pesch, K. Moessner, W. Saad, and H. V. Poor, “6G for vehicle-to-everything (V2X) communications: Enabling technologies, challenges, and opportunities,” *Proceedings of the IEEE*, vol. 110, no. 6, pp. 712–734, 2022.
- [86] M. H. C. Garcia, A. Molina-Galan, M. Boban, J. Gozalvez, B. Coll-Perales, T. Şahin, and A. Kousaridas, “A tutorial on 5G NR V2X communications,” *IEEE Commun. Surv. Tutor.*, vol. 23, no. 3, pp. 1972–2026, 2021.

- [87] Y. Yu, Z. H. Jiang, J.-D. Zhang, and W. Wu, "Broadband millimeter-wave endfire circularly polarized array with a low-profile feeding structure," *IEEE Trans. Antennas Propag.*, vol. 70, no. 8, pp. 7270–7275, 2022.
- [88] K. Ding, X. Fang, A. Chen, and Y. Wang, "A novel parallel-series feeding network based on three-way power divider for microstrip antenna array," *IEEE Antennas Wirel. Propag. Lett.*, vol. 12, pp. 757–760, 2013.
- [89] M. Y. Mohamed, A. M. Dini, M. M. Soliman, and A. Z. M. Imran, "Design of 2 x 2 microstrip patch antenna array at 28 GHz for millimeter wave communication," in *2020 IEEE International Conference on Informatics, IoT, and Enabling Technologies (ICIoT)*. IEEE, 2020, pp. 445–450.
- [90] E. A. Ball, "Investigation into series-fed microstrip patch arrays at 26 GHz, 28 GHz and 48 GHz—design, simulation and prototype tests," in *2021 IEEE Texas Symposium on Wireless and Microwave Circuits and Systems (WMCS)*. IEEE, 2021, pp. 1–6.
- [91] A. Chletsou, E. Newsom, and J. Papapolymerou, "Experimental characterization of a helical antenna integrated in the rear of a vehicle for C-V2X communications," *IEEE J. Microwaves.*, 2023.
- [92] M. Li, Z. Zhang, M.-C. Tang, D. Yi, and R. W. Ziolkowski, "Compact series-fed microstrip patch arrays excited with dolph–chebyshev distributions realized with slow wave transmission line feed networks," *IEEE Trans. Antennas Propag.*, vol. 68, no. 12, pp. 7905–7915, 2020.
- [93] S. Zhao, J. Chen, and Y. Shi, "All-solid-state beam steering via integrated optical phased array technology," *Micromachines*, vol. 13, no. 6, p. 894, 2022.
- [94] C. Fulton, M. Yeary, D. Thompson, J. Lake, and A. Mitchell, "Digital phased arrays: Challenges and opportunities," *Proceedings of the IEEE*, vol. 104, no. 3, pp. 487–503, 2016.
- [95] G. Han, B. Du, W. Wu, and B. Yang, "A novel hybrid phased array antenna for satellite communication on-the-move in Ku-band," *IEEE Trans. Antennas Propag.*, vol. 63, no. 4, pp. 1375–1383, 2015.
- [96] R. J. Mailloux, *Phased array antenna handbook*. Artech house, 2017.
- [97] A. H. Naqvi and S. Lim, "Review of recent phased arrays for millimeter-wave wireless communication," *Sensors*, vol. 18, no. 10, p. 3194, 2018.

- [98] Y. Yuan, S. J. Chen, and C. Fumeaux, “Varactor-based phase shifters operating in differential pairs for beam-steerable antennas,” *IEEE Trans. Antennas Propag.*, vol. 70, no. 9, pp. 7670–7682, 2022.
- [99] Z. Wang and Y. Dong, “Metamaterial-based pattern-switchable linear array for 2-D discrete beam-scanning using hybrid digital coding method,” *IEEE Trans. Antennas Propag.*, vol. 71, no. 3, pp. 2515–2526, 2023.
- [100] J.-Q. Han, F.-Y. Meng, and Y.-H. Liu, “Series-fed circularly polarized 2-Bit reconfigurable beam-steering antenna array,” in *2024 International Conference on Microwave and Millimeter Wave Technology (ICMMT)*, vol. 1. IEEE, 2024, pp. 1–3.
- [101] J. M. Wen, C. Yu, Y. X. Li, Y. M. Pan, and S. Y. Zheng, “A compact dual-beam steering antenna array based on a simplified beamforming network,” *IEEE Trans. Antennas Propag.*, vol. 71, no. 9, pp. 7620–7625, 2023.
- [102] Y. Qiao, Y. Niu, L. Su, S. Mao, N. Wang, Z. Zhong, and B. Ai, “Deep reinforcement learning based mmWave beam alignment for V2I communications,” *IEEE Trans. Mach. Learn. Commun. Netw.*, 2024.
- [103] M. Ko, H. Lee, and J. Choi, “Planar LTE/sub-6 GHz 5G MIMO antenna integrated with mmwave 5G beamforming phased array antennas for V2X applications,” *IET Microw. Antennas Propag.*, vol. 14, no. 11, pp. 1283–1295, 2020.
- [104] H. Zakeri, R. Azizpour, P. Khoddami, G. Moradi, M. Alibakhshikenari, C. H. See, T. A. Denidni, F. Falcone, S. Koziel, and E. Limiti, “Low-cost multiband four-port phased array antenna for sub-6 GHz 5G applications with enhanced gain methodology in radio-over-fiber systems using modulation instability,” *IEEE Access*, 2024.
- [105] J. W. Kunzler and K. F. Warnick, “Wideband radio frequency interference cancellation for high-sensitivity phased array receivers with true time delays and truncated hadamard projection,” *IEEE Trans. Antennas Propag.*, vol. 70, no. 9, pp. 8069–8076, 2022.
- [106] A. Ludvig-Osipov, J.-M. Hannula, P. Naccachian, and B. L. G. Jonsson, “Physical limitations of phased array antennas,” *IEEE Trans. Antennas Propag.*, vol. 69, no. 9, pp. 5512–5523, 2021.
- [107] K. F. Warnick, D. B. Davidson, and D. Buck, “Embedded element pattern loading condition transformations for phased array modeling,” *IEEE Trans. Antennas Propag.*, vol. 69, no. 3, pp. 1769–1774, 2020.

- [108] M. R. Al-Amin, R. S. Malfajani, E. Baladi, and M. S. Sharawi, "Connected antenna arrays with beamsteering capability for on-package millimetre-wave applications," *IEEE Open J. Antennas Propag.*, vol. 5, no. 2, pp. 414–429, 2024.
- [109] V. Kumar, A. Mohan, and B. Ghosh, "Beam-steering transmitarray antenna for 5G application," in *2023 IEEE Wireless Antenna and Microwave Symposium (WAMS)*. IEEE, 2023, pp. 1–4.
- [110] A. Rammohan *et al.*, "Revolutionizing intelligent transportation systems with cellular vehicle-to-everything (C-V2X) technology: Current trends, use cases, emerging technologies, standardization bodies, industry analytics and future directions," *Veh. Commun.*, p. 100638, 2023.
- [111] Q. Zhang, Z. Zhao, J. Zheng, F. Li, J. Tang, Y. Huang, Y. Ren, and X. Chen, "Multifunctional frequency selective absorber enabling FR1 and FR2 5G OTA tests in a hybrid reverberation chamber," *IEEE Trans. Instrum. Meas.*, vol. 72, pp. 1–10, 2023.
- [112] D. Shin, W.-H. Lim, and H. L. Lee, "Highly integrated in-band full-duplex TRX antennas for mmwave V2X communications," *IEEE Trans. Vehicular Tech.*, vol. 72, no. 5, pp. 6404–6411, 2023.
- [113] S. A. Busari, *et al.*, "Millimetre-wave massive MIMO for cellular vehicle-to-infrastructure communication," *IET Intell. Transp. Syst.*, vol. 13, no. 6, pp. 983–990, Jun. 2019.
- [114] C. Kykkotis, P. S. Hall, R. A. Lewis, and A. D. Searle, "Millimetre wave antennas for future vehicle communications," in *IEEE 49th Veh. Technol. Conf.*, vol. 2. IEEE, May. 1999, pp. 1585–1588.
- [115] D. Rongas, A. Paraskevopoulos, L. Marantis, and A. G. Kanatas, "An integrated shark-fin reconfigurable antenna for V2X communications," *Prog. Electromagn. Res.*, vol. 100, pp. 1–16, Feb. 2020.
- [116] H. A. Elmobarak, M. Himdi, X. Castel, S. K. A. Rahim, and T. K. Geok, "Flexible patch antenna array operating at microwaves based on thin composite material," *IEEE Access*, vol. 10, pp. 115 663–115 672, 2022.
- [117] B. Liu, P. Tang, J. Zhang, Y. Yin, G. Liu, and L. Xia, "Propagation characteristics comparisons between mmwave and visible light bands in the conference scenario," in *Photonics*, vol. 9, no. 4. MDPI, 2022, p. 228.

- [118] J.-M. Xie, B. Li, Y.-P. Lyu, and L. Zhu, “Single-and dual-band high-order bandpass frequency selective surfaces based on aperture-coupled dual-mode patch resonators,” *IEEE Trans. Antennas Propag.*, vol. 69, no. 4, pp. 2130–2141, 2020.
- [119] S. Jabeen, Q. U. Khan, and S. A. Sheikh, “A single-layer s/c/k/ka bands shared aperture antenna with novel feed structure for k/ka bands,” *IEEE Trans. Antennas Propag.*, vol. 71, no. 8, p. 6965–6970, Aug. 2023.
- [120] M. Kacar, T. M. Weller, and G. Mumcu, “3D printed wideband multilayered dual-polarized stacked patch antenna with integrated MMIC switch,” *IEEE Open J. Antennas Propag.*, vol. 2, pp. 38–48, 2020.
- [121] M. Simone, A. Fanti, and G. Mazzarella, “5G wideband stacked patch antennas,” in *Proc. 15th Eur. Conf. Antennas Propag. (EuCAP)*, 2021, pp. 1–5.
- [122] L. Wang, J. Shi, K. Xu, and Z. W. Yin, “Compact dual-strip coupled dual-patch antenna for millimeter-wave AiP applications,” *IEEE Antennas Wireless Propag. Lett.*, vol. 20, no. 4, pp. 577–581, Apr. 2021.
- [123] J. Xu, *et al.*, “Low-profile wideband vertically folded slotted circular patch array for Ka-band applications,” *IEEE Trans. Antennas Propag.*, vol. 68, no. 9, pp. 6844–6849, Sep. 2020.
- [124] N. Hussain, *et al.*, “A metasurface-based low-profile wideband circularly polarized patch antenna for 5G millimeter-wave systems,” *IEEE Access*, vol. 8, pp. 22 127–22 135, 2020.
- [125] W. Wan, *et al.*, “Low-profile broadband patch-driven metasurface antenna,” *IEEE Antennas Wireless Propag. Lett.*, vol. 19, no. 7, pp. 1251–1255, Jul. 2020.
- [126] Y. Q. Guo, Y. M. Pan, and S. Y. Zheng, “Design of series-fed, single-layer, and wideband millimeter-wave microstrip arrays,” *IEEE Trans. Antennas Propag.*, vol. 68, no. 10, pp. 7017–7026, Oct. 2020.
- [127] H. Wang and I. Park, “Coplanar strip line-fed series dipole array antenna for high-gain realization,” *IEEE Trans. Antennas Propag.*, vol. 69, no. 8, pp. 5106–5111, Aug. 2021.
- [128] S. Long, M. McAllister, and L. Shen, “The resonant cylindrical dielectric cavity antenna,” *IEEE Trans. Antennas Propag.*, vol. 31, no. 3, pp. 406–412, 1983.
- [129] R. Li, G. DeJean, J. Laskar, and M. M. Tentzeris, “Investigation of circularly polarized loop antennas with a parasitic element for bandwidth enhancement,” *IEEE Trans. Antennas Propag.*, vol. 53, no. 12, pp. 3930–3939, Dec. 2005.

- [130] J. R. James and P. S. Hall, *Handbook of microstrip antennas*. IET, 1989, vol. 1.
- [131] F. Bowman, *Introduction to Bessel functions*. Courier Corporation, Apr. 2012.
- [132] A. Bellary, K. Kandasamy, and P. H. Rao, “Analysis of wave propagation models with radio network planning using dual polarized MIMO antenna for 5G base station applications,” *IEEE Access*, vol. 10, pp. 29 183–29 193, March, 2022.
- [133] W. Wang and Y. Zheng, “Wideband gain enhancement of a dual-polarized MIMO vehicular antenna,” *IEEE Transactions on Vehicular Technology*, vol. 70, no. 8, pp. 7897–7907, 2021.
- [134] H. Ward, “Properties of dolph-chebyshev weighting functions,” *IEEE Trans. Aerosp. Electron. Syst.*, no. 5, pp. 785–786, 1973.
- [135] T. Mitha and M. Pour, “Principles of adaptive element spacing in linear array antennas,” *Sci. Rep.*, vol. 11, no. 1, p. 5584, Dec. 2021.
- [136] S. Kumar, *et al.*, “Fifth generation antennas: A comprehensive review of design and performance enhancement techniques,” *IEEE Access*, vol. 8, pp. 163 568–163 593, 2020.
- [137] A. S. Mohammed, S. Kamal, M. F. B. Ain, R. Hussin, F. Najmi, S. A. Sundi, Z. A. Ahmad, U. Ullah, M. F. B. M. Omar, M. Othman *et al.*, “Mathematical model on the effects of conductor thickness on the centre frequency at 28 GHz for the performance of microstrip patch antenna using air substrate for 5G application,” *Alex. Eng. J.*, vol. 60, no. 6, pp. 5265–5273, 2021.
- [138] N. Nguyen-Trong, S. J. Chen, and C. Fumeaux, “High-gain dual-band dual-sense circularly polarized spiral series-fed patch antenna,” *IEEE Open J. Antennas Propag.*, vol. 3, pp. 343–352, 2022.
- [139] Y. Xu, K.-M. Luk, A. Li, and J. Sun, “A novel compact magneto-electric dipole antenna for millimeter-wave beam steering applications,” *IEEE Trans. Vehicular Tech.*, vol. 70, no. 11, pp. 11 772–11 783, 2021.
- [140] Z. M. Xiao, Y. M. Pan, and S. Y. Zheng, “Millimeter-wave widebeam dielectric resonator antenna and its wide-angle beam-scanning phased arrays using the field distribution of quasi-te 112 modes,” *IEEE Trans. Antennas Propag.*, 2023.
- [141] Y. Hasan and M. A. Rahman, “Design of a wide dual-band monopole microstrip antenna with beam steering capability,” in *2021 International Conference on Electronics, Communications and Information Technology (ICECIT)*. IEEE, 2021, pp. 1–4.

- [142] Z. Qu, Y. Zhou, S. Alkaraki, J. R. Kelly, and Y. Gao, “Continuous beam steering realized by tunable ground in a patch antenna,” *IEEE Access*, vol. 11, pp. 4095–4104, 2023.
- [143] L. Steinweg, C. Carta, and F. Ellinger, “A hybrid true-time and phase-delayed approach for millimeter-wave beam steering,” *IEEE Trans. Microw. Theory Techn.*, vol. 70, no. 9, pp. 4318–4327, Sep. 2022.
- [144] Y. T. Lo and S. Lee, *Antenna Handbook: Theory, Applications, and Design*. Boston, MA, USA: Springer, 2013.
- [145] W. T. Li, *et al.*, “Low-profile wideband dual-polarized antenna for millimeter-wave beam steering applications,” *IEEE Trans. Antennas Propag.*, 2023.
- [146] Q. Ren, A. U. Zaman, and J. Yang, “Dual-circularly polarized array antenna based on gap waveguide utilizing double-grooved circular waveguide polarizer,” *IEEE Trans. Antennas Propag.*, vol. 70, no. 11, pp. 10 436–10 444, 2022.
- [147] H. Xu, *et al.*, “Planar wideband circularly polarized cavity-backed stacked patch antenna array for millimeter-wave applications,” *IEEE Trans. Antennas Propag.*, vol. 66, no. 10, pp. 5170–5179, Oct. 2018.
- [148] W. Li, X. H. Tang, and Y. Yang, “A Ka-band circularly polarized substrate integrated cavity-backed antenna array,” *IEEE Antennas Wireless Propag. Lett.*, vol. 18, no. 9, pp. 1882–1886, Sep. 2019.
- [149] B. Feng, *et al.*, “A compact wideband circularly polarized magneto-electric dipole antenna array for 5G millimeter-wave application,” *IEEE Trans. Antennas Propag.*, vol. 68, no. 9, pp. 6838–6843, Sep. 2020.
- [150] H. Askari *et al.*, “A wideband circularly polarized magnetoelectric dipole antenna for 5G millimeter-wave communications,” *Sensors*, vol. 22, no. 6, p. 2338, 2022.
- [151] Z. Zhang, S. Yang, F. Yang, Y. Chen, S.-W. Qu, and J. Hu, “Ultralow scattering design of wideband conformal arrays based on optimally loaded resistors,” *IEEE Trans. Antennas Propag.*, vol. 70, no. 8, pp. 6692–6702, 2022.
- [152] D. Wu, J. Liang, and L. Ge, “A wideband dual-circularly polarized series-fed corner-truncated patch array using coplanar proximity coupling,” *IEEE Trans. Antennas Propag.*, 2024.
- [153] R.-L. Li and H. Nakano, “Numerical analysis of arbitrarily shaped probe-excited single-arm printed wire antennas,” *IEEE Trans. Antennas Propag.*, vol. 46, no. 9, pp. 1307–1317, Sep. 1998.

- [154] X. Bao and M. Ammann, “Dual-frequency dual-sense circularly-polarized slot antenna fed by microstrip line,” *IEEE Trans. Antennas Propag.*, vol. 56, no. 3, pp. 645–649, Mar. 2008.
- [155] S. Sadeghi-Marasht, M. S. Sharawi, and A. Zhu, “Dual-band circularly polarized antenna array for 5G millimeter-wave applications,” *IEEE Open J. Antennas Propag.*, vol. 3, pp. 314–323, 2022.
- [156] U. Ullah, M. Al-Hasan, S. Koziel, and I. B. Mabrouk, “A series inclined slot-fed circularly polarized antenna for 5G 28 GHz applications,” *IEEE Antennas and Wireless Propag. Lett.*, vol. 20, no. 3, pp. 351–355, Mar. 2021.
- [157] U. Ullah, *et al.*, “Series-slot-fed circularly polarized multiple-input–multiple-output antenna array enabling circular polarization diversity for 5G 28 GHz indoor applications,” *IEEE Trans. Antennas Propag.*, vol. 69, no. 9, pp. 5607–5616, Sep. 2021.
- [158] D. Jang, N. K. Kong, and H. Choo, “Design of an on-glass 5G monopole antenna for a vehicle window glass,” *IEEE Access*, vol. 9, pp. 152 749–152 755, Nov. 2021.
- [159] H. Wang, K. E. Kedze, and I. Park, “A high-gain and wideband series-fed angled printed dipole array antenna,” *IEEE Trans. Antennas Propag.*, vol. 68, no. 7, pp. 5708–5713, Jul. 2020.
- [160] G. Zhai, *et al.*, “Gain enhancement of printed log-periodic dipole array antenna using director cell,” *IEEE Trans. Antennas Propag.*, vol. 62, no. 11, pp. 5915–5919, Nov. 2014.
- [161] S. D. Joseph and E. A. Ball, “Series-fed millimeter-wave antenna array based on microstrip line structure,” *IEEE Open J. Antennas Propag.*, vol. 4, pp. 254–261, 2023.
- [162] S. Afoakwa and Y.-B. Jung, “Wideband microstrip comb-line linear array antenna using stubbed-element technique for high sidelobe suppression,” *IEEE Trans. Antennas Propag.*, vol. 65, no. 10, pp. 5190–5199, Oct. 2017.